8-2016

Targeted Nano-Therapeutices for the Reversal of Calcification and ECM Degradation in Abdominal Aortic Aneurysms

Nasim Nosoudi
Clemson University

TARGETED NANO-THERAPEUTICES FOR THE REVERSAL OF CALCIFICATION AND ECM DEGRADATION IN ABDOMINAL AORTIC ANEURYSMS

A Dissertation
Presented to
the Graduate School of
Clemson University

In Partial Fulfillment
of the Requirements for the Degree
Doctor of Philosophy
Bioengineering

---

by
Nasim Nosoudi
August 2016

Accepted by:
Dr. Narendra Vyavahare, Committee Chair
Dr. Martine Laberge
Dr. Jeoung Soo Lee
Dr. Alexey Vertegel
Dr. Bruce Gray

ABSTRACT

Abdominal aortic aneurysm (AAA) is focal ballooning and dilation of abdominal aorta. AAAs are the 13th primary cause of death in the US, taking the lives of approximately 15,000 Americans each year [1]. The best prevention of AAA is early detection when the AAA is smaller than 3 cm. The only current treatment option for well-developed AAA is surgical repair of the aneurysmal vessel. Since the enactment of the Screening Abdominal Aortic Aneurysms Very Efficiently Act (SAAVE) act, patients with Medicare are covered for one-time ultrasound imaging for aneurysm, which allows smaller scale AAAs to be discovered. Unfortunately, after this initial detection there is no currently known treatment to slow the growth of these aneurysms. Monitoring can be continued through the use of ultrasound imaging or plain film radiography, which shows calcification related to the AAA, but there is no effective way to show a full picture of focal wall weakening [2]. When the AAA has a diameter greater than 5.5 cm, elective surgery is typically performed as the risk of surgery is less than the risk of a ruptured AAA.

Excessive activity of metalloproteinases (MMPs) has been associated with aortic elastin damage and degeneratio[3]. Also AAA is often associated with calcification, which increases the risk of AAA rupture [4]. Based on this knowledge, we hypothesized that combined treatment MMP inhibitors locally to stop the degradation of elastin, and pentagalloyl glucose (PGG) to regenerate lost elastin can be an effective treatment option for early to middle stage aneurysms in order to prevent disease progression. Furthermore, we hypothesized that calcification associated with well-developed AAA can be removed

first with ethylene diamime tetraacetic acid (EDTA), a well-known metal ion chelator and then degraded elastin can be regenerated with PGG. The overall goal of this study was to develop a minimally invasive, non-toxic, targeted vascular drug delivery system that both prevents elastin degradation and aids elastin regeneration, thereby acting as a multi-functional treatment option for elasto-degenerative vascular diseases including AAAs. In order to achieve this goal, we used nanoparticles (NPs) developed in our laboratory to target degraded elastin by conjugating elastin antibody that specifically recognizes only degraded elastin. First, using calcium chloride-induced AAA rat model, we show targeted delivery of such nanoparticles loaded MMP inhibitor (BB-94) lead to suppression of MMP activity in abdominal aortic aneurysms and prevented aneurysmal expansion. Next, we demonstrated that nanoparticles can be loaded with PGG. In AAA model in rats, we show PGG can be delivered at the site of AAA by targeted NPs. Such PGG delivery inhibited elastin degradation and lead to suppression of AAA. Finally, we tested whether moderate size calcified aneurysms could be reversed by dual therapy. We created moderate size AAA in rats by calcium chloride injury, and then first delivered EDTA loaded NPs systemically to remove calcification followed by delivery of PGG loaded NPs. Only dual therapy showed reversal of calcification in the aorta as well as reversal of AAA and regeneration of elastic lamina. NPs with EDTA alone or blank NPs did not cause regeneration of elastic lamina in the aorta.

DEDICATION

I would like to dedicate this work to my parents, Amir, and teachers who inspired me.

ACKNOWLEDGMENTS

First and foremost, I would like to express my sincere gratitude to my advisor, Dr. Naren Vyavahare, for his support, guidance, criticism, mentorship and commitment throughout my Ph.D. journey. His broad knowledge and innovative thinking have greatly helped the success of this research as well as my growth as a scholar and academic.

I would also like to extend my appreciation to my committee members—Dr. Martine Laberge; Dr. Jeoung Soo Lee; Dr. Alexey Vertegel and Dr. Bruce Gray—for their advice during my research.

I would next like to thank Dr. Guzelya Korneva for her invaluable help with HPLC.

My sincere appreciation is extended to Dr. John Parrish and all the staff at the Godley Snell Research Centre.

I am also grateful to the Department of Bioengineering and Clemson University.

Special thanks to Maria Torres for being the nicest Graduate Student Services Coordinator ever.

Special thanks to all my friends in Clemson, specially my lab members, Saketh, Vaideesh and Yang and my undergraduate students, Aniqa, Steven and Joe.

I would like to extend my thanks to those animals that helped me giving their lives to accomplish this study.

I would like to acknowledge the financial support provided by the National Institute of Health and the Hunter Endowment.

I would like to acknowledge Dr. Michael Gelinsky and Dr. Anja Lode for mentoring me.

TABLE OF CONTENTS

Table of Contents (Continued)

Page

LIST OF TABLES

LIST OF FIGURES

List of Figures (Continued)

Figure Page

List of Figures (Continued)

Figure Page

List of Figures (Continued)

Figure Page

CHAPTER I

INTRODUCTION

Abdominal aortic aneurysm (AAA) is the dilation or ballooning of part of the aorta located in the abdominal region. There are typically no symptoms associated with AAAs until it reaches an advance stage, and the bursting of the AAA is often fatal. AAAs less than 5.5 cm wide are considered to have a low chance of rupturing and are designated as small AAAs. Any abdominal aortic aneurysm larger than 5.5 cm wide[5] is considered a large AAA and often an operation to repair is advised if the risk of rupture is greater than that of surgery[6]. Males 65-years-old and older and those who have smoked 100 cigarettes or more are offered a routine ultrasound screening for AAA through Medicare. Routine screening is now allowing diagnosis of early stage aneurysms. Unfortunately, there are no known pharmacological approaches for treating small AAA in humans or retarding AAA growth[7]. However, there are multiple drugs that have been found to prevent AAA formation and progression in small animal studies. These findings have generated a large amount of interest to treat patients with small aneurysms, and have led to some initial investigative studies. In one study, 121 patients who received a Beta blocker had a significantly lower mean growth rate than those who did not (0.36 versus 0.68 cm per year)[8,9]. Another class of successful drugs, statins, are suggested for AAA patients to reduce atherosclerosis development[10]. Additionally, there have been at least 14 independent in-vivo studies on doxycycline that have shown it limits aneurysm progression. Systemic delivery of doxycycline is known to decrease inflammatory markers in AAA in humans, but it has not been confirmed to reduce AAA expansion

rates[10,11]. We believe one reason behind the failure of these drugs is that systemic administration at approved dosage levels does not provide the necessary therapeutic levels at the site of AAA. If we were able to deliver the drugs locally, it would improve the therapeutic efficacy and prevent systemic side effects.

Furthermore, inhibition of ECM degrading enzymes can halt the progression of the disease but it cannot reverse already degraded ECM. One of the hallmarks of aneurysm is the degradation of elastic lamina in the medial region of the aorta. Elastic fibers are created during early development and are made up of a cross-linked elastin core (amorphous elastin) residing in a network of microfibril associated glycoproteins (MAGPs), latent TGF-beta binding protein (LTBP) and fibulins[12].

Elastic fibers can undergo degeneration during inflammatory diseases[13]. Atherosclerotic disease or excessive smoking can cause chronic inflammation in arteries that can lead to elastic fiber degeneration and formation of aortic aneurysms. Once degraded, it is rarely remodels in elderly patients. Little work has been done on the regeneration of elastin for AAA treatment. This is important because other ECM components such as collagen and glycosaminoglycans are remodeled during disease but older diseased cells are unable to repair and remodel degraded elastin[14].

During this dissertation research, we have explored the use of targeted nanoparticles that can deliver synthetic MMP inhibitors to the aneurysmal aorta to reduce MMP activities, protect elastin from proteolytic damage, and improve the integrity of the abdominal aorta. We further investigated whether nanoparticle based targeted treatment can aid in deposition of newly formed cross-linked elastin by cells (delivery of

polyphenols) while reducing inflammation and calcification (by delivery of the chelating agent EDTA) in the artery. Overall, our plan was to find treatments that were effective in halting and reversing aneurysms and healing AAAs.

We were successful in formulating polymeric nanoparticles (NPs) based on either poly-l-lactic acid (PLA) or bovine serum albumin (BSA) that had been decorated with elastin antibodies to be able to recognize and attach to damaged aortic elastin. Such NPs were successfully loaded with synthetic MMP inhibitor, polyphenolic compound PGG, and EDTA.

This dissertation has been formatted in the following sections:

1. In Chapter II, we present a comprehensive overview of the cardiovascular system, its structure, function, biomechanics, elastic moduli, elastin in aorta, vascular disease, specially AAA, and treatment recommendations as well as pharmacological treatment options available today.

2. In Chapter III, we provide the rational of the research and specific aims.

3. In Chapter IV, we discuss the prevention of abdominal aortic aneurysm progression by targeted inhibition of matrix metalloproteinase activity with Batimastat-loaded nanoparticles.

4. In Chapter V, we present targeted therapy with nanoparticle loaded with pentagalloyl glucose (PGG) to protect vascular elastic lamina from MMP-mediated degradation and show that it prevents progression of abdominal aortic aneurysm (AAA) in calcium chloride injury mediated AAA development in rats.

5. In Chapter VI, we present dual therapy using EDTA loaded nanoparticles along with PGG loaded nanoparticles to reverse abdominal aortic aneurysm in an advance stage in a calcium chloride injury mediated AAA development in rats.

6. Chapter VII provides conclusion of the present research and future directions needed to take this research further as a therapy for clinical suppression of AAA.

CHAPTER II

LITERATURE REVIEW

The Cardiovascular System

The cardiovascular system functions to carry blood and lymph throughout the body[15]. It is divided into four sub units: the heart, macrocirculation, microcirculation, and lymph vascular systems[16]. Blood vessels vary with size and function, but each has three layers, or tunics, which means "coat" in Latin. The deepest layer, the tunica intima, makes up the typically simple squamous endothelial lining of the vessel. The tunica media, the middle layer, consists of smooth muscle and some connective tissue fibers, and the outermost layer, the tunica externa, is primarily connective tissue with fibroblasts[17] (See Figure 1).

Arteries carry blood from the heart to various organs and can be categorized by their size. Those with a diameter below 0.5 mm are known as arterioles. Muscular or distributive arteries are medium sized, and elastic arteries are the largest. Capillaries, the smallest blood vessels, are responsible for gas transfer and are 7–9 μm in diameter[18]. Veins bring blood to the heart from various organs. They have three categories based on the size as well. Venules are the smallest followed by medium and large veins. Compared to veins, arteries have thicker walls as they need to withstand more pressure[19].

Biomechanics of Aorta

The rupture of aneurysmal vessel wall counts as a mechanical failure, so the biomechanics of AAA has been studied extensively[21]. The mechanical properties of AAA could be used for predicting of AAA rupture risk so the ultimate goal of studying

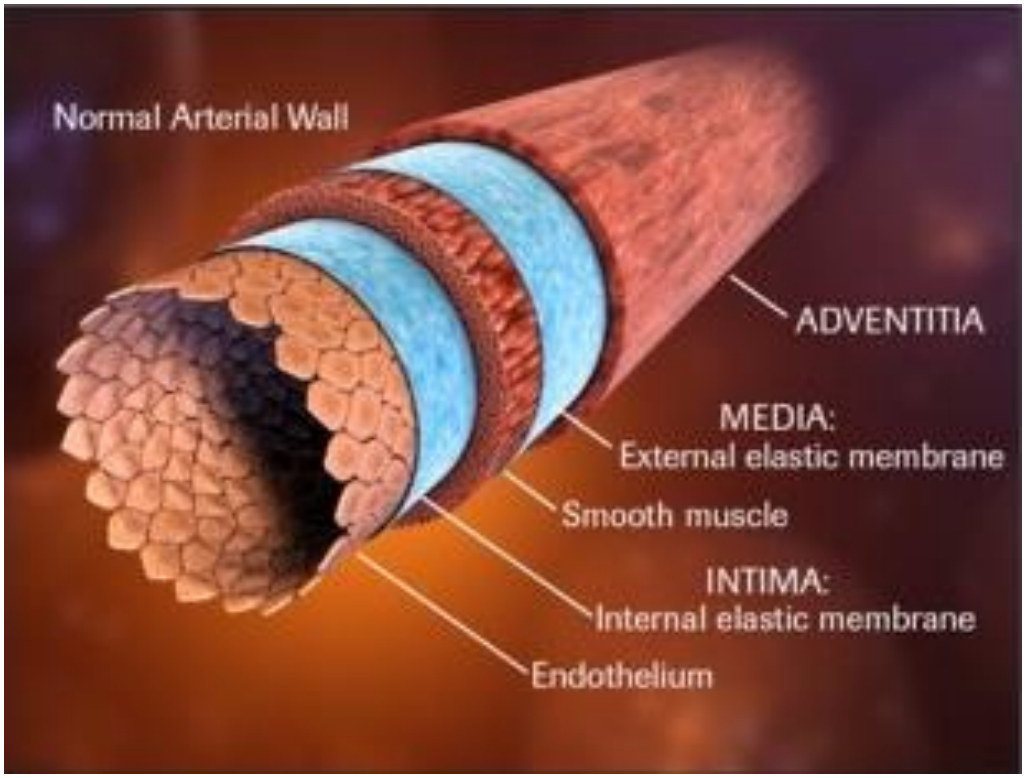

Figure 1. Sections of blood vessels composed of three main layers[20].

mechanical properties is to predict AAA rupture[22]. Blood vessels can attribute most of their mechanical properties to their makeup of collagen and elastin fibers, ground substances, and smooth muscle cells. Alan Burton and his colleagues were the first group to make the connection between the microstructure of the vessel and its resulting macroscopic mechanical properties[23]. Using the differential digestion of elastin and collagen in the arteries, they were able to measure the corresponding variations in the mechanical properties of the wall. Their finding resulted in the formation of a theoretical analysis of the arterial wall that spawned a number of notable studies expanding on the subject[23,24].

Young's modulus or elastic modulus is determined as the slope of the linear portion of a uniaxial stress strain curve[25]. Elastic modulus of AAA could provide parameters for analysis of AAA wall stress distribution and predicting rupture of AAA[22].

The Blood Pressure and Its Effect on the Aortic Wall

When studying the arterial pressure in the aorta, the aorta can be compared to an inflated tube-like construction[26]. This pressure can be translated directly to tension based mechanical stress on the wall, with the circumferential and axial stresses acting as the major stresses (See Figure 2). During inflation, the wall undergoes an isochoric deformation, where tissue volume is constant, leading to weakening of the wall in the circumferential and axial directions.

As a rule, as the aortic diameter increases, the wall becomes proportionally thicker. Medial lamellar units (MLU) increase with wall thickness. Thus, each MLU carries a tension of about 2 ± 0.4 N/m, and it's been shown that substantial decrease in wall thickness and the number of MLU's happens during aneurysmal changes[27,28].

Stiffness is the slope of the load-deformation curve[29]. Aorta stiffness increases with strain which means that at hypertensive loading the aorta will be stiffer than during normal arterial pressure[27,30]. When stiffness of aneurysmal and healthy vessel was compared, result showed that aneurysmal section were stiffer than the healthy section with less collagen and elastin content[21].

Stiffness of the artery depends on its intrinsic elasticity. Pulse wave velocity (PWV) is a direct measure of large arterial stiffness[31]. Circumferential cyclic Green-Lagrange is another method of measuring arterial stiffness[32]. PWV and circumferential

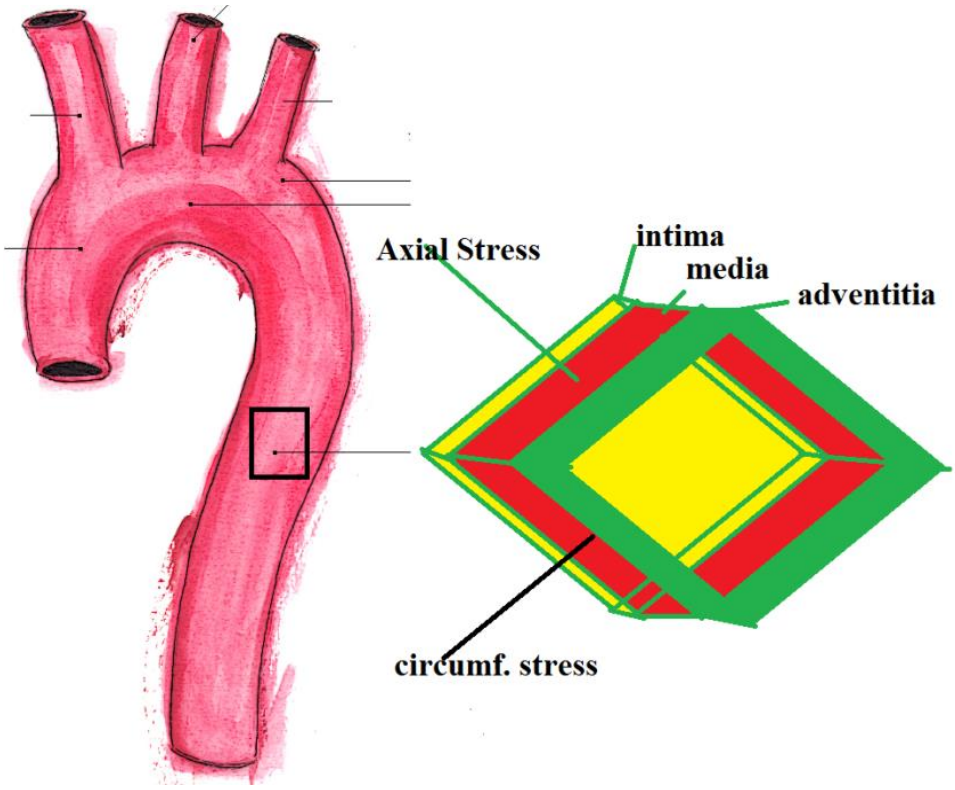

Figure 2. Different types of stress in aortic wall.

cyclic Green-Lagrange strain use ultrasound and offer a noninvasive assessment of stiffness along an arterial section[33].

Structure of Aortic Elastin

Making up roughly 50% of the arterial ECM, elastin is the most prevalent structural protein of the arteries[34]. Elastin is made up of elastic fibers that have two major components, one amorphous and one fibrillar. The extensively cross-linked elastin of the amorphous component comprises 90% of the fiber. The fibrillar component, is a collection of microfibrils, that are rich in acidic glycoproteins and is about 8-16 nm long[35].

Amorphous elastin forms from monomers of soluble tropoelastin. Tropoelastin arises during prenatal development when elastogenic cells including smooth muscle cells (SMCs), endothelial cell, fibroblasts and chondroblasts express the elastin gene[36]. Humans only contain one tropoelastin gene, ELN. As we age, ELN expression decreases dramatically as elastin production decreases. In middle-aged people, elastin production is almost non-existent, so we must rely on the elastin deposition that occurs in the womb and early in life[37]. In order to make elastin, tropoelastin molecules must interact and then crosslink, forming insoluble elastin. Fibrillin-1 largely makes up microfibrils in ECM that likely anchor the forming elastic fibers[38]. Lysyl oxidases are a group of five enzymes including LOX, and LOXL 1-4, which cross-link tropoelastin and aid the process[39].

Initially, tropoelastin is expressed then secreted into the ECM. In a closer look, the mature tropoelastin begins to accumulate on the surface on the cell to create 1 micron spherules. This accumulation of tropoelastin aids coacervation of tropoelastin molecules. Eventually, the tropoelastin is oxidized by the lysyl oxidase enzymes and then participate in aldol condensation and Schiff base reactions to crosslink elastic fibers. The microfibrils that exist in the ECM are transported to where the new elastin is being formed, by members of the fibulin protein family. The elastin produced as the final product is very stable and able to give human tissue the ability to stretch and recoil[40] (See Figure 3).

Elastin binding protein (EBP), made of a 67-kDa peripheral subunit attached to two membrane bound proteins of 61 and 55 kDa, is the mechanism that specifically targets

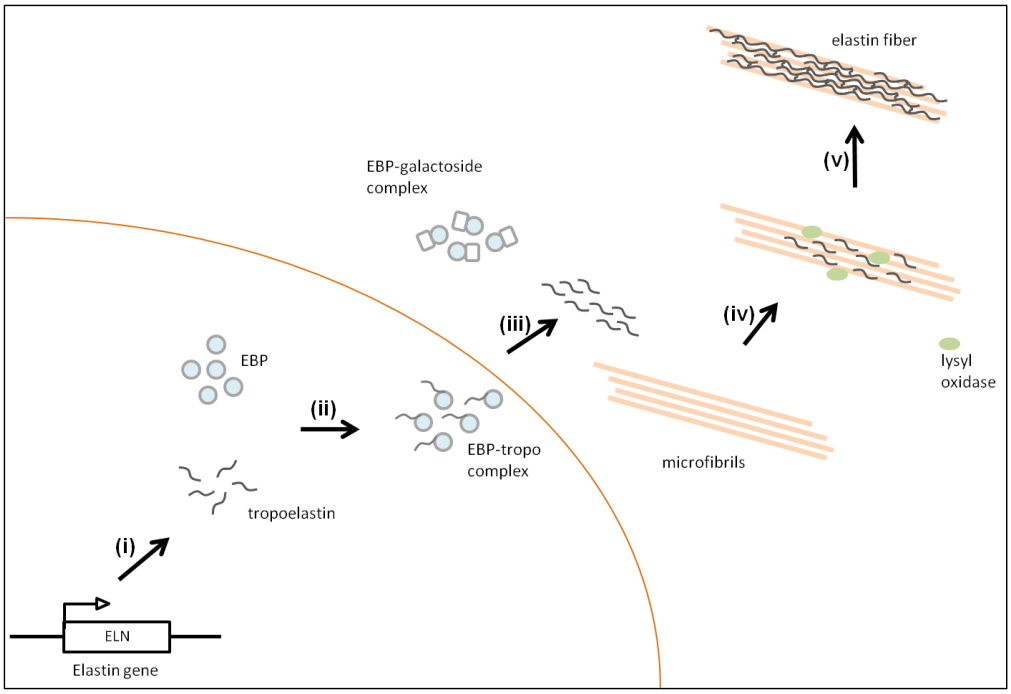

Figure 3. Elastin assembly[40].

tropoelastin molecules to fibre formation sites on the surface of cells. Initially, tropoelastin binds to an EBP complex that is intact. The 67-kDa subunit loses its affinity for tropoelastin and the membrane bound protein when a sugar moiety binds to the EBP. The loss of affinity lease to tropoelastin being released onto growing elastic fibers [35].

Smooth muscles cells (SMCs) and fetal lung fibroblasts go through a different process of binding to tropoelastin. SMCs, much like chondrocytes, use heparin sulfate chains through proteoglycans on the cells surface to bind to the tropoelastin. In the fetal lung, fibroblast, use heparan sulfate moiety and integrin αvβ3 receptors[41].

Vascular Diseases

Vascular disease may result from any circulatory system disorder. It includes Peripheral Artery Disease, Aneurysms, Renal (Kidney) Artery Disease, Buerger's Disease, Peripheral Venous Disease and etc.[42] Vascular disease is a subgroup of cardiovascular disease (CVD). CVD, often brought on by risk factors such as high blood pressure, high LDL cholesterol, and smoking, is the primary cause of death in the United States. At least one of these risk factors is present in nearly half (49%) of Americans[43]. Other lifestyle choices and medical conditions, namely diabetes, excessive weight, poor diet, lack of physical activity[44], and overuse of alcohol, can increase the risk of heart disease[25]. The prevalence of heart disease across the United States is shown in Figure 4.

Abdominal Aortic Aneurysm (AAA)

Weakening and resulting focal bulging of the abdominal aorta are known as abdominal aortic aneurysms (AAAs)[46]. The AAA disease is diagnosed when the minimum diameter between the anterior and posterior walls of the aorta is 3.0 cm[47]. Much like other cardiovascular diseases, AAAs occur more frequently in males and often dependent of risk factors including advanced age, tobacco use, and family history. American College of Cardiology/American Heart Association (ACC/AHA) guidelines list the occurrence of AAAs between 2.9 and 4.9 cm in diameter as 1.3% for 45-54 year old men and 12.5% for 75-84 year old men[48]. While there is limited data on the mechanical strength of the human aorta, experts concur that an

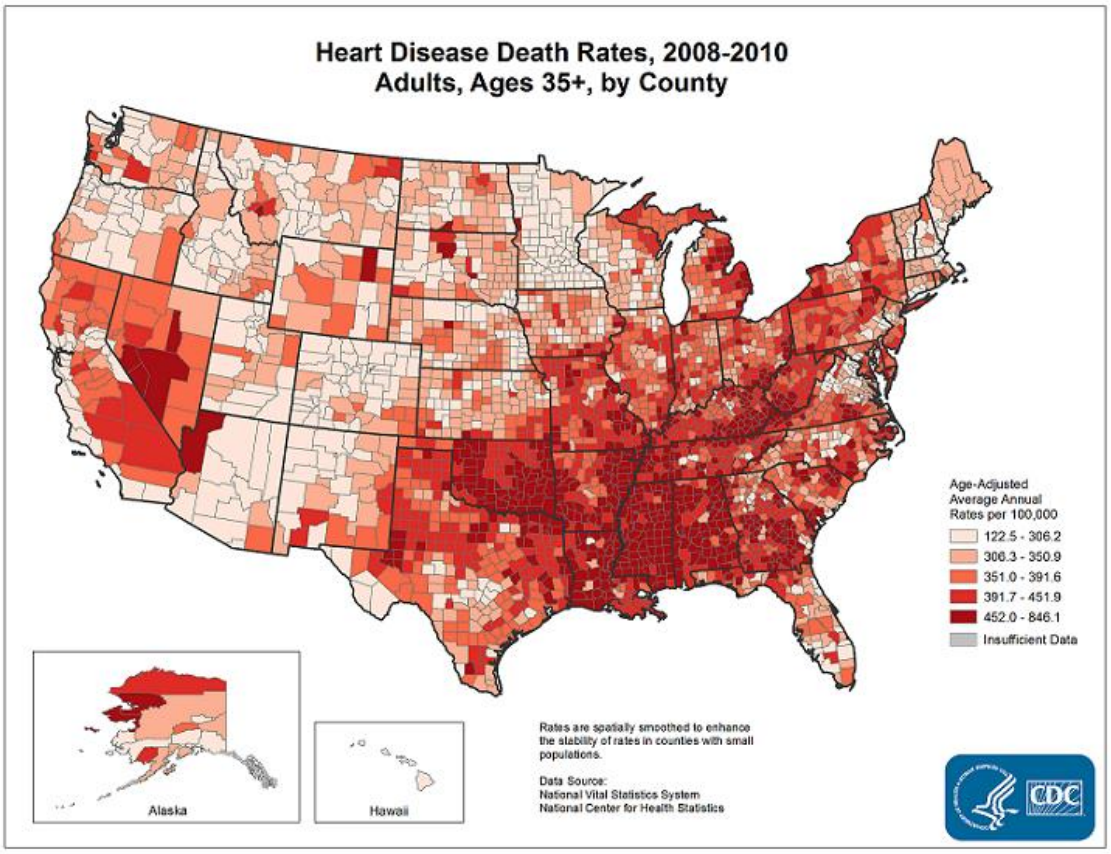

Figure 4. Heart disease rate of death across the US[45].

aneurysmal aorta is mechanically weaker than healthy aorta, both longitudinally and circumferentially, and the resulting weakness is the main cause of rupture[49,50].

Risk of Rupture

Randomized studies comparing immediate repair and monitoring of small AAAs largely comprise the general theory of AAA progression and risk of rupture. The results show that the yearly risk of rupture is less than or equal to 1% for those AAAs with a diameter below 5.5cm, but it increases with the size of the aneurysm. For individuals that have an AAA greater than 6 cm, it jumps to 10% and then to over 25% for people with

one lager than 8 cm. The risk of rupture also increases for smokers, women, people with poor lung function, and higher mean arterial blood pressure[51].

Treatment Recommendations

Early stage AAA has no major symptoms thus it makes the threat of rupture that much more serious [52]. A treatment plan has to take into consideration both the disease progression, risk of rupture, and patient life expectation as well as the mortality potential that comes with attempted prophylactic surgery. The guidelines currently set in place by the ACC/AHA state patients with AAAs between 4.0 and 5.4 cm are to be checked by ultrasound or CT scans, while patients with AAAs larger than 5.5 cm should have the risk of rupture eliminated through surgery[53]. Furthermore, asymptomatic male patients with an AAA less than 5.0 cm and asymptomatic female patients with an AAA below 4.5 cm should not undergo interventional repair techniques, but repair can be beneficial on an AAA between 5.0-5.4 cm[6].

EVAR vs. Open Surgery

The most common and effective methods for repairing abdominal aortic aneurysms are abdominal endovascular aneurysm repair (EVAR) and the more traditional open surgery (shown in Figure 5). EVAR involves a small incision in the groin that allows the placement of a stent graft in the aneurysm, whereas open surgery involves a synthetic graft being placed in the walls of the aneurysm[54]. Comparing EVAR with open repair in cases that were a good fit for open repair showed that thirty days mortality was

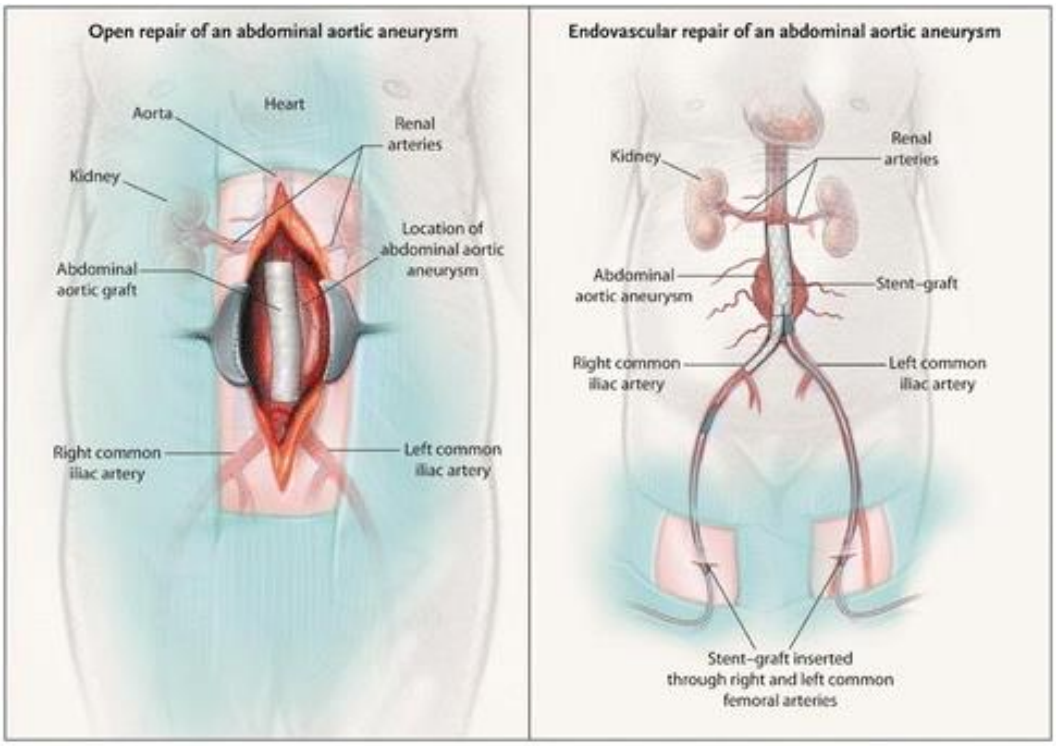

Figure 5. Open Repair vs EVAR[57].

1.6 % for EVAR and 4.7 % for open repair of AAA. Given the 30 days post-surgery outcome, this may help both surgeon and patient in choosing treatment options[6,55,56].

Mortality of Ruptured AAA (rAAA)

In a study in a specific geographical area, the mortality rate for rAAAs was assessed and found to be 6.3/100,000 inhabitants for the annual incidence. In one the clinical studies[58], about 37% or 82 out of 221 patients did not make it to the hospital before they died. Of those patients who were admitted, 79.8% went through immediate surgery. For the entire hospital, the mortality rate was 63.3%, while the cumulative mortality was 76.9% when non-admitted cases were included.

Animal Models for AAA

In any animal model, the goal is to model human disease pathology as closely as possible, in order to effectively evaluate the mechanisms that occur in humans. For aneurysms, currently no exact model exists, and so conclusions are drawn based on assumptions the biochemical and cellular mechanisms that occur in the animals are comparable to those in humans. Of course, each different experimental model of AAA has its own pros and cons. Most techniques of physical, chemical, and genetic manipulations on healthy vasculature have been used on almost every typically tested species. Table 1 shows the advantages and disadvantages of animal species for AAA research.

Surgically Induced Aneurysms

Blunt trauma and/or crush injuries to the arterial wall are two of the most common ways to create the mechanical weakness necessary to induce an experimental AAA[60]. Artificially reducing the arterial diameter in certain locations can create the turbulence and shear stress that result in enough dilation to cause an aneurysm. An aneurysm phenotype can also be created through the implantation of arterial tissues from a foreign species[61]. The resulting immune rejection requires about four weeks to progress until it is deemed to effectively mirror an aneurysm. Each of these techniques of creating aneurysms achieves the desired purpose at the cellular level which trauma to the arterial wall and a strong immune response. This is characterized microscopically by a congregation of T-cells, B cells, and macrophages and a loss of both extracellular and medial cellular components, which is also seen in human aneurysms[59].

Table 1. Advantages and disadvantages of animal species for AAA research[59].

Animal	Species advantages	Species disadvantages
Mouse	• Fairly low costs • Well-characterized genome facilitates genetic manipulation	• Very small aorta • Genetically manipulated models can be expensive
Rat	• Fairly low costs • Larger size of vessels compared to mice	• Genetic manipulation is difficult
Swine	• Similar arterial morphology to humans	• Variable aneurysm formation following elastase perfusion
Rabbit	• Relatively low costs	• Poor public perception of studies based in rabbit species
Canine	• Large peripheral arteries • Able to survive prolonged anesthesia	• High cost • Poor public perception of studies based in canine species
Sheep	• Large arteries	• High cost
Turkey	• Form spontaneous aneurysms	• N/A

Chemically Induced Aneurysms

According to initial clinical research, elastolysis of the aortic media was a major player in pathophysiological beginning of a human AAA, and elastase was at the center of the destruction occurring the elastic tissue of the aortic wall[62]. Atherosclerosis, the hardening of the elastic wall, also showed similar patterns of calcification and fragmentation of elastic tissue that appeared in AAAs[63]. Therefore, the administration of chemical solutions of elastase and calcium chloride to the infrarenal aorta is the most well established practice for generating aneurysms in most animal species[59].

Elastase-Induced Aneurysms

In the 1960s, transient intraluminal perfusion with pancreatic elastase into the abdominal aorta was first documented as a technique to induce experimental AAAs[64]. The use of temporal analysis to compare aneurysm progression in humans to that in rats

that have undergone elastase infusion has found a number of similarities. Notably, this analysis has demonstrated that the medial elastic tissue destruction is increased due to inflammatory response created by aortic dilation, while the rate of aneurysm formation post-aortic elastase treatment is not correlated [59].

Calcium Chloride-Induced Aneurysms

Calcification is closely associated with aneurysms, and heavy calcification is seen in about 80% of human AAAs[65]. Knowing the commonality of calcification in AAAs, in 1988 Gertz et. al.,[66] conducted a pioneering study on male New Zealand rabbits, determining that the application of $CaCl_2$ to the adventitia of the carotid artery resulted in the formation of an aneurysm. In the study, the researchers immersed the entire adventitial surface of the right common carotid artery in a 0.5M $CaCl_2$ solution for 15 min. After three weeks, the luminal diameter of the treated arterial segment had increased by an average of 61% as compared to the opposite carotid artery which was treated with sodium chloride (NaCl) instead. A histological examination using scanning electron microscopy (SEM) revealed endothelial cell fragmentation where the calcium chloride was administered, as well as, elastin calcification, loss of vascular smooth muscle cells, and a strong immune response characterized by the presence of neutrophils, monocytes, foreign body giant cells, and lymphocytes. This study was the first recorded model of a human aneurysm[67]. Other studies have tried to recreate the model with variable conditions including Freestone et al. They used a 0.25 M v solution instead, but even 12 weeks after surgery there was no AAA formation. A second attempt was made using a 0.05M thioglycollate and $CaCl_2$ solution in addition to a high cholesterol diet, and

AAA formation was seen in just three weeks[68]. This model was successful in both rabbits and rodents. Another technique applying a 13.6 mEq/10 mL $CaCl_2$ solution applied to abdominal aorta of C57BL/6 mice resulted in AAA formation, degradation of elastin, reduction of VSMC, and lymphocyte and macrophage infiltration[69]. $CaCl_2$ has been documented to increase endothelial permeability and induce VSMC apoptosis when applied to vasculature, as well as causing the infiltration of the adventitia and media of the aorta by inflammatory cells[70,71]. These documented animal models have been shown to closely mirror human AAAs in terms of their pathology due to aortic calcification, increased presence of inflammatory cells, degradation of elastin, neovascularization, oxidative stress, and VSMC apoptosis. The main issue with the $CaCl_2$ AAA model is that it does not result in intraluminal thrombus and rupture as is seen in human AAAs[67].

Genetically Manipulated Models of AAA

Sophisticated techniques of altering genes have allowed researchers to more specifically dissect the mechanisms that lead to pathogenic phenotypes, thus allowing researchers to obtain a better idea of therapeutic targets. Genetically modified organisms (GMOs) are growing in number and complexity as techniques are being improved and expanded, allowing medical researchers to apply their knowledge of GMOs to their research. An example of this is the process of creating "gene knockout mice", which are genetically deficient due to the targeted disruption of one or more alleles. These mice are gaining an integral role in research regarding the pathophysiology of vascular diseases. Only a few have been used in AAA research at this point, but their presence will likely

increase. Below the specific relevance of gene knockout mice to human AAA research will be discussed.[59].

Angiotensin II and Hyperlipidemic Mice

Aortic aneurysms in mice have been created by infusing octapeptide angiotensin-II (ang-II) subcutaneously. When the ang-II is delivered to hyperlipidemic strains of mice, typically deficient in apolipoprotein E (Apo E−/−) or in low-density lipoprotein receptor (LDLR−/−), the mice's pre-existing disposition to aneurysms is inflamed, resulting in small aneurysm formation. While this model successfully creates atherosclerotic plaque similar to that seen in human AAAs, the AAAs in mice occur sporadically and occasionally supra-renally, which does not occur in humans[72-74].

Pharmacological Management of Small Abdominal Aneurysm

Even though AAA has high rates of mortality and morbidity, ranking in the top fifteen of most recurrent causes of death in men over 55 in western societies[75], little is known about the cause and development of AAA. Non-invasive observational imaging such as ultrasound, computerized tomography(CT), scans, or magnetic resonance imaging (MRI), combined with angiography[76] is used to make a diagnosis. Images revealing an abdominal aorta with a diameter of 3 cm and above typically indicate the formation of an aneurysm. Currently, surgical techniques including conventional and endovascular repair on AAAs are used in high rupture risk patients, defined as those with an AAA with a diameter of 5.5 cm or greater, and have been deemed effective treatment methods. Unfortunately, that is about the extent of treatment for AAA patients, leaving

those with smaller aneurysms, less than 5.5 cm, without an effective treatment. They are generally recommended to wait until the aneurysm grows to the size where an operation is deemed worth the risk, anxiously waiting as their condition worsens[77].

While what causes the degeneration of aneurysms may not be not known, it is established that AAAs are connected with chronic transmural inflammation[78] and the breakdown and elimination of essential proteins in the connective tissue of the outer aortic wall. Simply, three steps can summarize the progression of AAAs (See Figure 6). First, the vascular wall begins to increase production of substances that trigger inflammation, although these specific substances are not well known. Next, infiltrating cells release molecular mediators. Finally comes the release of metalloproteinases and their respective inhibitors, controlled by the inflammatory agents and infiltrated cells from the earlier steps. Activated macrophages are responsible for producing of the MMPs, specifically of MMP-9 and MMP-2, that are not counter-balanced by the activity of their inhibitors (TIMPs)[79]. This imbalance is primarily responsible for degradation of collagen and elastin, which are integral part of the ECM. The destruction of the collagen and elastin interferes with the ordered lamellar structure in the tunica media of the aorta, leading to the formation of the aneurysm[80]. When examining human AAA tissue, an excessive presence of inflammatory infiltrates containing both lymphocytes and macrophages have been discovered in both the media and the adventitia, validating the

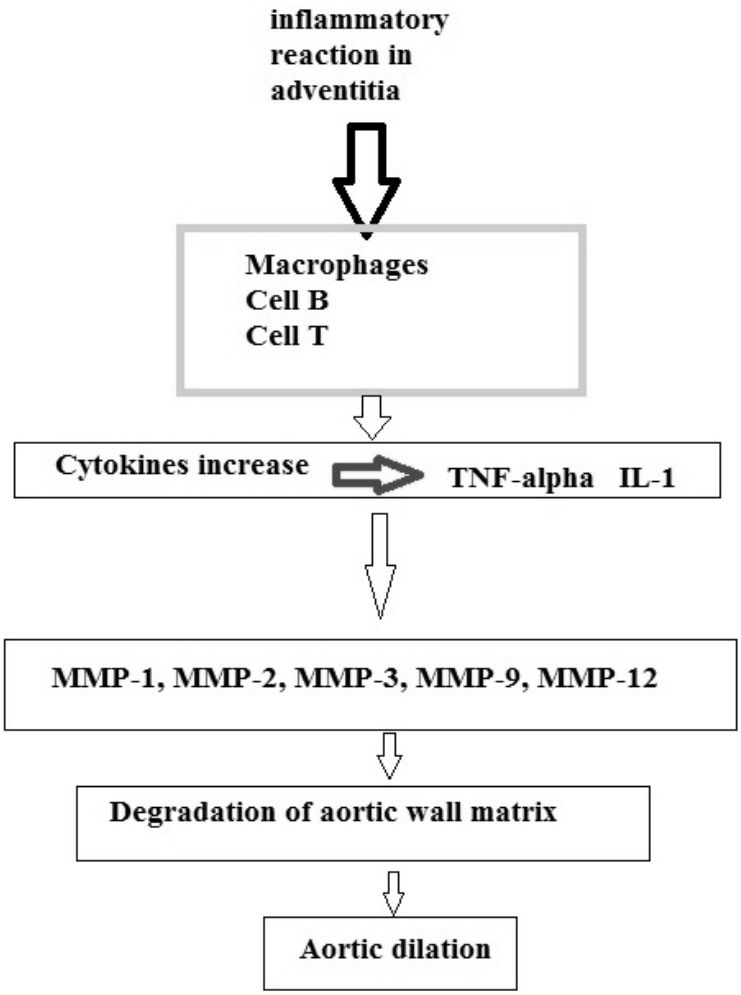

Figure 6. Flow chart showing progression of molecular mediators during formation of abdominal aortic aneurysm[76].

above theory. Additionally, a correlation between increasing aneurysm diameter and higher density of inflammatory cells in the adventitia has been confirmed[81].

The main goal of current research related to AAAs is to find new treatments that prevent the expansion of small aneurysms. At this time, majority of research in this field is concentrated on the third step of formation, trying to either decrease the presence of metalloproteinases or prevent their activities (See Figure 7). Some drugs including

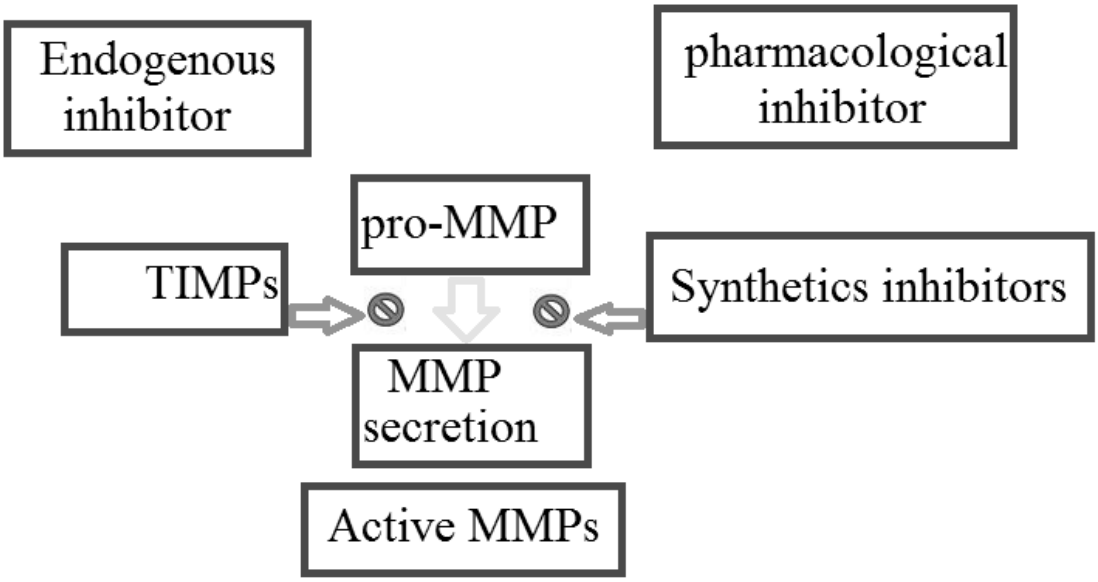

Figure 7. Preventing MMPs activation as a therapy for AAA.

doxycyclines, statins, and synthetic MMP inhibitors have shown potential and are undergoing testing.

New Medications for AAA Treatment

Doxycycline

Tetracyclines were discovered in 1948, as a product of the fermentation of *Streptomyces aureofaciens*[82]. Based on their origin, they can be classified into one of three different groups, either natural products, semi-synthetic compounds, or chemically modified tetracyclines[83]. Besides being powerful antibiotics, tetracyclines are known to inhibit MMPs and aid in T-lymphocyte transmigration by preventing chemotaxis and the mass movement of neutrophils. Additionally, doxycycline specifically targets endothelial cells where it inhibits MMP synthesis. By doing this, doxycycline is capable of

decreasing both protein and mRNA levels which in turn alters endothelial migration that occurs during angiogenesis[76].

Statins

Statins, which are widely used to lower lipid levels, are specifically hydroxymethylglutamyl-coenzyme A (HMG-CoA) reductase inhibitors[84]. Statins have also been demonstrated to prevent atherosclerosis progression for reasons unrelated to the benefits of lower lipid levels, which are known as "pleiotropic statins effects". Specifically, these pleiotropic statins' effects may include anti-oxidant effects, anti-inflammatory effects, and reduction of MMP secretion, which have been shown to prevent AAA development in a number of studies[85]. For example, three separate types of statins, pravastatin, simvastatin, and fluvastatin, have been shown to reduce MMP-9 production in the AAA and its infiltrated cells[86]. Further studies on simvastatin have shown it to increase TIMP-1 production although it had no effect on the infiltration of inflammatory cells into the AAA[87]. Atorvastatin, on the other hand was effective in suppressing the recruitment of macrophages directly by MMP-12 inhibition, primarily by inhibition of the expression of intercellular adhesion molecule-1 within the vascular wall[88]. Despite these positive results, it should be noted that in some human studies there has been no noticeable effects on AAA growth by statins. Furthermore, no association has been found between AAA expansion and a statin-based treatment or serum low-density lipoprotein (LDL) concentration. However, these studies are contrasted by other studies in which statins did show an ability to reduce or delay AAA expansion in humans. One of these studies conducted by Feeney et. al,[89] reported that pre-hospital statin use resulted

in a significant survival benefit in patients with a ruptured AAA. A separate observational study of 130 patients that were monitored for 2 years found that there was no expansion of aneurysms in the 75 patients that were administered statins[90]. A few other studies have also show similar benefits for statins, suggesting that there is a decrease in aneurysm expansion rate for patients being treated with statins as opposed to those who were not[91]. Further investigation about statins has revealed important information about the molecular pathways through which statins can inhibit the growth of AAAs. Pravastatin was particularly ineffective in this setting; however, it was effective in increasing TIMP-1 content. This shows that increased TIMP-1 expression is unrelated to HMG-CoA inhibition, and its benefits are not limited by MMP-9 inhibition[92]. Another suspicion of the benefits of pravastatin is that it may be involved in preventing apoptosis, often elevated in AAAs, because pravastatin has been shown to increase the expression of Bax, a proto-oncogene known to induce apoptosis, but not the expression of Bcl-2, a proto-oncogene that reduces apoptosis. When analyzing the ratio of Bax/Bcl-2, an important index of apoptosis, it was unchanged, rendering any conclusions about pravastatin affecting apoptosis in AAAs invalid[93]. Based on this, it can be hypothesized that TIMP-1 influences other factors that prevent AAA progression, such as growth factor-like activity, anti-inflammatory activity, and aortic smooth muscle cell proliferation. Although the specific molecular mechanism used by statins has yet to be determined, statins may still function to control AAA growth. Studies evidencing the usefulness of statins' pleiotropic effects in reducing aneurysmal wall inflammation,

diminishing MMP expression, and enhancing TIMP synthesis show potential for their ability to prevent AAA growth[76].

Synthetic Inhibitors of MMPs

MMPs known formally as matrix metalloproteinases are a group of endopeptidases that contain zinc and are calcium dependent[94]. They function to remodel tissue, by degrading parts of the ECM such as elastins, collagens, proteoglycans, and matrix glycoproteins. Hormones, growth factors, and cytokines are able to regulate MMPs[95]. Most commonly, MMPs are produced via excretion from a number of pro-inflammatory cells like macrophages, neutrophils, and lymphocytes and connective tissues cells such as fibroblasts, osteoblasts, and endothelial cells[73]. The zymogens that these enzymes are expressed as are processed further to reach active form by other proteolytic enzymes including plasmin, furin, serine proteases, and others[96]. Currently, there are 26 known human MMPs (See Figure 8) that can be categorized into 4 groups: collagenases, gelatinases, stromelysins, and matrilysins[97]. There is a further subclass known as membrane-type MMPs (MT-MMPs), which either have an intracellular and transmembrane domain, a membrane linker domain, or are membrane associated. They also have an extra transmembrane domain to anchor them to the surface of the cell. The remainder of the MMPs has a distinct domain, either a hinge region, a catalytic domain, an N-terminal domain, or a C-terminal hemopexin-like domain. The membrane is important for macromolecular substrate recognition and TIMP interaction[94,98].

No.	MMP No.	Class	Enzyme
1	MMP-1	Collagenases	Collagenase-1
2	MMP-8		Neutrophil collagenase
3	MMP-13		Collagenase-3
4	MMP-18		Collagenase-4
5	MMP-2	Gelatinases	Gelatinase-A
6	MMP-9		Gelatinases-B
7	MMP-3	Stromelysins	Stromelysin-1
8	MMP-10		Stromelysin-2
9	MMP-11		Stromelysin-3
10	MMP-27		Homology to stromelysin-2 (51.6%)
11	MMP-7	Matrilysins	Matrilysin (PUMP)
12	MMP-26		Matrilysin-2
13	MMP-14	MT-MMP (membrane type)	MT1-MMP
14	MMP-15		MT2-MMP
15	MMP-16		MT3-MMP
16	MMP-17		MT4-MMP
17	MMP-24		MT5-MMP
18	MMP-25		MT6-MMP
19	MMP-12	Other enzymes	Macrophage metalloelastase
20	MMP-19		RASI 1
21	MMP-20		Enamelysin
22	MMP-21		MMP identified on chromosome 1
23	MMP-22		MMP identified on chromosome 1
24	MMP-23		From human ovary cDNA
25	MMP-28		Epilysin
26	MMP-29		Unnamed

Figure 8. Matrix metalloproteinase enzymes[94].

Mechanism of Action

The majority of matrix metalloproteinase inhibitors act as chelating agents, meaning they block activity by binding to the zinc at the active center of the enzyme[99].

Synthetic MMP inhibitors have been created primarily through the use of a peptide sequence that the targeted protease can recognize. This peptide sequence has also had a number of chemical functionalities attached that allow it to react with the zinc ion at the active site inhibiting the enzyme. There are a few key requirements for a molecule to function properly as an MMP inhibitor, including, an attached functional group that can chelate the zinc (II) ion of the active site, a functional group with a hydrogen bond that can bind with the backbone of the enzyme, and at least one side chain capable of van der Waals interactions on the subsites of the enzyme[100]. Functional groups capable of chelating the zinc ion would include hydroxamate (CONH–O), carboxylate (COO), and thiolate (S), among others. Using methods including structure-based design and combinatorial chemistry, a number of different structural classes of MMP inhibitors have been discovered. Current MMP inhibitors in use include marimastat, trocaid, CGS-27023A, prinomastat, AG3340, BAY 12-9566, Ro 32-3555[94].

Pioneering Hydroxamate Structures

Hydroxamate-based MMP inhibitors are much like their name, inhibitors that use a hydroxamate (=CONHOH) group to bind to the zinc[101]. Two of these inhibitors, Ilomastat and Batimastat (BB-94) were the first to undergo patient testing.

Batimastat (Figure 9), is a broad-spectrum MMP inhibitor and more commonly referred as BB-94, has been effective in inhibiting inflammatory responses in rats, decreasing the aneurysm expansion[103].

BB-94 has been shown to decrease inflammatory response to aneurysms, in addition to acting as a metalloproteinase inhibitor[103]; unfortunately, due to a lack of bioavailability it is limited for long term use. A second generation of these, Marimastat, is used orally in cancer treatment but 30% of patients had musculoskeletal side effects. Most studies on Marimastat have examined intimal hyperplasia and aneurysms in human ex vivo tissue[104]. While initially promising, these drugs have shown few therapeutic benefits in humans and have thus been overlooked for their potential to treat other conditions.

Typically, hydroxamate-based MMP inhibitors tested in *in vitro* tumors cells have shown exceptional anticancer behavior however, when tested clinically, they did not perform adequately. This could be explained at least in part because these broad-spectrum inhibitors work on other metalloproteinases unrelated to pathology like disintegrin and metalloproteinase (ADAMs) proteases. Testing on patients has shown these have caused muscular and skeletal pain in multiple patients, which seems to be related to the dosage level[105,106]. However, if the MMP inhibitors had their structures altered to create a specificity of targets to cut down on toxicity, they would likely have shown the clinical cancer chemotherapy benefits that were initially expected[107].

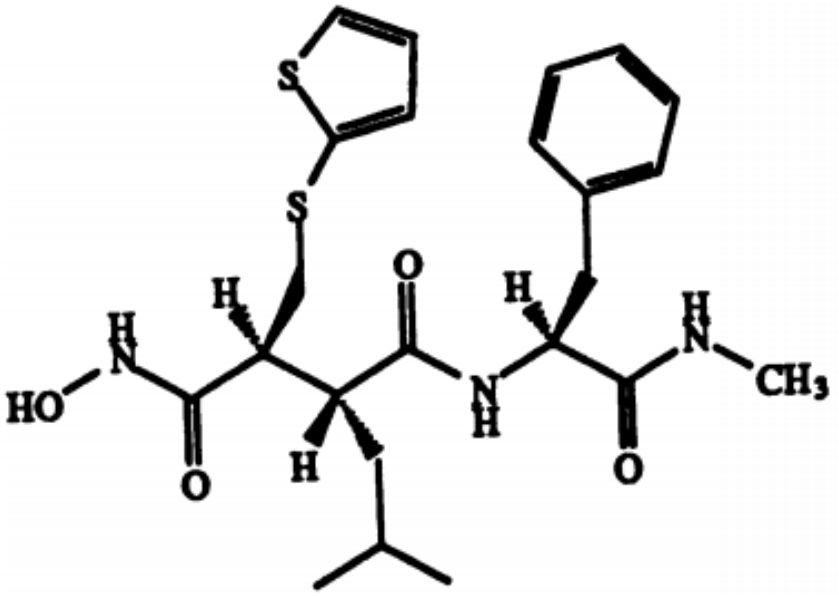

Figure 9. Batimastat structure[102].

New Generation Hydroxamate-Based MMP Inhibitors

MMI-270 (See Figure 10) is likely the single most important structure from earlier generations that has carried over. The molecule allows for a number of key benefits including water solubility, oral availability, and low molecular mass in a broad spectrum inhibitor. However, they do have a noticeable limitation of drug metabolism. The metabolism issues stems from amide reduction resulting in the loss of the hydroxamate zinc-binding group, leading to hydrolysis to the carboxylate, then conjugation to glucuronide[107].

Angiotensin Converting Enzyme Inhibitors (ACEI)
and Angiotensin Receptor Blockers

Blood pressure is another factor that is important to consider when examining AAA and ACEIs are a type of drug used for regulation of blood pressure. While the

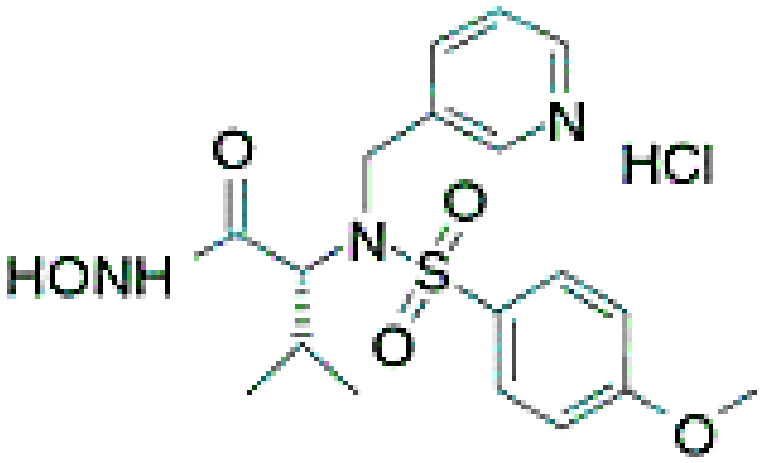

Figure 10. MMI270 (CGS27023A) structure[108].

mechanisms of action of ACEIs are not known, they do affect aneurysm progression according to several studies. Treating experimental animals with Angiotensin-II has been shown to decrease elastin content in the AAA and aortic wall[109]. Additionally, collagen production in the vascular wall increases and arterial wall size decreases in established AAA patients when they are given ACEIs[110]. Furthermore, research by Liao et. al, has shown that by using different ACEIs, elastin decreases could be controlled independently of arterial blood pressure lowering while preventing changes in inflammation of aortic wall[111]. Another study conducted by Alsac et. al., testing an ACEI, perindopril, demonstrated its ability to reduce aneurysm growth through both the inhibition of MMP synthesis and changing elastin levels [112]. ACEI treatments have also been shown to limit aneurysm ruptures compared to no treatment in clinical trials, which other blood pressure lowering drugs including beta-blockers, calcium channel blockers, antagonists of angiotensin-II receptors, and diuretics have been unable to do[113]. Unfortunately, studies have also seen detrimental effects of ACEI in regards to AAA growth. One such study

from the UK on 1700 patients actually found that the aneurysm growth rate was higher in patients who had the ACEI treatment than those that did not[114]. Due to these findings, it is clear that there is a need for more randomized studies in order to understand the true nature of ACEIs and what their actual therapeutic benefits are.

As mentioned above, angiotensin II-receptor antagonists (ARBs) are blood pressure lowering drugs, but they also have been tested for their potential of preventing AAA growth[115]. Using an experimental model in which apolipoprotein deficient mice were subjected to the chronic release of angiotensin II until their aortas dilated and eventually ruptured, researchers found that the administration of losartan was able to prevent aneurysm formation. Further, they found when transforming growth factor-B was antagonized by losartan, progressive matrix degradation was prevented. With these promising results, the need for more studies, clinical especially, to determine their ability to prevent AAA growth is obvious[116].

Natural Substances

Some natural substances have been used to treat AAA. Vitamin E improved AAAs and reduced the combined end point of fatal+nonfatal aortic rupture in Ang II animal model[117]. Periadventitial administration of PGG(a polyphenol) delays the development of AAA in a calcium chloride injury rat model[14].

Polyphenols

Polyphenols are a large and varied family of natural substances. They exist as simple molecules or complex structures, but they all have at least one benzenic cycle with

one or more hydroxyl function and are derived from the metabolism of either polyacetate or shikimic acid. They are present in all vascular plants and are secondary metabolites.

Currently, thousands of polyphenolic compounds have been studied in plants and they been grouped into classes. These classes are broken down based on the variations in the basic chemical makeup that lead to differences in the methylation, oxidation, hydroxylation, and glycosylation, as well as their links to other secondary metabolites or primary metabolites such as carbohydrates, proteins, and lipids[118]. Polyphenols consist of a hydrophobic core surrounded by phenolic (-OH) groups on the exterior of the compound. This structure allows them to be broken down into condensed, complex or hydrolysable varieties. They can also be divided into ligands, flavonoids, phenolic acids, and stilbenes based on the number of phenolic rings and their accompanying structural elements[119]. To create hydrolysable tannins, gallic acid (3, 4, 5-trihydroxyl benzoic acid) must be esterified to a core polyol. If a more complex hydrolysable tannin is desired, the galloyl groups can be either esterified or oxidatively crosslinked. Gallotannins, the simplest of the hydrolysable tannins, are merely polygalloyl esters of glucose, and pentagalloyl glucose (β-1,2,3,4,6-Pentagalloyl-O-D-Glucopyranose) is the most prototypical of these [117]. Pentagalloyl glucose (PGG) is comprised of five identical ester linkages which involve the core sugar's aliphatic hydroxyl groups (See Figure 11). PGG's alpha anomer is not common in nature, but PGG does have numerous isomers, as do the rest of gallotannins. All of these isomers have a molecular weight of 940 g/mol. What vary based on the different structures of the isomers are the biochemical properties, specifically the ability to precipitate proteins, susceptibility to hydrolysis, and

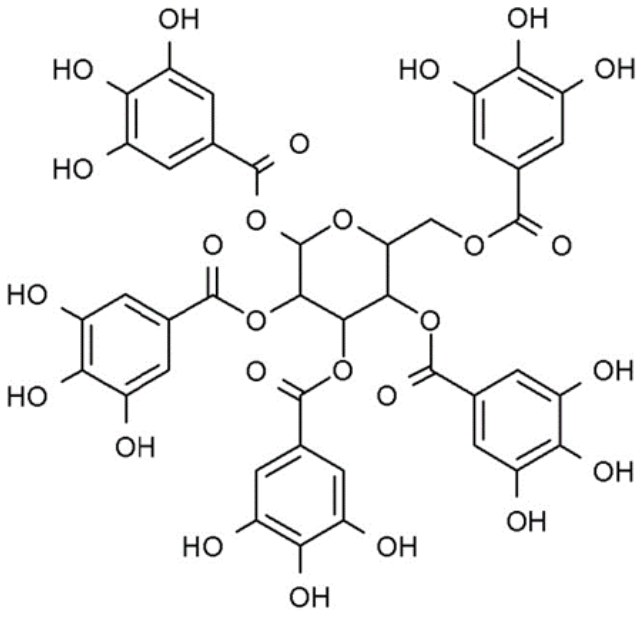

Figure 11. PGG structure[120].

chromatographic behavior. While PGG is best known for its anti-oxidant properties, its elasto-regenerative properties have been demonstrated both *in vivo* and *in vitro*[121-123].

Systemic delivery of the aforementioned drugs has failed to translate into significant clinical advances. Systemic toxicity and low concentration of drug delivered to the diseased area could possibly be the main reasons behind this failure. To address these issues we need a targeted drug delivery system. This offers an efficient drug loading in a biodegradable polymer with an increased circulation time *in vivo* to reach targeted sites and remaining at the site by specific chemical bonds and finally offering the release of the encapsulated drug in a controlled fashion. Such a delivery system also offers tailoring its physical and chemical properties to suit various needs[124].

Use of Nanoparticle Based Theranostic Agents in the Vascular Diseases

Nanotechnology that has the potential to fight cardiovascular diseases by making an immediate impact can be divided into four categories. First, tissue engineering using nanofibers can be used to rebuild damaged or lost tissue, for example allowing for the replacement of defective heart muscle[125] or blood vessels[126]. Second, molecular imaging paired with nanotechnology based agents can be used to identify, diagnose and track diseases[127]. Nano-based carriers can be used as targeted therapeutics which allow for precise treatments, limiting drug side effects and ensuring the injured area receives the drug. Finally, nanotechnology can be used to improve diagnostic devices, including implantable biosensors, allowing for better feedback and control as to what is occurring in the body. Targeted nano therapeutics in cardiology are especially helpful because injections of nano particles do not put the patient at risk of embolism formation, like the larger particles associated with intravenous delivery (IV)[128].

Targeted Drug Delivery

The ability to send drugs, using a nanocarrier to the site of injury as opposed to systemic or more generalized treatments, is currently the ultimate goal of pharmaceutical research[129]. Targeted drug delivery serves to maximize the benefits of a drug because of the localization of the therapeutic pharmacological activity to the specific tissue or organ in need. The encompassing idea of targeted drug delivery is to use various systems, physical, biological, molecular, in order to increase the concentration of the active agent at the site where it is needed. This would allow for reduced drug dosage while increasing

treatment efficacy and decreasing drug toxicity[130]. While drug delivery is excellent in theory, putting it into practice is much more challenging. In order to successfully execute targeted drug delivery, careful consideration must be made as to the metabolism and reactivity of the drug, as well as how the distribution and rate need to occur[131]. Other important concepts that need to be considered are nanocarrier biocompatibility, local blood flow, amount and distribution of drug receptors, interactions of nearby biological and cellular membranes with nanocarrier and the ability of enzymes to metabolize the nanocarrier[132 133].

Biological nanocarrier which are developed around the use of antibodies on surface, sound very effective theoretically; however, in practice, they encounter some issues centered around the antibody-polymer conjugate's distribution[134]. These issues include problems with the polymer carrier capacity of the antibodies conjugation sites and changes to the antibody's specificity based on the polymer molecules being conjugated. Thus far, the final issue has been the largest antagonist of achieving pharmacologically active concentrations at the desired local concentrations in the body[135].

Polymeric Particles

Polymeric particles are the most heavily researched organic nanoparticles because of their ability to hold many types of drugs, release them over an extended amount of time and ease of linking targeting ligands to the surfaces[136]. Polymeric particles are also very stable in both *in vitro* and *in vivo* settings. Additionally, polymers have long been used in medicine[137], including medical devices. Another advantage of polymers like poly-lactic acid (PLA), poly-glycolic acid (PGA) and poly-lactic-co-glycolic acid

(PLGA), their co-polymer, is their biodegradability, which is very desirable for delivery applications[138]. Poly-anhydrides and poly-orthoesters are also biodegradable, and been used for nanoparticle synthesis. When hydrophobic polymers such as the ones stated above are combined with hydrophilic polymers their co-polymers are effective in synthesizing carriers of drugs[139]. Poly-ethylene oxide (PEO), poly-propylene oxide (PPO), and poly-ethylene glycol (PEG) are all common copolymers used for this purpose. Another type of polymer used in drug delivery is responsive polymers, because they are able to react to temperature, pH, electromagnetic radiation, and other stimuli[140]. The benefit of enclosing drugs within nanoparticles is two-fold. First, the drug is protected from potential degradation by enzymes or hydrolysis, in both *in vivo* and *in vitro* conditions[141]. Secondly, the encapsulation allows for flexibility in delivery techniques, allowing for more patient friendly approaches such as oral administration of insulin using polymer-based nanoparticles[142]. Most types of substances, including RNA, DNA[143], proteins, and peptides[144], can be contained in these nanocarriers. Furthermore, these carriers can be used for either specific targeting or simple localized delivery[145]. When they are used as treatment for cancer, the particles are specifically designed to be small and hydrophilic increasing the time they remain in blood. Because of the enhanced permeability and retention (EPR) effect seen in tumors due to blood vessel leakage or limited lymphatic drainage, the nanoparticles accumulate within the tumor[146]. Mucosal surfaces are another common area in which localized release methods are used. Eyes, lungs, nose, the gastrointestinal tract, and others are the target of particles coated with a mucoadhesive polymer that extends contact time between the drug and surface and

stabilizes the drug during interactions with digestive enzymes. Active targeting typically functionalizes the surface of the nanoparticles using anything from receptor binding to peptides to antibodies and others in order to ensure delivery to the targeted tissue [147]. Human serum albumin nanoparticles created to allow for loperamide transport across the blood-brain barrier are a perfect example of this active targeting. The nanoparticles are attached to transferrin or monoclonal transferrin receptor antibodies so that they can reach the transferrin receptor in the brain[148]. In summation, all the developments in targeted drug delivery, specifically the advances in the use of nanoparticles, allow for better treatments and reduced systemic toxicity during treatments[149,150].

Bovine Serum Albumin (BSA) Nanoparticles

Albumin has long been the standard for modeling protein behavior in sustained release drug delivery systems because of its stability and commonality. This globular protein is also biodegradable, nontoxic, and non-antigenic, making it a great candidate for use in controlled drug delivery[151]. Abraxane®, an albumin-bound nanoparticle loaded with Paclitaxel, is a successful example of this, having been approved in 2006 to treat metastatic breast cancer by the Food and Drug Administration (FDA)[152]. Molecularly, albumin is made up of six subdomains and six sites for fatty acids to bind. Hydrophobic drugs, including curcumin, are also capable of binding to these fatty acid sites, offering protection from degradation and thus making them more bioavailable[153]. BSA particles usually use glutaraldehyde as a cross linker and are prepared by a process of coacervation or desolavation under mild conditions[149]. Because of the toxicity of glutaraldehyde, other

options for cross linking have been suggested and include polyethyleneimine (PEI), formaldehyde[154] and 1-ethyl-3-(3-dimethylaminopropyl) carbodiimide (EDC)[149].

Particle Size

Pharmaceutical nanoparticles, or nanocarriers, are essentially submicron sized particles that serve to hold and/or transport a drug. Based on their target or usage, they are between 10 and a few hundred nanometers and are either dry, solid particles or colloidal dispersions[155].

Particle size affects degradation, targeting, clearance and uptake mechanisms [156,157]. A reduction in particle size allows an improved dissolution rate and maximizes how much drug is available for absorption. Nanoparticles for drug delivery can be tailored to release their contents at an optimal rate by changing particle size[156].

Surface Modification

Surface modification to the nanocarrier allows for increased residence time in blood[158]. The particles are administered intravenously and do not dissolve immediately, an immune response (opsonization) to the blood proteins that are absorbed onto the particles' surface will occur[159]. The particles will then be quickly removed from circulation by the mononuclear phagocyte system (MPS) which will consume and dispose of the particles, eliminating therapeutic effects[160]. Opsonization can be staved off by either a non-covalent attachment of polymers or surfactants to the nanocarriers' surface, or molecular covalent attachments to the surface. Poly-ethylene glycol (PEG)[161] is the most commonly used particle to be grafted or adsorbed to the surface. When used

on bovine serum albumin (BSA) loaded poly(lactic-co-glycolic acid) (PLGA) nanoparticles, a steric PEG coating increased the half-life of the particles from 13.6 min to 4.5 hrs.[150].

Particle Charge (Zeta Potential)

While surface coatings like PEGylation can improve the efficacy of nanoparticles, changing the charge of the nanoparticle can have major effects as well[162]. Changing charge is well documented to alter protein adsorption and cellular internalization during circulation[163]. This is reflected in the fact that nanoparticles that are positively charged have higher rates of phagocytosis than neutral and negatively charged particles, decreasing their blood circulation half-life[150]. Another study determined that endosomes were more likely to escape due to surface charge. Those results were based on the behavior of negatively charged polystyrene nanoparticles that stayed in endosomal compartments of smooth muscle cells, not reaching the cytosol[164].

Targeting AAA

There have been a few studies that have successfully targeted AAA using diagnostic or therapeutic targeting. Small AAA can be diagnosed using a novel, noninvasive technique if nanoparticles can enhance visualization. Bonnard et al. managed to successfully target AAA via P-Selectin, expressed by activated platelets in AAA, by using microparticles functionalized by fucoidan. Two weeks after elastase perfusion, the microparticles, injected into rats via penis vein, were radiolabeled with 99mTc. Single photon emission computed tomography (SPECT) imaging was used to successfully

image AAA[165]. Another group proved that surface functionalization of doxycycline loaded PLGA nanoparticles with cationic amphiphiles can be useful in targeting AAA. These particles bind to elastin via hydrophobic interactions in cell culture of aneurysmal smooth muscle cells[166]. AAA was successfully targeted via anti-elastin decorated nanoparticles in different animal models of AAA. These nanoparticles could target damaged elastin but not healthy elastin[167].

CHAPTER III

KNOWLEDGE GAP AND SPECIFIC AIMS

Knowledge Gap

Up to 90% of detected AAAs are small enough that they do not require surgery. However, they are not treated because there are no current pharmacological treatments to prevent AAA expansion approved by the FDA. A safe treatment that could prevent the expansion of small AAA would benefit many patients who are left to wait until their AAA grows large enough to require surgery. Our intention is to develop a minimally invasive, non-toxic, biodegradable vascular delivery system that targets AAA in order to prevent elastin degradation and regenerate elastin as a novel AAA therapy.

Filling in the Knowledge Gap

We have developed a nanoparticle system that has been functionalized with an elastin antibody, in order to achieve our goal. This system can recognize and bind to damaged elastin in the aorta when delivered systemically. We then load a MMP inhibitor and deliver it to the site of AAA and confirm the MMPs activity suppression. Later, we will use an elastin regenerator instead of a MMP inhibitor to see the effect of elastin preservation in AAA therapy. Finally, in order to provide a therapy for a more advanced AAA, where calcification is involved, we will deliver calcium chelator to site of the AAA first, followed by an elastin regenerator to stabilize elastin.

Specific Aims and Rationale

Aim1

To investigate whether MMP inhibitors like batimastat (BB-94) loaded nanoparticles (NPs) can be targeted to the site of abdominal aortic aneurysm (AAA) and whether they can stop growth of AAAs by suppressing local MMPs activity in a calcium chloride mediated injury model of aneurysms in rats.

Approach

We will optimize loading of BB-94 in PEGylated poly-lactic acid (PLA) NPs that are conjugated with anti-elastin antibodies, necessary for targeting damaged elastin. We will study drug loading efficiency, *in vitro* release, drug activity, and cellular uptake of NPs. NPs with optimum drug loading and release profile will be delivered intravenously in rats where AAAs have been created by perivascular application of calcium chloride. We will study the MMPs activity and AAA growth suppression with time. We will also study organ distribution and systemic toxicity of NPs.

Rational

Several clinical trials for systemic MMP inhibition as a cancer treatment failed because of poor bioavailability, dose limiting toxicity, and systemic side effects, such as musculoskeletal problems, which limited the dose that could be tolerated[168]. Clinical trials of systemic delivery of MMP inhibitor beta-blocker-propranolol did not show significant changes in the growth rate of aneurysms, but caused systemic side effects and reduced patient compliance[169], thus dampening enthusiasm for pharmacological therapy

for AAA. The side effects caused by MMP inhibitors in cancer patients led to the use of substantially lower doses of MMP inhibitors in clinical trials for aneurysm prevention [170]. Because our targeted treatment's site-specificity permits very low doses of the drug, such therapy will be an attractive option for preventing expansion of aneurysms in patients without causing systemic side effects.

Aim 2

To investigate whether PGG loaded nanoparticles (NPs) can be targeted to the site of an AAA and whether they increase elastin matrix deposition, thus allowing AAA regression in a calcium chloride mediated injury model of aneurysms in rats.

Approach

We will optimize loading of PGG in bovine serum albumin (BSA) NPs that are conjugated with anti-elastin antibodies. We will study drug loading efficiency, in vitro release, drug activity, and cellular uptake of NPs. We will study in detail about elastin morphology, degradation, and regeneration by fastin and desmosine analyses and by transmission electron microscopy (TEM) and histology. Using ultrasound imaging, mechanical properties of the aorta will be assessed to see whether elastin regeneration helps biomechanically to restore arterial function. As calcification is seen in AAAs, we will also test if duel therapy of EDTA NPs to remove calcium and PGG NPs to restore arterial elastin will be beneficial.

Rational

It has been established that elastin degradation is a primary cause of AAA[171], and whether AAA is large or small, regression of it and restoration of normal arterial architecture would be preferable. Although no one previously could show elastin regeneration, our group demonstrated the protective effect of PGG in terms of protecting damaged and non- damaged elastin from protease degradation and the ability of PGG to help tropoelastin molecules to assemble and make new crosslinked elastin by vascular smooth muscle cells[121]. We have already developed NPs that target to AAA. We would like to use these NPs to deliver PGG at the site of aneurysms. Such site-specific targeting of PGG would help arterial elastin restoration. With the regeneration of elastin, we can reverse the progression of aneurysms.

Aim3

To investigate whether elastin-specific vascular calcification associated with AAA can be first removed when targeted nanoparticles deliver chelating agent EDTA to the site of vascular calcification and if PGG targeted delivery thereafter can regenerate elastic lamina.

Approaches

In the rat model of calcium chloride, NP based EDTA therapy will be optimized and NP based PGG will be used. We will create a moderate stage aneurysm and will treat them first with EDTA nanoparticles. After that, we will treat them with PGG nanoparticles. After six (6) weeks and organ harvesting, we will study in detail about

elastin regeneration by desmosine analysis. Circumferential strain of the aorta will be assessed to see whether elastin regeneration helps biomechanically to restore arterial function.

Rational

Degeneration of elastin plays a crucial role in the pathology and progression of AAA, a disease characterized by the loss of structural integrity of the arterial wall. AAA is often associated with calcification, which increases the risk of AAA rupture [4]. Current option for AAA is the replacement of weakened aorta with a vascular graft. Our group has shown earlier that treatment with pentagalloyl glucose (PGG) increased elastin matrix deposition by healthy and aneurysmal vascular smooth muscle cells *in vitro* [121]. Furthermore, we have shown that EDTA nanoparticles can remove calcification from calcified artery with minimal dose of EDTA using the same nanoparticles technology [172.] We would like to use combination therapy of EDTA and PGG to be delivered at the site of aneurysms. Such dual therapy of EDTA followed by PGG would help reduce calcification and promote arterial elastin restoration, thus reversing the disease.

CHAPTER IV

PREVENTION OF ABDOMINAL AORTIC ANEURYSM PROGRESSION BY TARGETED INHIBITION OF MATRIX METALLOPROTEINASE ACTIVITY WITH BATIMASTAT-LOADED NANOPARTICLES

Abstract

Rationale

The side effects caused by MMP inhibitors in cancer patients led to the use of substantially lower doses of MMP inhibitors in clinical trials for aneurysm prevention. Clinical trials of systemic delivery of a MMP inhibitor, propranolol—which is a beta-blocker—did not show significant changes in the growth rate of aneurysms, but caused systemic side effects and reduced patient compliance, thus dampening enthusiasm for pharmacological therapy for AAA. Because our targeted treatment's site-specificity permits very low doses of the drug to be used, this therapy will be an attractive option for preventing expansion of aneurysms in patients without systemic side effects.

Objective

Our previous study showed that poly D, L-lactide (PLA) nanoparticles (NPs) conjugated with an anti-elastin antibody can be targeted to the site of an aneurysm in a rat model of AAA. Here, we tested whether such targeted NPs can deliver the MMP inhibitor batimastat (BB-94) to the site of an aneurysm and prevent aneurysmal growth.

Approach and Results

BB-94-loaded PLA NPs-targeted to the aneurysmal aorta were studied in a calcium chloride injury-induced AAA in rats. Intravenous injections of elastin antibody-

conjugated BB-94-loaded NPs (EL-NP-BB94) targeted the site of aneurysms and delivered BB-94. Such targeted delivery inhibited MMP activity, elastin degradation, calcification, and aneurysmal development in the aorta (269% expansion in control vs. 40% EL-NP-BB94) at a low dose of BB-94. The systemic administration of BB-94 alone at the same dose was ineffective in producing MMP inhibition.

Conclusions

Targeted delivery of MMP inhibitors using NPs may be an attractive strategy to inhibit aneurysmal progression.

Introduction

Abdominal aortic aneurysm (AAA) characterized by dilation of the abdominal aorta, is one of the top-10 causes of death among older men.[173] Although the cause of AAA remains unknown in the majority of cases, several key regulators of AAA pathogenesis are known. Matrix metalloproteinases (MMPs) have been shown to play a major role in progressive extracellular matrix (ECM) degradation in AAA.[174,175]. Under inflammatory conditions, infiltrating macrophages, vascular smooth muscle cells, endothelial cells, and adventitial fibroblasts secrete pro-MMPs; cleavage of the pro-MMP subunit activates the MMPs, causing ECM degradation. MMP activity may be naturally suppressed by tissue inhibitors of matrix metalloproteinases (TIMPs), which comprise a family of four protease inhibitors: TIMP1, TIMP2, TIMP3, and TIMP4.[176]. An improper balance between MMPs and TIMPs shifts equilibrium towards matrix degradation in

several vascular conditions, such as AAA, atherosclerosis, hypertension, and calcification.[177]

Several types of MMPs are expressed in AAA tissue, including MMP-1, MMP-2, MMP-3, MMP-9, and MMP-12.78 MMP-9 and MMP-2 knockout mice do not develop aneurysms, suggesting that these MMPs play a major role in the development of AAA3. A number of synthetic MMP inhibitors (e.g., doxycycline- and hydroxamate-based) are known to decrease MMP activity[178] and prevent medial destruction.[179]. Synthetic MMP inhibitors with a hydroxamate (-CONHOH) group bind zinc atoms and suppress MMP enzymes[180]. Among the many hydroxamate-based MMP inhibitors are marimastat, solimastat, prinomastat, cipemastat, and Batimastat (BB-94)[181,182]. It has been shown that BB-94 was one of the first synthetic MMP inhibitors to be tested clinically to reduce MMPs in cancers with advanced malignancies[183]. However, its effectiveness is limited by its poor water solubility when administered orally, requiring parenteral administration. In several studies, systemic administration of MMP inhibitors effectively reduced aneurysmal onset in animal models[182,184], but systemic delivery can cause off-target inhibition of the MMP activities essential for normal homeostasis[185]. Although there are no in vivo studies of targeted delivery of MMP inhibitors to the aneurysm site, a recent in vitro study showed the potential of delivering doxycycline-loaded nanoparticles (NPs) for localized elastic matrix stabilization and regenerative repair in AAA[166]. Doxycline was also shown to reduce mRNA stability for MMP-2 and inhibit MMP activity that way[186].

In this study, we tested the hypothesis that systemic delivery of elastin-antibody conjugated polymeric nanoparticles loaded with BB-94 would be targeted specifically to

the aneurysm site, will slowly release the drug at the aneurysm site, and inhibit local MMP activity and subsequent aneurysms. Such targeted MMP inhibition would require smaller and less frequent drug doses than systemic administration, which would minimize systemic side effects.

Materials and Methods

Synthesis of Batimastat-Loaded Nanoparticles (EL-NP-BB94)

Poly (D,L-lactide) (PLA) NPs were prepared using the solvent-diffusion-based nano-precipitation method.[167] PLA (10 mg, average MW 75k-120k) (Sigma Aldrich, St. Louis, MO) was dissolved in 1 ml acetone (VWR International, Radnor, PA). 1,2-distearoyl-*sn*-glycero-3-phosphoethanolamine-N-(methoxy(polyethylene glycol) – 2000) (2 mg, DSPE-PEG (2000) Maleimide, Avanti Polar Lipids, Inc., Alabaster, AL) and BB-94 (Sigma Aldrich, St. Louis, MO) were dissolved in dimethylsulfoxide (Sigma Aldrich, St. Louis, MO), and this solution was then added to the PLA solution. The polymer solution was added drop-wise (16 µl/sec) to water and kept under sonication (Omni Ruptor 4000) for 20 minutes at 4°C. Following sonication, the particles were washed twice with distilled water by centrifugation at 14000x g for 30 minutes at 4°C and then re-suspended in distilled water. The non-solvent (water) to solvent (acetone) ratio was 1:15 for all experiments. Three different batches containing ratios of 5:1, 10:1, and 15:1 polymer to BB-94 were prepared in which the ratio between the two polymers (PLA: DSPE-PEG(2000) Maleimide) was 4:1.

Nanoparticle Yield

The total final dry weight of the NPs was recorded, and NP yield was calculated using the formula shown below:

$$\text{NP yield } \% = \frac{\text{Final dry weight}}{\text{Initial weight}} \times 100 \qquad (1)$$

Nanoparticle Characterization

Particle size, ζ-potential and Transmission Electron Microscopy (TEM) were performed to characterize the NPs. The NP suspension (1 mg) was diluted in HPLC-grade water, and the ζ-potential and particle size were measured with a 90Plus particle size analyzer (Brookhaven Instruments Co., Holtsville, NY). Transmission Electron Microscopy (TEM) was used to study NPs morphology. A drop of 0.1 mg/ml NPs-water suspension was placed on a formvar-coated copper grid and dried overnight in vacuum desiccator. Grid-mounted samples were imaged using a Hitachi H7600 TEM.

Nanoparticle Degradation Studies

Blank NPs were suspended in phosphate buffered saline (PBS) and stirred at 37^{o}C to test the polymer degradation. Degradation of the NPs was monitored by measuring the weight of the remaining NPs at different time points (1, 7, 14, 21, and 28 days) after lyophilization. The percent weight loss was calculated using the difference between the remaining dry weight and the initial weight. We also tested blank NPs degradation by gel permeation chromatography (GPC). Nanoparticles (5 mg) were suspended in 5 mL of DI water at stirred at 37^{o}C. At week 1 and week 4, NPs were isolated by filtration and lyophilized. NPs were dissolved in chloroform at a concentration of 1mg/ml. The

solution was filtered directly into chromatography vials using 0.2µm PTFE filters. Polymer molecular weight was assessed by Size Exclusion Chromatography/Gel Permeation Chromatography(SEC/GPC) using a Shodex KF-804L column on a Waters HPLC/GPC system equipped with an Autosampler, column heater, and refractive index (RI) Detector. Chloroform was used as the mobile phase at a flow rate 0.65 ml/min, and the column was kept at 30°C during all separation runs. The injection volume for GPC analysis was 50 µL. Polystyrene standards of 9, 35, 50, 100 and 200 kDa were used as markers, and a control sample of PLA (Average MW 75,000-120,000 kDa) was used to validate the calibration curve reliability.

Loading Efficiency and Release Profile of BB-94

Loading efficiency was calculated by dissolving NPs in dimethylsulfoxide, determining BB-94 concentration at λ (max) = 285 nm using UV spectrophotometry, and using the equation shown below:

$$\%\ \text{Loading} = = \frac{\text{BB}-94\ \text{weight}}{\text{total weight of NPs}} \times 100 \qquad (2)$$

To study release kinetics, a known amount of NPs was suspended in phosphate buffered saline (PBS) and incubated at 37°C on a shaker. Suspensions were centrifuged for 30 minutes at 10000×g at room temperature (RT). The supernatant was removed, and the sediment was freeze-dried and characterized for BB-94 concentration by dissolving it in 100 µl dimethylsulfoxide and measuring absorbance by UV spectrophotometry.

Percent release was calculated as the following:

$$\%\ BB\text{-}94\ Released = \frac{(\text{Initially loaded BB}-94) - (\text{Residual BB}-94)}{\text{Initially loaded BB}-94} \times 100 \qquad (3)$$

Conjugation of Elastin Antibody to NPs

Traut's reagent (34 µg, G-Biosciences, Saint Louis, MO) was used for thiolation of 10 µg of rabbit anti-rat elastin antibody (United States Biological, Swampscott, MA), and the mixture was incubated in HEPES buffer (20 mM, pH=9.0) for an hour at room temperature. Thiolated antibodies were rinsed with HEPES buffer and added to the NPs (4 µg antibody per 1 mg NPs) and then incubated overnight for conjugation. After incubation, antibody-conjugated NPs were washed twice with PBS, centrifuged (10000 rpm for 10 minutes), and suspended in 0.3% rat serum albumin for an *in vivo* study animal study.[167]

BB-94 Activity

To test if the BB-94 loaded in the NPs was still in active form, sodium dodecyl sulfate-polyacrylamide gel electrophoresis (SDS-PAGE) zymography was performed. Briefly, NPs were dissolved in dichloromethane (Aldrich, MO) and DI water at a ratio of 3:1. This mixture was mixed vigorously and centrifuged for 10 minutes at 10000×g to extract BB-94 from the NPs. The DI water containing BB-94 was subsequently collected and lyophilized. The activity of the extracted BB-94 from the NPs was tested by two different methods. In the first approach, culture medium collected from rat aortic smooth muscle cell (RASMC) cultures was loaded into a SDS-PAGE zymography gel, and extracted BB-94 was added to the development buffer(500ng/ml) (50 mM Tris Base, 5 mM $CaCl_2 \bullet 2H_2O$, 200 mM NaCl, 0.02% brij 35). After 24 hours incubation in the development buffer, gels were stained with 0.5% coommasie blue for an hour at room temperature and were destained with 5% water, 40% methanol, 10% acetic acid. After

this, the gels were photographed using epi-illuminated white light in a Bio-Rad Gel Doc instrument. Zymography bands were quantified using Image J software and data was reported as RDU. In the second approach, BB-94 activity was tested in RASMCs cultures. Briefly, RASMCs were grown to 80% confluency at 37°C and 5% CO_2 in DMEM containing 10% FBS and 1% penicillin-streptomycin (ScienCell Research Laboratories, Carlsbad, CA). After 24 hours, cells were treated with extracted BB-94 (500 nM) in serum-free medium for 24 hours. After treatment, conditioned medium was collected. The total protein of the culture medium was quantified using Bicinchoninic Acid (BCA) protein assay (Pierce, Rockford, IL) with 10 µg total protein loaded per well and prestained molecular weight standards (Precision Plus Protein Standard, Bio-Rad, Hercules, CA). Gel zymography was performed as described in the previous section.

Reverse Zymography for TIMP Activity

Equal amounts of protein from RASMC-conditioned cell culture media (BB-94 treated or control) were loaded in 15% reverse zymogram gel containing 1.5% gelatin and collagenase (20 units) under nondenaturing and nonreducing conditions. After 24 hours incubation in the development buffer, gels were stained with 0.5% coommasie blue for an hour and were destained. The gel pictures were captured using epi-illuminated white light and a Bio-Rad Gel Doc instrument; bands were analyzed and quantified using Image J, and data was reported as RDU.

RASMCs and Rat Aortic Endothelial Cells (RAOEC)

A standard MTT assay was performed to measure the cytotoxicity of NPs to RASMCs and RAOECs. RASMCs and RAOECs were cultured with NPs for 24 hours. MTT colorimetric assays (Sigma Aldrich, St. Louis, MO) were performed according to the manufacturer's protocol to confirm cell viability. Control and NP-treated cells were washed with PBS and incubated for 3 hrs. with 3-(4,5-dimethyl-thiazol-2-yl)-2,5-diphenyltetrazolium bromide (MTT) solution (5 mg/ml). Formazan crystals formation was detected at 570 nm and viability was shown as % MTT reduction compared to control. MTT activity was normalized to control.

Elastin-Antibody Conjugated Nanoparticle Uptake by Macrophages

Elastin-antibody conjugated NPs were loaded with fluorescent dye, 1, 1-dioctadecyl-3, 3, 3, 3-tetramethylindotricarbocyanine iodide (DIR), as described previously[167]. Macrophages (RAW 264.7, ATCC® TIB-71™) were grown in 24-well tissue culture plates followed by incubation with EL-DIR-NPs (1 mg/ml) at 37°C in 5% CO_2 for 4 hours and 24 hours. Cells were washed three times with sterile PBS and imaged before and after washing using EVOS® XL Cell Imaging System to determine NP uptake. As controls for charge and size, we prepared two different batches of NPs, one with positive surface charge and one with smaller NP size. To create a positive surface charge, NPs were coated with chitosan[187] (molecular weight 600K-800K) (ACROS, NJ). To study cytotoxicity, rat bone marrow macrophage cells (Cell Biologics, Inc., RA-6030F) were grown in 24-well tissue culture plates followed by incubation with BB94 NPs (0.5, 1, 2 mg/ml). A standard Live /Dead assay was performed after 24 hours.

Feasibility of Nanoparticle Targeting *in vivo*

Local elastin damage in the rat abdominal aortic region was induced by perivascular application of calcium chloride.[69] After ten days, rats were divided into two groups and went through treatment with batimastat loaded NPs or blank NPs. Briefly, 19 male Sprague-Dawley (SD) rats (5-6 weeks old) were placed under general anesthesia (2% to 3% isoflurane). The infrarenal abdominal aorta was exposed and treated periadventitially by placing 0.50 mol/L $CaCl_2$-soaked sterile cotton gauze on the aorta for 15 minutes. The treated area was flushed with warm saline, and the abdominal incision was closed with sutures. Animals were allowed to recover and were given a normal diet for ten days. Adventitial inflammation and elastic lamina degradation has previously been shown to occur within ten days in this model. NPs loaded with BB-94 and conjugated with elastin antibody (named EL-NP-BB94 henceforth, ~10mg/kg body wt.) were suspended in 200 µl of 0.3% rat serum albumin (Sigma Aldrich, St. Louis, MO) and were injected through the tail vein (n=5). Control animals received elastin antibody-conjugated blank NPs (named EL-NP-Blank henceforth) (n=5). Three additional rats were injected with elastin antibody conjugated and DIR dye-loaded NPs (named EL-NP-DIR henceforth) to monitor delivery of the NPs by *in vivo* imaging. As a negative control, IgG antibody-conjugated NPs loaded with DIR dye (named IgG-NP-DIR henceforth) were injected through the tail vein (n=3). To study if the systemic delivery of low-dose BB-94 affects MMP activity in the aorta, three rats received the same amount of BB-94 (600 µg of BB-94 /kg body wt.) dissolved in 200 µL PBS solution with 0.01% Tween 20 (Merck, Germany) by intraperitoneal injection.

Two days (48 hrs.) after treatment, the rats were euthanized and thoracic and abdominal aortic tissue segments were explanted and snap-frozen in liquid nitrogen. Total protein from the aortic samples was extracted by pulverizing liquid nitrogen-frozen tissue samples and homogenizing them in RIPA extraction buffer (50 mM Tris-HCl pH 7.4, 150 mM NaCl, 1 mM EDTA, 1% Triton X-100, 1% Sodium deoxycholate, 0.1% SDS, with protease inhibitor cocktail) (Roche Diagnostic GmbH, Germany) according to the manufacturers protocol. Sections of thoracic and abdominal aortic tissue were embedded in Optimal Cutting Temperature compound (OCT) for cryostat sectioning. For DIR-loaded NP groups, whole fresh aorta and all organs were harvested and imaged using Caliper IVIS Lumina XR (Hopkinton, MA) with Ex/Em of 745/795 nm for studying targeting and bio distribution of NPs.

MMP Activity in Rat Aorta

The total protein from the harvested aortic tissue after 48 hours of treatment was quantified using the BCA protein assay kit (Pierce, IL). An internally quenched peptide substrate, which is specific to MMP-2 and 9 (excitation 280 nm, emission 360 nm, MMP Substrate III, Anaspec, CA), was used to measure the MMP activity. One mg of substrate dissolved in 50 µl dimethylsulfoxide was diluted in 10 ml of development buffer (50 mM Tris Base, 5 mM $CaCl_2 \bullet 2H_2O$, 200 mM NaCl, 0.02% brij 35). Development buffer (96 µl) was mixed with 2 µl of the extracted protein along with 2 µl of substrate stock solution and incubated for one hour at 37°C. Endpoint florescence intensity was read using a fluorescence plate reader.

Nanoparticle Targeting to Inhibit Aneurysm Progression

To study long-term aneurysmal inhibition, another set of 13 rats was used. AAAs were induced by perivascular application of calcium chloride[69]. Ten days after injury, NPs (~10mg/kg body wt.) were injected via tail vein once a week for four weeks (n=5 EL-NP-BB94, n=5 EL-NP-Blank, and n=3 EL-NP-DIR). Rats were euthanized on day 38, and organs and aorta were harvested. IVIS imaging was used to confirm targeting and bio distribution in the EL-NP-DIR group. Aortic tissues from the EL-NP-Blank and EL-NP-BB94 groups were harvested as described above.

In situ Zymography

To examine the activity of MMPs in the aortic tissue samples *in situ*, zymography was performed on histological sections of aorta isolated at 48 hours and 38 days after NP injection. Gelatinolytic activity was demonstrated in unfixed cryostat sections (8 μm thick) using DQ-gelatin as a substrate (Life, IL). Cryostat sections of the abdominal aorta were air-dried for 10 minutes. One part DQ-gelatin (1 mg/ml of DI water) was mixed with nine parts 1% agarose (Promega, WI) in PBS containing DAPI (1 μg/ml) (Life Technologies, IL). A drop of the mixture was added to each section, and each section was then incubated in development buffer for one hour at 37° C. As a positive control, in one sample MMP activity was blocked by MMP inhibitor 1, 10-phenanthroline monohydrate (0.2mmol/L) (Life Technologies, OR). Images were captured using EVOS® XL cell imaging system.

Histological Analysis

Formalin-fixed samples were embedded in paraffin, and 5 µm sections were mounted on glass slides and heated overnight to adhere the tissues to the slides and melt the paraffin. Subsequently, the slides were deparaffinized with xylenes and graded ethanol and stained with hematoxylin and eosin for tissue morphology, Verhoeff-van Gieson (VVG) for elastic fibers, and Alizarin Red S with a Light Green SF counterstain for calcification.

Immunostaining for Macrophages (CD80)

Aortic sections from the 38 day aneurysm study were used. Tissues preserved with formalin were embedded in paraffin and sectioned as previously described. Subsequently, the slides were deparaffinized with xylenes and graded ethanol, and antigen retrieval was done using the HCl method. The slides were incubated overnight at room temperature with the primary antibody, Mouse Anti Rat CD80 (Bio-Rad, Hercules, CA). Subsequently, the slides were incubated for 1 hour with the secondary antibody, Cy7 goat anti-mouse IgG (H+L) (Bioss Inc., MA), and DAPI nucleic acid stain and then imaged with a fluorescent microscope, EVOS® XL Cell Imaging System.

Aneurysmal Development

Initial external diameter was measured at the time of the $CaCl_2$ injury. Final aortic diameter was recorded before euthanasia on day 38. Aneurysmal development was calculated as shown below:

$$\text{Aneurysmal development\%} = \frac{Final\ diameter - Initial\ diameter}{Initial\ diameter}\ x\ 100\% \qquad (4)$$

Statistical Analysis

In vitro experiments were performed in triplicate and repeated twice; for in vivo studies, five animals were used per group per time point. Student's t test was performed using Microsoft Excel, and exact permutation test was performed using the NPAR1WAY procedure in SAS. The data are expressed as the mean ± standard deviation; results were considered to be significant when P-values ≤ 0.05.

Results

Nanoparticle Characterization

NPs were prepared with three different initial BB-94 concentrations (5:1, 10:1, 15:1 polymer-to-drug ratio). No significant differences were found for the percent yield of NPs among the three batches. Increasing the initial BB-94 concentration during NP preparation did not increase the final BB-94 loading in the NPs. Particle-surface charge was dependent on initial polymer to BB-94 ratios. All BB-94-loaded NPs were negatively charged; however, a higher polymer to BB-94 ratio led to a more negative surface charge (see Table 2).

NP Degradation and BB-94-Release Study

A higher polymer-to-BB-94 ratio led to a smaller NP size, which was confirmed visually by TEM (See Figure 12).

When suspended in DI water, Blank-NPs lost substantial weight (65±4.5%) in four weeks; the majority of weight loss occurred in the first week (45.65±6.8) (See Figure 13).

Table 2. Characterization of nanoparticles and BB-94 loading.

Polymer/ BB-94 ratio	% Yield n=4	% Loading n=3	NP size (nm) n=3	ζ-potential (mV) n=3
15:1	62.9± 33.9	5.7 ± 2.5	123.8 ± 24.9#	-83.1 ±2.8#*
10:1	44.2 ± 3	8.4 ± 2.7	153.5 ± 26.8#	-47.2±5.5#*
5:1	38.4 ± 18	6.7 ± 0.4	196.3 ± 3.3	-29.1±5.1

*Represents statistical significance (Student's unpaired t-test, $P < 0.05$),
#Represents statistical significance (exact permutation test, $P < 0.05$) compared to 5:1 group**.**

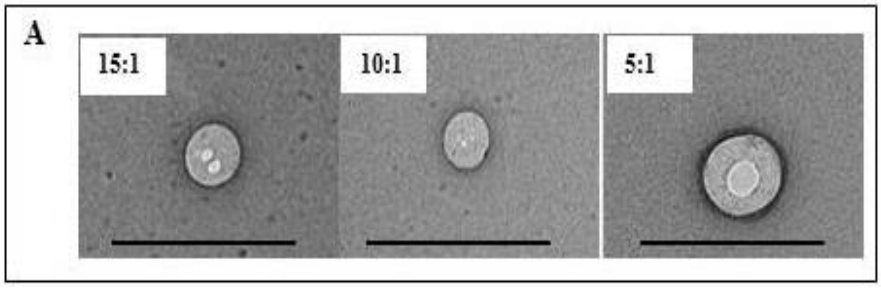

Figure 12. TEM images of 15:1, 10:1, and 5:1 polymer to BB-94 ratio NPs.

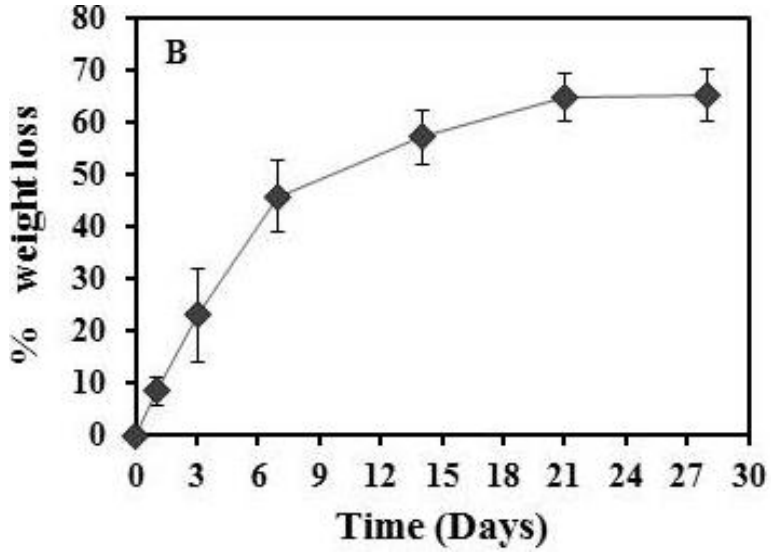

Figure 13. Weight loss of blank NPs over four weeks.

This data was also corroborated by NP degradation seen in the GPC study.

Polymer nanoparticles as prepared showed one broad peak at retention time at ~9 min. With time, low molecular weight products (with retention time ~12-13 min) appeared suggesting polymer degradation (See Figure 14).

In vitro BB-94 release from the NPs was gradual and lasted for up to eight days. Although final BB-94 loading was similar for all polymer-to-BB-94 ratios, the BB-94 release profile varied with the starting BB-94 concentration (See Figure 15). Slower release was observed in NPs with a 5:1 polymer-to-BB-94 ratio, while significant burst release was observed when the initial BB-94 concentration was lower (10:1 or 15:1 polymer: BB-94 ratio). BB-94 release was more controlled for the batch with a higher starting BB-94 concentration (5:1 polymer: BB-94 ratio), so these NPs were chosen for further study.

Activity of BB-94

The activity of the BB-94 loaded in the NPs was examined using gel zymography. When extracted BB-94 was added to the development buffer, pro-MMP-2 (72 kDa), active MMP-2 62kD), and MMP-9 (92 kDa) activities were inhibited completely (See Figure 16).

When BB-94 extracted from the NPs was added to the RASMC cultures, ninety percent of MMP-9 (92 kDa) and ten percent of MMP-2 (62 kDa) activity were inhibited. Notably, more MMP-2 remained in the pro-form (inactivated, 72kD) when BB-94 was added to cell cultures (See Figure 17).

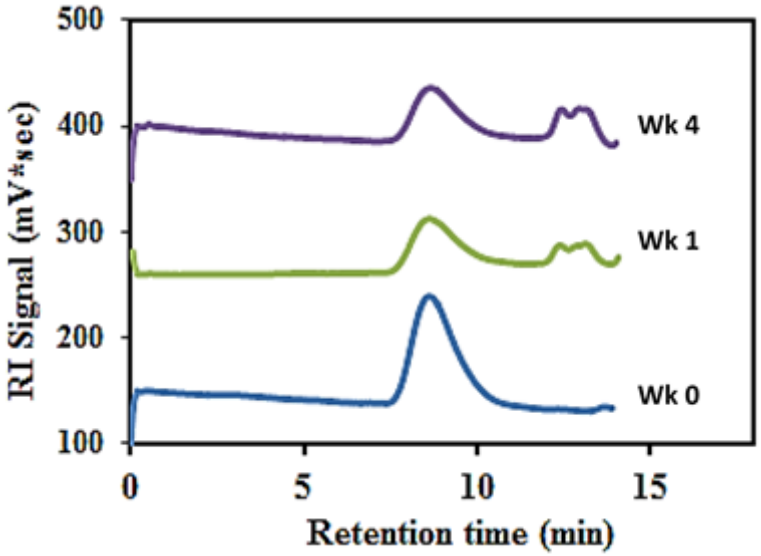

Figure 14. GPC curves show peaks for degradation products at retention time (~13 min) at week 1 and 4.

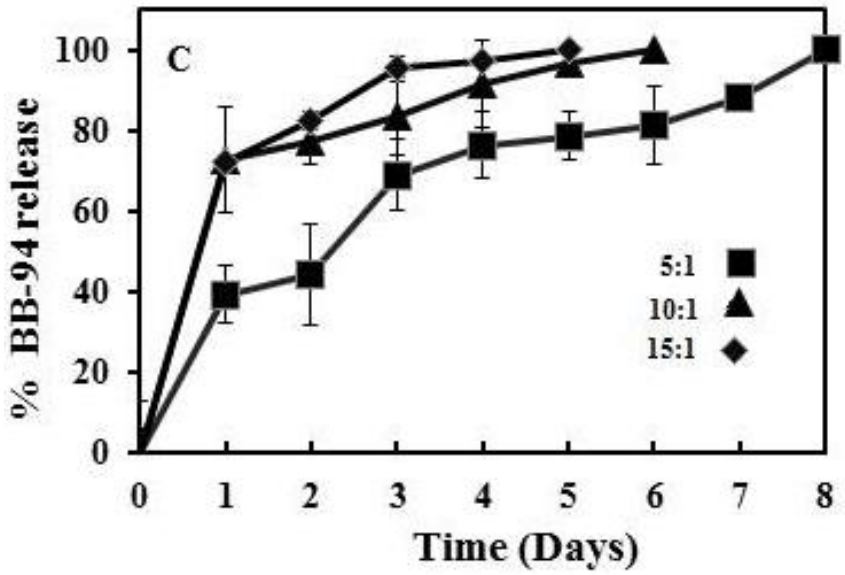

Figure 15. Release kinetics of BB-94 for 8 days.

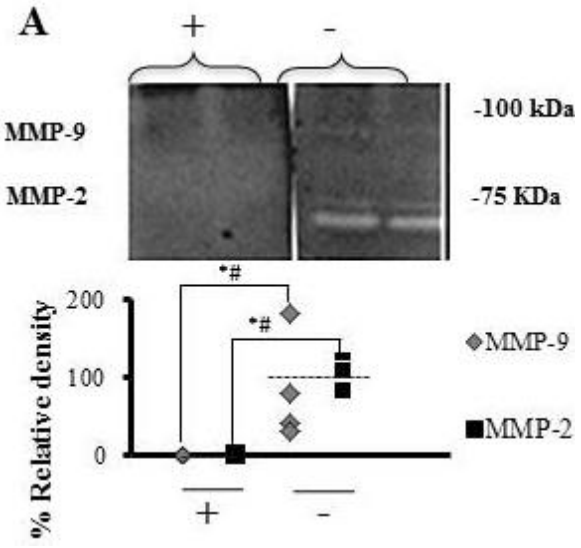

Figure 16. Gel zymography study when BB-94 was used in development buffer. * (Student's unpaired t test, $P < 0.05$) and # (exact permutation test, $P < 0.05$). (n=6 for zymography). Dashed line represents the mean value.

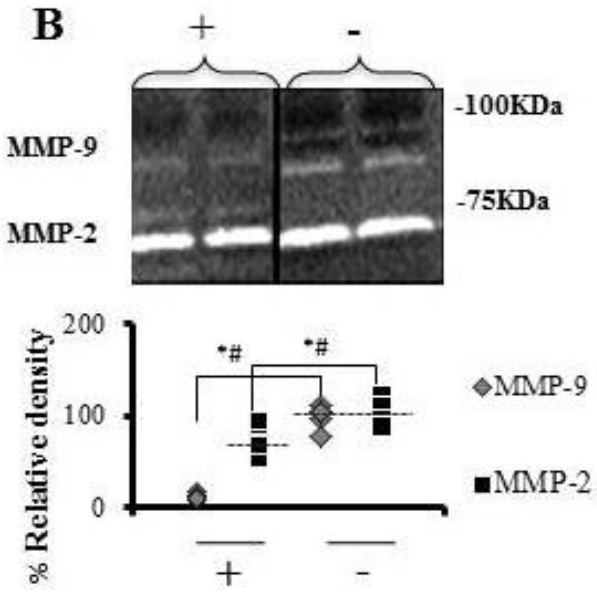

Figure 17. Gel zymography study: Conditioned media. * (Student's unpaired t test, $P < 0.05$) and # (exact permutation test, $P < 0.05$). (n=6 for zymography). Dashed line represents the mean value.

There was no significant difference in the expression of tissue inhibitors of metalloproteinase-2 (TIMP-2) (21 kDa) between control and BB-94-treated cells (See Figure 18). These results suggest that BB-94 loaded NPs inhibited MMPs without affecting TIMP-2 levels.

NP Cytotoxicity and Cellular Uptake

RAOEC and RASMC viability showed no significant change in 24 hours in the presence of NPs when compared to the control (See Figure 19A&B). We have already shown that such NPs are not taken up by VSMCs[167]. Inflammatory cells such as macrophages are commonly present at the site of AAA. Thus, we determined if our NPs were resistant to macrophage uptake. NPs labelled with a DIR dye were incubated with macrophage cell cultures for 24 hours (ζ-potential: -29.1±5.1, size: 196.28±3.2 nm). Due to the negatively charged surface of the chosen NPs, no macrophage uptake was observed (See Figure 19-a_1,a_2,a_3). When the surface-charge was changed to positive with the addition of chitosan, (ζ-potential: +20.28±4.93), NPs could be seen in the cell cytoplasm which suggests that they were taken up by macrophages (See Figure 19C- b_1,b_2,b_3). When NP size was changed to ~125 nm and the surface charge remained negative (ζ-potential: -83 ±2.8), there was again significant uptake by macrophages (See Figure 19C-c_1,c_2,c_3). Overall, ~200 nm NPs with negative surface charge that were chosen for further studies were resistant to macrophage uptake. Bone marrow macrophages viability showed no significant change in 24 hours for blank and BB-94 loaded NPs at thirteen fold concentration used *in vivo* (See Figure 19D).

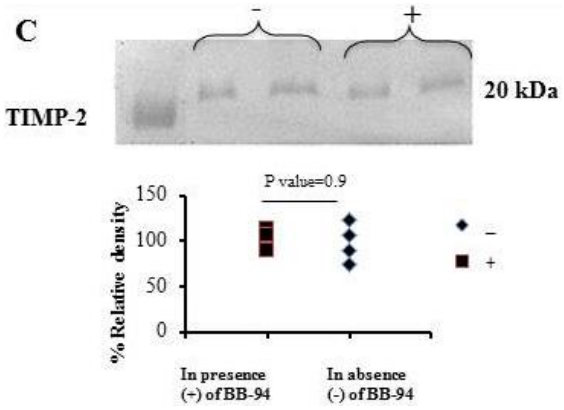

Figure 18. Reverse gel zymography(n=4).

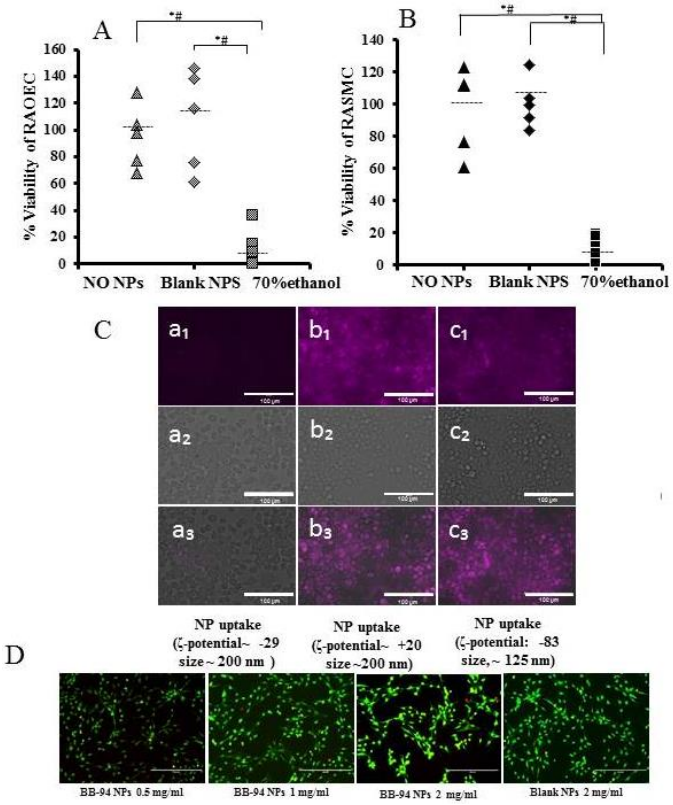

Figure 19. Cells viability and uptake in presence of NPs. * (Student's unpaired t test, $P < 0.05$) and # (exact permutation test, $P < 0.05$) (n=6). Dashed line represents the mean value.

In vivo NP Targeting and MMP Inhibition

We have shown that NPs with a surface conjugated anti-elastin antibody can target the site of aortic injury in this animal model.[167] We confirmed *in vivo* targeting, by observing localized fluorescence at the injury site of the abdominal aorta for the EL-NP-DIR group, suggesting excellent targeting to the injured aorta (See Figure 20A), while no fluorescence was observed in the injured aorta for control IgG-NP-DIR group (See Figure 20A).

We next examined if NPs loaded with BB-94 would target the injury site and inhibit local MMP activity. Fluorescence intensity data when normalized to total protein content showed that the abdominal aorta had ~50% higher MMP activity than the thoracic aorta in the EL-NP-Blank group (See Figure 20B). This result suggests that MMPs were activated by CaCl2-mediated injury and that blank NPs targeted to the abdominal aorta did not suppress MMP activity. The EL-NP-BB94 group showed 56% lower MMP activity in the abdominal aorta in comparison to the thoracic aorta, suggesting that MMP activity was completely suppressed at the injury site (See Figure 20B). When the same concentration of BB-94 was delivered by intraperitoneal injection (IP), MMPs in the abdominal aorta showed 63% higher activity than the thoracic aorta, suggesting that systemic delivery of the same dose of BB-94 was ineffective in suppressing local MMP activity in the abdominal aorta (See Figure 20B). These results were further confirmed by *in situ* zymography studies on histological sections of abdominal aorta in different groups. The green fluorescence in this assay is caused by the

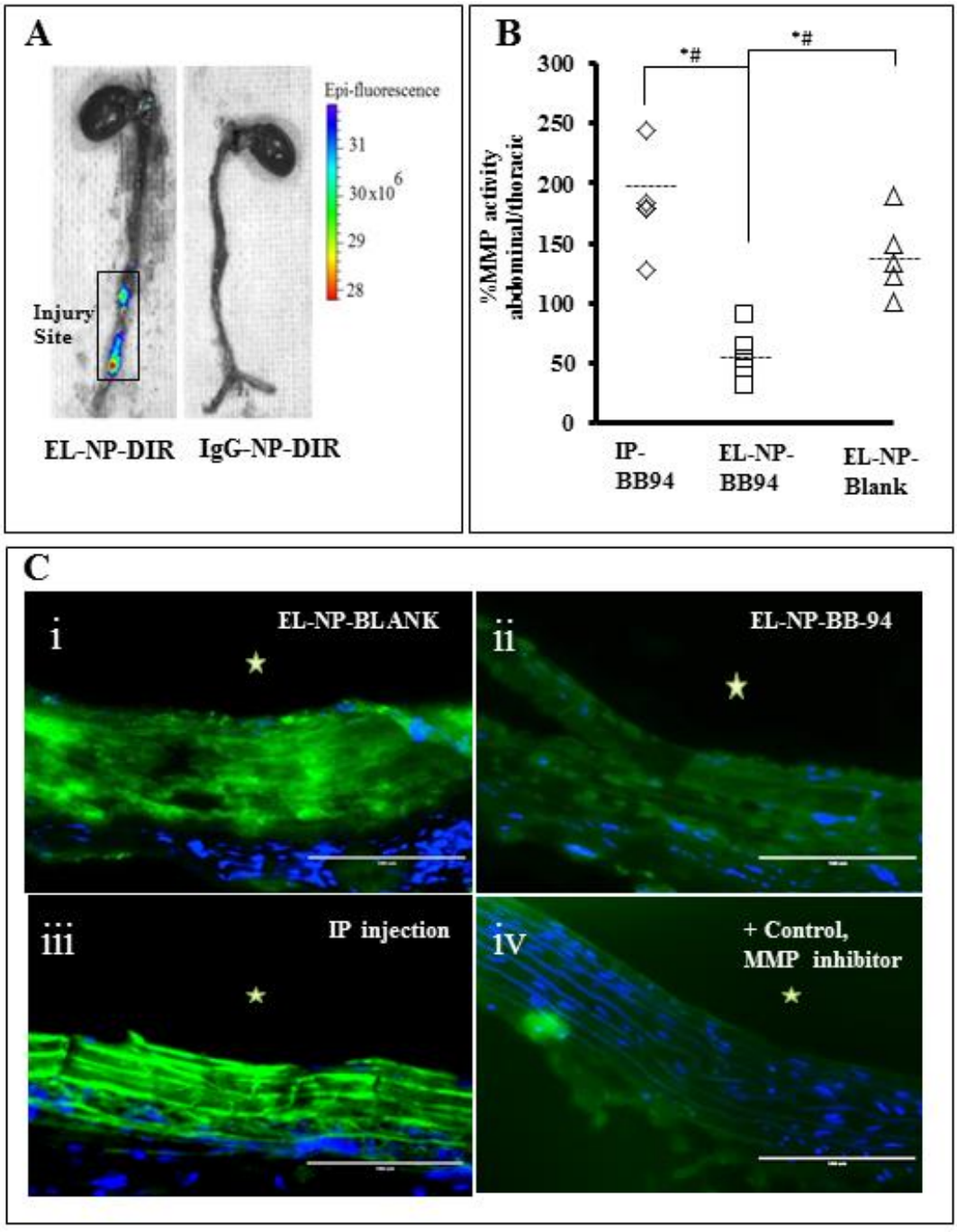

Figure 20. Targeting and MMPs activity after 10 days. * (Student's unpaired t test, $P < 0.05$) and # (exact permutation test, $P < 0.05$) (n=5). Dashed line represents the mean value. * Indicates lumen. Bar = 100 μm.

enzymatic degradation of DQ gelatin, which directly corresponds to the MMP activity in the sections. Intense green fluorescence corresponding to higher MMP activity was found in the sections of the abdominal aorta in the control animals receiving EL-NP-Blank or IP injected BB-94 (IP-BB-94); a significant suppression of MMP activity was observed in the BB-94 NP group (EL-NP-BB94), (See Figure 20C). This was similar to the positive controls, where MMP activity was inhibited by the addition of 1, 10-Phenanthroline during *in situ* zymography.

Long-term Targeting and Bio Distribution of NPs

With encouraging results in the 48-hour targeting experiment, we next determined if such targeting can inhibit MMP activity and aneurysmal development for prolonged periods. Because our BB-94-release study showed slow release for up to seven days, we decided to inject elastin-antibody conjugated NPs once weekly for four weeks. After injections (4 injections over a total of 38 days after first $CaCl_2$ injury), a three-fold increase was seen in the fluorescence signal in the abdominal aorta for the EL-NP-DIR group as compared to a single injection (Figure 21A compared to Figure 20A), indicating more NPs accumulated at the injury site. The fluorescence signal of DIR (% florescence/dry weight of organ) increased in the abdominal aorta from 26.3 to 78.7%. At the same time, the signal decreased from 0.78 to 0.003% for the kidneys, from 15 to 2.7% for the liver, and from 48 to 18% for the spleen in comparison to the 2-day study (Figure 21 B). These data show that additional NPs accumulated at the injury site, while other organs were clearing non-targeted NPs. More importantly, the NPs were seen

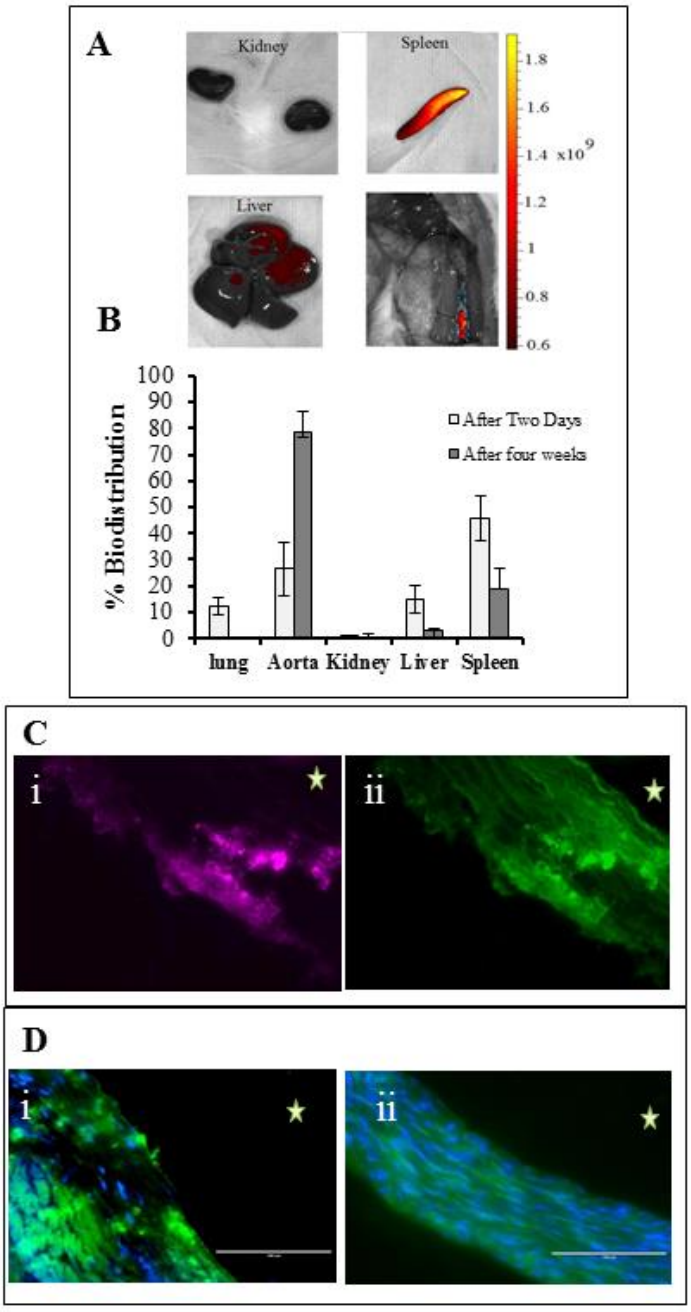

Figure 21. Targeting after 4 weeks. Cross-section of abdominal aorta showing NPs(purple). Matrix metalloproteinase activity in abdominal aortic sections by in situ zymography at 38 days.

infiltrating from the adventitial side of the aneurysmal aorta through the vasa vasorum rather than from the luminal side and then attaching to the degraded elastic lamina deep within the medial layer (See Figure 21C).

Long-Term Inhibition of MMPs and Aneurysmal Development

When NPs were injected weekly for four weeks after $CaCl_2$ injury, MMP activity was still suppressed in animals receiving EL-NP-BB94 NPs (similar to the 48-hour study), while MMPs remained elevated in the EL-NP-Blank group (Figure 21D).

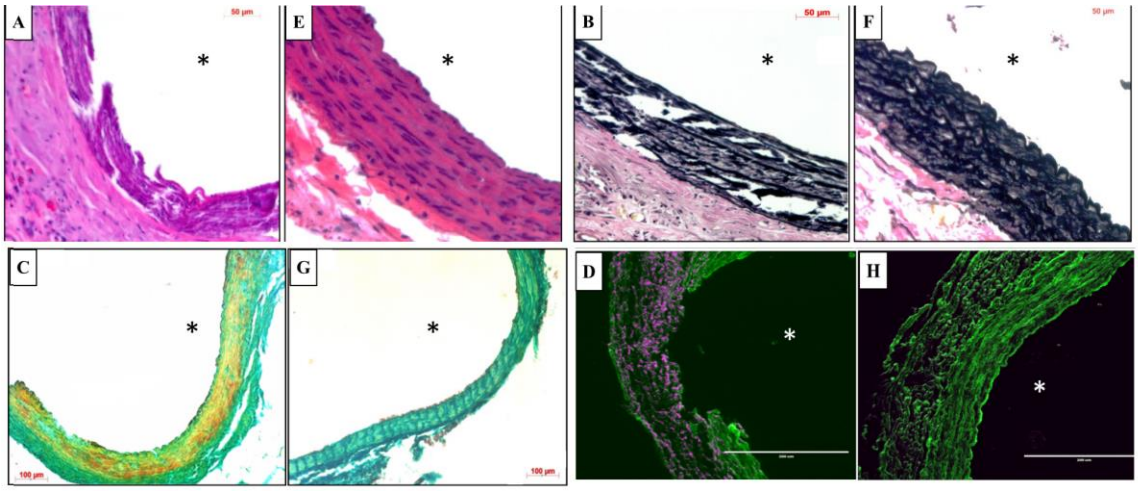

Figure 22. Histological analysis at 38 days.

Hematoxylin and eosin staining showed significant inflammation in the adventitia in the EL-NP-Blank group, while the EL-NP-BB94 group maintained greater structural integrity and had little inflammation (Figure 22A and Figure 22E respectively). Verhoeff-van Gieson (VVG) staining revealed the elastic lamina was broken and damaged in the EL-NP-Blank group while elastin preservation was observed in the EL-

NP-BB94 group (Figure 22B and Figure 22F). Similarly, alizarin red S staining showed heavy medial calcification in the EL-NP-Blank group and a substantial reduction in calcification in the BB94-treated group (EL-NP-BB94) (Figure 22C and Figure 22G). Macrophage immunohistochemistry revealed that the blank NPs group had a higher density of M1 macrophages in the adventitia and ruptured media in comparison to the BB-94 group (Figure 22D and Figure 22H).

Discussion

This study demonstrates that the use of targeted NPs carrying a potent MMP inhibitor can successfully inhibit local MMP activity in inflammatory vascular conditions such as AAA. We optimized NP size, surface charge, and BB-94 loading. Our data agree with the literature: During NP preparation, the particle size increased with increasing drug concentration and the negative surface charge decreased.[188] Particle size and drug loading are important parameters that dictate the release of a drug from NPs. The negative surface charge facilitates electric repulsion among NPs, thus increasing NP stability.[189] Surprisingly, increasing initial BB-94 concentration did not lead to a higher amount of BB-94-loading, with the maximal loading being only 6-8% of BB-94 in PLA. This may have occurred due to the physical properties of the original drug.[190] Although drug-loading was similar, drug dispersion within NPs, and thus ultimate release, varied with initial drug concentration. Our study shows that higher polymer content (15:1 and 10:1 polymer to BB-94 ratio) results in burst release on day 1. This may have occurred due to the smaller particle size with higher surface area for drug diffusion. NPs in the 5:1

polymer-to-BB-94-ratio batch had the biggest particle size and showed a more-controlled release because of either lower surface area or better drug encapsulation. Our NP degradation data with blank NPs showed significant weight loss after 7 days and an increase in polymer degradation products as assessed by GPC, suggesting that drug diffusion and polymer degradation occurred simultaneously.

Maintaining drug activity during NP synthesis is necessary for success in targeting. We showed that BB-94 extracted from NPs suppresses MMP activity both in gel zymography and in cell cultures. We found that BB-94 added to the development buffer during gel zymography was more effective in inhibiting MMPs (both the active and pro forms) than when it was added to cell culture media. It is possible that BB-94 dissociated during gel electrophoresis when the cell culture media was loaded in gels, thus causing lower MMP inhibition. The findings from reverse zymography showed no significant difference in the expression of TIMP-2 protein within the groups; this is consistent with the literature showing that BB-94 has no effect on TIMPs.[191]

Particle size and charge are important criteria in targeting NPs to the vasculature. It has been shown that NP-targeting of vascular ECM in an aneurysm site occurred for particle sizes below 200 nm.[167] That study also showed that a negatively charged NP surface prevents NP uptake by vascular smooth muscle cells. Because macrophages are phagocytic and present at the aneurysmal site, we determined if a negative surface charge would also prevent the uptake of NPs by macrophages. We showed that macrophages do not take up ~200 nm BB-94-loaded NPs (5:1 polymer to BB-94 ratio, negative surface

charge). Based on these results and previous VSMC-uptake results, these NPs would remain in the ECM.

Elastin-antibody conjugation on the NP surface also allowed us to target these NPs to the site of elastin damage found in the aneurysm site due to the fact that this antibody recognizes only core amorphous elastin that is exposed during elastic lamina degradation.[167] Our data with DIR dye-loaded NPs confirmed that they targeted only the injury site while sparing the healthy aorta. More importantly, we found that NPs entered preferentially from the adventitial side through the vasa vasorum and lodged deep in the media when delivered systemically. This is clinically advantageous because the intraluminal thrombus generally present in an aneurysm can obstruct NP-targeting from the luminal side. Notably, more degradation and inflammation is seen clinically in the adventitia.[192]

MMPs, in particular MMP-9 (gelatinase B/92 kDa) and MMP-2 (gelatinase A/72 kDa), play a significant role in AAA development and progression.[78] The goal of targeted treatment is to suppress MMP activity at the site of AAA so that further ECM degradation can be prevented. Our MMP fluorogenic assay showed that the MMP-2 and MMP-9 activity (represented as a ratio of abdominal aorta over thoracic aorta in the same animal) was 50% higher in the EL-NP-Blank and BB-94 IP groups, suggesting that sustained MMP activation was induced by CaCl2 injury and was not inhibited in the abdominal aorta by these treatments. Only when BB-94 was delivered by targeted NPs (EL-NP-BB94) was a significant decrease in MMP activity seen in the abdominal aorta for prolonged periods, suggesting that targeted NPs delivered BB-94 at the site of injury

and inhibited local MMP expression. This can occur by the suppression of macrophage activation as we have observed; this result is consistent with previous studies[103]. These data are corroborated by the qualitative *in situ* zymography findings on histological sections of the abdominal aorta, which show suppression of gelatinolytic activity in tissues in the EL-NP-BB94 group alone [193]. Others have shown that a daily IP injection of 15 mg of BB-94 inhibited the expansion of AAA in elastase-induced aneurysms in rats However, the study lasted for only seven days, and AAA was treated only by the systemic inhibition of MMPs. We show that targeted NPs with very low concentrations of BB-94 injected only once weekly (equivalent to 25 μg total BB-94/animal/day) can significantly inhibit aneurysm expansion in a four week study. This corresponds to a 580-fold lower BB-94 concentration than others have used systemically[103]. Several clinical trials for systemic MMP inhibition as a cancer treatment failed because of poor bioavailability, dose limiting toxicity, and systemic side effects, such as musculoskeletal problems, which limited the dose that could be tolerated.[168] The side effects caused by MMP inhibitors in cancer patients led to the use of substantially lower doses of MMP inhibitors in clinical trials for aneurysm prevention[170]. The propranolol treatment was successful in aneurysm-prone turkeys and caused an increase in the tensile strength of tissue rings from the abdominal aorta.[194] However, clinical trials of the systemic delivery of, beta-blockers like propranolol, did not show significant changes in the growth rate of aneurysms, but caused systemic side effects and reduced patient compliance[11,169], thus dampening enthusiasm for pharmacological therapy for AAA. Because our targeted treatment's site-specificity permits very low doses of the drug, such therapy will be an

attractive option for preventing the expansion of aneurysms in patients without causing systemic side effects.

In conclusion, we demonstrate that targeted delivery of very small doses of MMP inhibitor BB-94 by NPs is an effective way to suppress MMP activity and aneurysmal development in an experimental rat model of AAA.

CHAPTER V

TARGETED THERAPY WITH NANOPARTICLE LOADED WITH PENTAGALLOYL GLUCOSE (PGG) PROTECTS VASCULAR ELASTIC LAMINA FROM MMP-MEDIATED DEGRADATION AND PREVENTS PROGRESSION OF ABDOMINAL AORTIC ANEURYSM (AAA)

Abstract

Rationale

It has been established that elastin degradation is a primary cause of AAA[171], and whether AAA is large or small, regression of it and restoration of normal arterial architecture would be preferable. Although no one previously could show elastin regeneration, our group demonstrated the protective effect of PGG in terms of protecting damaged and non-damaged elastin from protease degradation and the ability of PGG to help tropoelastin molecules to assemble and make new crosslinked elastin by vascular smooth muscle cells[121]. We have already developed NPs that target to AAA. We would like to use these NPs to deliver PGG at the site of aneurysms. Such site-specific targeting of PGG would help arterial elastin restoration. With the regeneration of elastin, we can reverse the progression of aneurysms.

Objective

Degeneration of elastin plays a vital role in the pathology and progression of abdominal aortic aneurysm (AAA), a disease that is characterized by damage to the arterial wall. Our previous study showed that pentagalloyl glucose (PGG), a core derivative of tannic acid, hinders the development of AAAs in a clinically relevant

animal model when applied locally. In this study, we tested whether targeted nanoparticles (NPs) can deliver PGG to the site of an aneurysm and prevent aneurysmal growth by protecting elastin.

Approach and Results

PGG-loaded albumin NPs with a surface-conjugated elastin-specific antibody were prepared and characterized by size, surface charge, PGG release, cellular toxicity, and uptake. Aneurysms were induced by calcium chloride-mediated injury to the abdominal aorta in rats. NPs were injected into the tail vein after 10 days of $CaCl_2$-injury. Rats were euthanized after 38 days, and aneurysmal development was studied. PGG-loaded NPs were non-toxic and were not taken up by vascular smooth muscle cells, macrophages, or endothelial cells in vitro. NPs with a surface tethered elastin antibody targeted and delivered PGG to the aneurysmal site. Such PGG delivery led to reduction in macrophage recruitment, matrix metalloproteinase (MMP) activity, elastin degradation, calcification, and development of aortic aneurysm as compared to control blank NPs(57±25% vs. 158±47% dilation, respectively).

Conclusions

Targeted delivery of PGG protects aortic elastin from further degradation in aneurysm-prone arterial segments. It offers the potential for the development of effective and safe therapies for AAA.

Introduction

Abdominal aortic aneurysm (AAA) is a vascular disease characterized by the expansion of the abdominal aorta due to structural weakening of the aortic wall. Five-to-nine percent (5-9%) of people over 65 years of age suffer from AAA; the mortality rate for ruptured AAAs is 90%.[195] The cause of AAA is unknown in the majority of cases; however, the key regulators involved in the pathogenesis of this disease are known. Animal studies show the possible efficacy of medications like statins, RAS inhibitors, beta adrenoceptor blockers, nonsteroidal anti-inflammatory medications, and macrolides in the treatment of AAA, but relevant clinical studies are limited[196]. Extracellular matrix (ECM) degradation of the wall of the aorta is a key contributor to the progression of the disease [197]. Matrix metalloproteinases (MMPs) are enzymes that are responsible for the degradation of ECM components. As inflammation progresses, infiltrating cells secrete pro-MMPs, which are activated extracellularly and degrade the ECM, specifically elastin laminae[198]. Thus, one approach to mitigate the progression of AAA is to treat the injury site with MMP inhibitors, such as hydroxyamate-based MMP inhibitors like batimastat[103], marimastat[199], and prinomastat[97]. Our group has previously shown a significant reduction in the development of AAA with the targeted delivery of batimastat, a hydroxyamate-based MMP inhibitor[200]. However, enzyme inhibitors can only stop further degradation but cannot reverse the disease.

To completely restore the structural integrity of the aortic wall, it is necessary not only to prevent degradation, but to also allow for regeneration of the elastic lamina. In previous studies, we have shown that a plant-derived polyphenolic tannin, pentagalloyl

glucose (PGG), has the ability to prevent elastolytic degradation by binding to enzyme cleavage sites on elastin. This high affinity of PGG to elastin allows PGG to form a protective coating that prevents further degradation[14]. We showed that a single periadventitial administration of PGG prior to $CaCl_2$ injury in rats prevented degradation of elastin and hindered AAA development. Recently, we have shown that PGG significantly increased insoluble elastin in rat aortic smooth muscle cells (RASMCs) from both healthy and aneurysmal aortae[121].

In this study, we tested the hypothesis that PGG-loaded bovine serum albumin (BSA) NPs with a surface conjugated elastin antibody will allow for the targeted delivery of PGG to the site of aortic aneurysm in a $CaCl_2$ mediated injury model. We show that such systemic therapy both specifically targets the aneurysmal site while sparing the healthy aorta and delivers PGG to the site. This local release of PGG provides a protective barrier for elastin from degradation in early stage aneurysm. We further show that such NP therapy allows regeneration of the damaged elastic lamina and significantly suppresses aneurysmal expansion of the aorta.

Materials and Methods

PGG-Loaded NPs Preparation

Bovine serum albumin (BSA) NPs were prepared by coacervation[201]. Nanoparticles (NPs) were obtained by dissolving 250 mg of BSA (Seracare, MA, U.S.A.) in 4 mL of deionized (DI) water. Pentagalloyl glucose (PGG, 125 mg) was dissolved in 400 µl of dimethyl sulfoxide and added slowly to the BSA solution. After an hour of stirring, the mixture was added dropwise to 24 mL of ethanol under continuous

sonication (Omni Ruptor 400 Ultrasonic Homogenizer, Omni International Inc, Kennesaw, GA) for half an hour. Glutaraldehyde (EM grade 70%, EMS, PA, USA) was added during stirring at different concentrations of 0.3, 0.7, 1, 12, and 100 µg/mg protein (BSA). These batches are named 0.3, 0.7, 1 and 12 hereafter.

DIR Loaded NPs Fabrication

Nanoparticles (NPs) were obtained by dissolving 250 mg of bovine serum albumin (BSA; Seracare, MA, U.S.A.) in 4 mL of deionized water. 2.5 mg of fluorescent dye, 1, 1-dioctadecyl-3, 3, 3, 3-tetramethylindotricarbocyanine iodide (DIR) was dissolved in 100 µl of acetone and added later to the BSA solution. After an hour of stirring, the mixture was added dropwise to 24 ml of ethanol under continuous sonication (Omni Ruptor 400 Ultrasonic Homogenizer, Omni International Inc., Kennesaw, GA) for half an hour. For crosslinking, glutaraldehyde (EM grade 70%, EMS, PA, U.S.A.) was added during. For animal studies to get the highest loading, 42 µg glutaraldehyde per mg BSA was used. For *in vitro* studies, different recipes were followed. For normal negatively charged ~200 nm sized particles, 12 µg glutaraldehyde per mg BSA was used and nanoparticles were conjugated as will be described in the next section. For positively charged ~200 nm sized particles, 12 µg glutaraldehyde per mg BSA was used. For negatively charged ~50 nm sized particles, 6 µg glutaraldehyde per mg BSA was used and sonication time was 60 min.

Conjugation of Elastin Antibody to NPs

Ten milligrams (10 mg) of pentagalloyl glucose (PGG)/DIR loaded NPs were incubated with 2.5 mg heterobifunctional crosslinker α-maleimide-ω-N-hydroxysuccinimide ester poly (ethylene glycol) (Maleimide-PEG-NHS ester, MW 2000 Da, Nanocs Inc., NY, U.S.A.) to achieve a sulfhydryl-reactive particle system. Traut's reagent (34 µg, G-Biosciences, Saint Louis, MO) was used for thiolation of 10 µg of rabbit anti-rat elastin antibody (United States Biological, Swampscott, MA), and the mixture was incubated in HEPES buffer (20 mM, pH=9.0) for an hour at room temperature. Thiolated antibodies were rinsed with HEPES buffer and were added to NPs (4 µg antibody per 1 mg NPs) and incubated overnight for conjugation.

Nanoparticle Yield

To quantify the NP yield, the total final dry weight of the NPs was recorded, and NP yield was calculated using the formula below:

$$\text{NP yield } \% = \frac{\text{Final dry weight}}{\text{Initial weight}} \times 100\% \qquad (5)$$

Characterization of PGG Loaded Albumin NPs—
Particle Size, Zeta Potential

Particle size and zeta potential of the NPs in suspension were determined using a 90Plus Particle Size Analyzer (Brookhaven Instruments Co., Holtsville, NY).

Loading efficiency of PGG in the NPs was quantified by determining PGG concentration in the washed out ethanol at λ (max) = 765 nm using UV spectrophotometry and the equation shown below:

$$\% \text{ Loading} = \frac{\text{Initial PGG} - \text{washed PGG weight}}{\text{Total weight of NPs}} \times 100 \qquad (6)$$

In vitro Release Studies

Release kinetics was determined by suspending a known amount of NPs in phosphate buffered saline at 37°C on a shaker. Suspensions were centrifuged for 15 minutes at 4000×g at room temperature for various periods of time. The supernatant was collected and analyzed for PGG concentration by the addition ferric chloride, which binds to PGG, and the absorbance was read at 765 nm with a spectrophotometer. Percent release was calculated as:

$$\%\ PGG\ Released = \frac{\text{Amount of released PGG}}{\text{Initially loaded PGG}} \times 100\% \qquad (7)$$

In vitro Cytotoxicity of PGG Loaded NPs

Rat aortic smooth muscle cells, rat aortic endothelial cells and rat bone marrow macrophage cells (Cell Biologics, Inc., RA-6030F) were cultured and then incubated with NPs for blank (0.5 mg/ml) and PGG-NPs (0.5 mg/ml) for 24 hours. A Live/Dead assay (Life Technologies, Inc., MD, U.S.A.) was performed according to the manufacturer's protocol to confirm cell viability. Cell number was calculated from the activity of lactate dehydrogenase (LDH) using CytoTox 96® Non-Radioactive Cytotoxicity Assay (Promega).

Macrophage Uptake of NPs

Elastin-antibody conjugated NPs were loaded with the fluorescent dye, DIR (EL-NP-DIR), as described above. Macrophages (RAW 264.7, ATCC® TIB-71™) were grown in 24-well tissue culture plates and subsequently incubated with EL-NP-DIR (1 mg/ml) at 37°C in 5% CO_2 for 24 hours. Cells were washed afterwards with sterile

phosphate buffered saline for a total of three washes. Cells were imaged before and after the washing step using the EVOS® XL Cell Imaging System to determine NP uptake. Two different batches of NPs were prepared as controls for charge and particle size. One batch was prepared with a positive surface charge, and another batch was prepared with a smaller particle size as described in DIR loaded NPs fabrication section. Positive surface charge was created by coating the NPs with deacetylated low molecular weight chitosan[2] (Sigma, St. Louis, MO). Normal NPs were conjugated with elastin antibody while we didn't conjugate other two batches.

In vivo Study—Early Stage Aneurysm

The rat abdominal aortic section (infrarenal) was subjected to perivascular application of calcium chloride to induce local elastin degradation[200].

Briefly, male Sprague-Dawley rats (5-6 weeks old) (n=24) were placed under general anesthesia by inhalation of 2% to 3% isoflurane. Calcium chloride was applied periadventitially by placing a 0.50 mol/L $CaCl_2$-soaked sterile cotton gauze pad on the infra-renal abdominal aorta for 15 minutes. Afterwards, warm saline was used to flush the area, and sutures were used to close the incision. Animals were given a normal diet for ten days. Three animals were euthanized to study histological Changes after ten days. NPs loaded with PGG and conjugated with an elastin antibody (EL-NP-PGG, ~10mg/kg body wt.) were suspended in 200 µl of phosphate buffered saline and injected into rats (n=6) through the tail vein once every two weeks for a total of four weeks (2 injections total). Control animals received elastin antibody-conjugated blank NPs (EL-NP-Blank) (n=6). Nine other rats were injected with elastin antibody conjugated and 1, 1-

dioctadecyl-3, 3, 3, 3-tetramethylindotricarbocyanine iodide (DIR) dye-loaded NPs (EL-NP-DIR) to study the delivery of the NPs to the abdominal aorta through *in vivo* imaging. From these nine rats, three were euthanized one week after the first injection; the other three were euthanized two weeks after the first injection. The last three received one extra injection in week two for a total of two injections, and these rats were euthanized after four weeks. After euthanizing rats, the whole body and the individual organs were imaged using a Caliper IVIS Lumina XR (Hopkinton, MA) with Ex/Em of 745/795 nm, to calculate the biodistribution and targeting of the NPs to the site of injury in the aorta. Biodistribution was calculated based on the equation below:

$$\%\ \text{Biodistribution} = ((\text{Fluorescence in tissue})/(\text{Total fluorescence in all organs}))/(\text{Dry weight of tissue}) \times 100\% \quad (8)$$

Rats from the EL-NP-Blank and EL-NP-PGG groups were euthanized on day 38, and tissues were harvested and snap frozen or formalin fixed for further analysis.

Ultrasound Analyses of the Abdominal Aorta

A high-frequency ultrasound device (Vevo 2100, VisualSonics, Toronto, Canada) utilizing a linear array probe (MS 400D, frequency 30–55 MHz) was used to complete ultrasound imaging of the abdominal aorta. During the imaging, the animals were kept under light anesthesia by inhalation of 2% isoflurane, and fixed in the dorsal position on the imaging table. Vevo 2100 analysis software was used to process M-Mode ultrasound data. Three different cardiac heart beats were recorded for each M-Mode measurement made. Systolic and diastolic diameters were measured, and this data was used to

calculate the circumferential cyclic Green-Lagrange strain with the assumption that strain is uniform around the vessel according to the following equation:

$$\text{Circumferential strain} = \frac{1}{2}((D_{sys}/D_{dia})^2-1)*100\% \quad (9)$$

Where, Dsys = Systolic internal diameter and Ddia = Diastolic internal diameter

Measurement of Matrix Metalloproteinase (MMP) Activity in the Aorta and *In Situ* Zymography

Aortic tissues frozen in liquid-nitrogen were pulverized and homogenized in RIPA extraction buffer (50 mM Tris-HCl pH 7.4, 150 mM NaCl, 1 mM EDTA, 1% Triton X-100, 1% Sodium deoxycholate, 0.1% SDS, with protease inhibitor cocktail) (Roche Diagnostic GmbH, Germany) in accordance with the manufacturer's protocol to extract protein from the aortic tissues. The total protein from the explanted aortic tissue after 38 days was quantified using the BCA protein assay (Pierce, IL). MMP-2 and MMP-9 activity were measured using an internally quenched peptide substrate (excitation 280 nm, emission 360 nm, MMP Substrate III, Anaspec, CA). One mg of the substrate was dissolved in 50 µL of dimethyl sulfoxide, and the solution was diluted in 10 mL of development buffer (50 mM Tris Base, 5 mM $CaCl_2 \bullet 2H_2O$, 200 mM NaCl, 0.02% brij 35). 2 µL of substrate stock solution and 2 µL of the extracted protein were mixed with 96 µL of the development buffer and incubated for one hour at 37°C. A fluorescent plate reader was used to read endpoint florescence intensity.

To examine the activity of MMPs in the aortic tissue samples *in situ* zymography was performed on frozen sections. Gelatinolytic activity was demonstrated in frozen sections (8 µm thick) using DQ-gelatin as a substrate (Life Technologies, IL). Cryostat

sections of abdominal aorta were air-dried for 10 minutes at 4°C. One part DQ-gelatin (1 mg/ml of DI water) was mixed with nine parts 1% agarose (Promega, WI) in phosphate buffered saline containing DAPI (1 μg/ml) (Life Technologies, IL). A drop of the mixture was added to each section and incubated in development buffer for one hour at 37° C. As a positive control, in one sample MMP activity was blocked by MMP inhibitor 1, 10-phenanthroline monohydrate (0.2mmol/L) (Life Technologies, OR). Images were captured using the EVOS® XL cell imaging system.

Desmosine Content

The snap frozen samples of rat aortas (abdominal) were pulverized, lyophilized, and hydrolyzed in 6N HCl at 95°C for 12 h. The samples were dried under a continuous stream of nitrogen gas (~45 minutes) and subsequently reconstituted in 1.0 mL of 0.01 N HCl. The desmosine content was measured using an Enzyme Linked Immunosorbent Assay kit (MyBioSource, San Diego, U.S.A., catalog number MBS748709) according to the manufacturer's protocol. For comparison, three healthy abdominal aortas (non-injured) were studied for desmosine content.

Lysyl Oxidase (LOX) Activity Assay

Aortic tissue snap frozen in liquid nitrogen was pulverized and homogenized in 500 μl of 6 M urea, 50 mM Tris (pH 7.4), 1 mM PMSF Protease Inhibitor, 1 μM pepstatin A, and 6 μM leupeptin. The homogenates were shaken on a plate shaker at 4°C overnight. The homogenized tissues were then centrifuged at 10,000g for 30 min at 4°C. The pellets were then suspended in the same buffer and homogenized and centrifuged

again. The supernatant was collected, and LOX activity was measured by quantifying LOX concentration using the Amplite Fluorimetric LOX Assay Kit (AAT Bioquest, Sunnyvale, CA, U.S.A., catalog number 15255)[202].

Aneurysmal Development

Initial external diameter was measured at the time of $CaCl_2$ injury. Final aortic diameter was recorded before euthanasia on day 38. Aneurysmal development was calculated as mentioned before.

Histological Analysis

Formalin-fixed samples were embedded in paraffin, and 5 µm sections were made and mounted on glass slides. The slides were heated overnight 55-60°C to adhere the tissues to the slides and melt the paraffin. Subsequently, the slides were deparaffinized with xylenes and graded ethanol and stained with Verhoeff-van Gieson (VVG) staining for elastic fibers, Alizarin Red S staining with a Light Green SF counterstain for calcification, hematoxylin and eosin staining for tissue morphology, and phenol staining for PGG.

Immunostaining for Macrophages (CD68)

Tissues preserved with formalin were embedded in paraffin and sectioned as previously described. Subsequently, the slides were deparaffinized with xylenes and graded ethanol, and antigen retrieval was done using citrate buffer (Millipore, MA, Catalog number 21545). The slides were incubated overnight at 4°C with the primary antibody, Mouse Anti Rat CD68 (AbD Serotec, Catalog number, MCA341GA). Staining

was completed using a DAB kit (Enzo Life Sciences, NY, Catalog number ADI-950-122-0100).

Immunofluorescence for PECAM-1 (CD31)

Tissues from DIR rats preserved with formalin were embedded in paraffin and sectioned as previously described. Subsequently, the slides were deparaffinized with xylenes and graded ethanol, and antigen retrieval was done using citrate buffer (Millipore, MA, Catalog number 21545). The slides were incubated overnight at 4°C with the primary antibody, Rabbit Anti Rat CD31 (Novus Biologicals, Catalog number, Nb100-2284). Staining was completed using TRITC conjugated goat anti-rabbit IgG (Jackson ImmunoResearch Laboratory, Catalog number 111-025-003).

Alanine Aminotransferase (ALT) Analysis

Blood was drawn via a heart stick with a 3 mL syringe, and the blood was centrifuged at 3000 rpm for 3 min. The serum was examined for the activity of Alanine Aminotransferase (ALT) using a commercially available kit (Sigma, St. Louis, MO, Catalog number, MAK052).

Histological Analysis of Liver

Formalin-fixed samples were embedded in paraffin, and 5 μm sections were mounted on glass slides and heated overnight to adhere the tissues to the slides and melt the paraffin. Subsequently, the slides were deparaffinized with xylenes and graded ethanol and stained with hematoxylin and eosin for tissue morphology.

Statistical Analysis

Data were analyzed by one-way ANOVA followed by Tukey's test or Dunnett's test. Levene's test was used to verify the homogeneity of variances and normality assumption was checked using a Shapiro-Wilk test. Dunnett's procedure was used when comparing all other treatments to a reference and Tukey's was used for all pairwise comparison.

Exact permutation test was performed using the NPAR1WAY procedure in SAS. The data are expressed as the mean ± standard deviation; results were considered to be significant when P-values ≤ 0.05.

Results

Nanoparticle Yield and Loading

BSA NPs were prepared with the coacervation method. The batch with 12 µg glutaraldehyde/mg BSA had the best yield (~61%), which was significantly higher than the yield for other batches (See Figure 23A). The batch with 12 µg glutaraldehyde/mg BSA also showed good PGG loading as compared to the other batches (See Figure 23B).

Particle Size and ζ-Potential

NP size increased with increasing glutaraldehyde concentration during NP preparation. Increased size led to a decrease in ζ-potential; however, all NPs showed negative surface charge (See Figure 24).

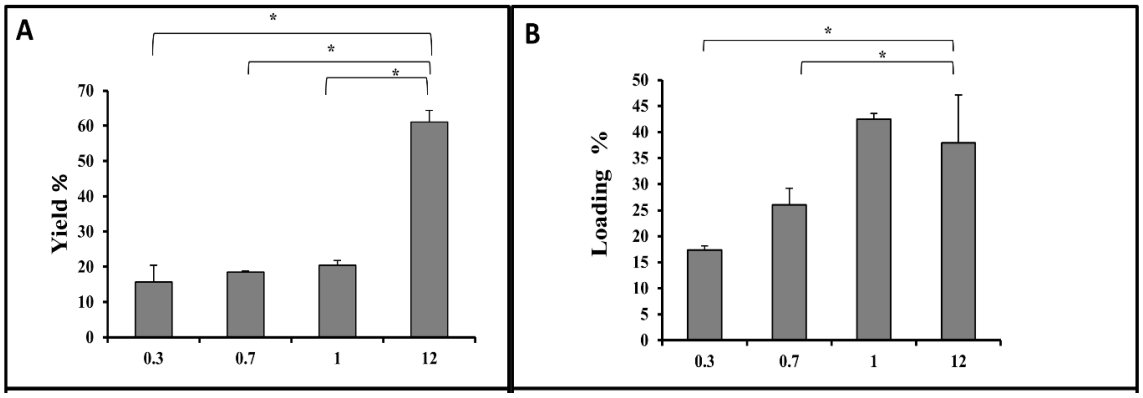

Figure 23. Yield and Loading of NPs with 0.3, .7, 1 and 12 µg glutaraldehyde per mg of BSA. (n=3). (*, P<0.05, Dunnett's test, compared to the 12 µg group).

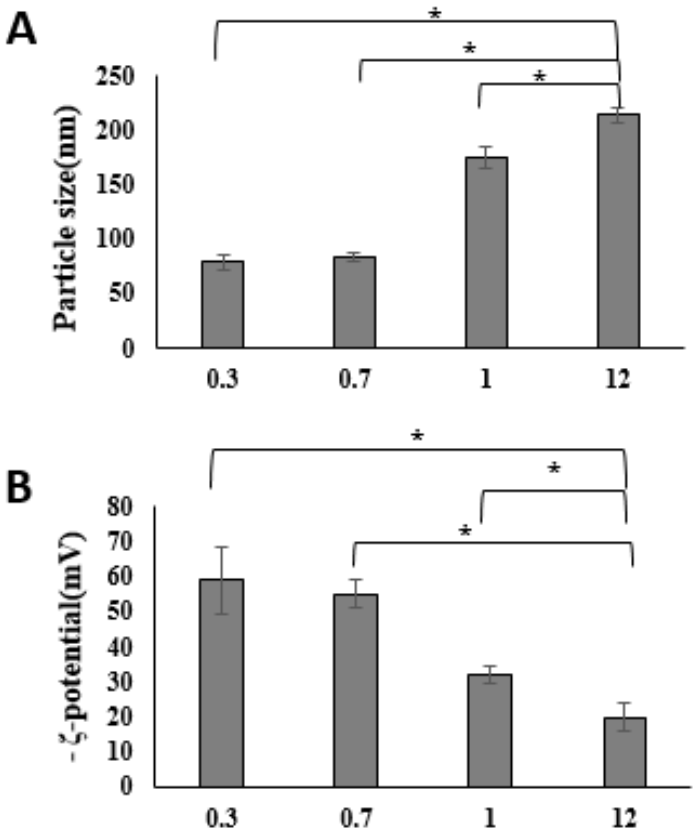

Figure 24. Zeta potential and particle size of NPs with 0.3, 0.7, 1 and 12 µg glutaraldehyde per mg of BSA. (n=3). (*, P<0.05, Dunnett's test, compared to the 12 µg group).

In vitro PGG Release from Nanoparticles

The PGG was released within 10 days with significant burst release in the first few hours from all batches of NPs except the batch in which 12 µg glutaraldehyde/mg BSA was added during sonication. This particular batch showed more controlled release of PGG that lasted for 60 days (See Figure 25); thus, these NPs were chosen for further studies.

In vitro Cytotoxicity and Macrophage Uptake

The rat aortic smooth muscle cell (RASMCs), the rat aortic endothelial cell (RAOEC), and the rat bone marrow macrophage (BMM) viability as assessed by live-dead assays showed no significant change after 24 hours of incubation with NPs in comparison to the control (See Figure 26).

No significant changes were observed in number of cells based on LDH assay (See Figure 27).

Because many macrophages are present at the AAA site, we assessed macrophage uptake of NPs *in vitro*. NPs loaded with 1, 1-dioctadecyl-3, 3, 3, 3-tetramethylindotricarbocyanine iodide (DIR) dye (ζ-potential~ -31, size~ 200 nm) were incubated with cells for 24 hours. Macrophage uptake was not detected due to the negative charge and optimum size of the NPs (See Figure 28, I and II). When the surface-charge was changed to be positive with the addition of chitosan, (ζ-potential: +13, size~ 200 nm) or when NPs were smaller (ζ-potential: -37, size~ 50 nm), NPs were seen in the cell cytoplasm, indicating cellular uptake (See Figure 28, III-VI). Thus, we

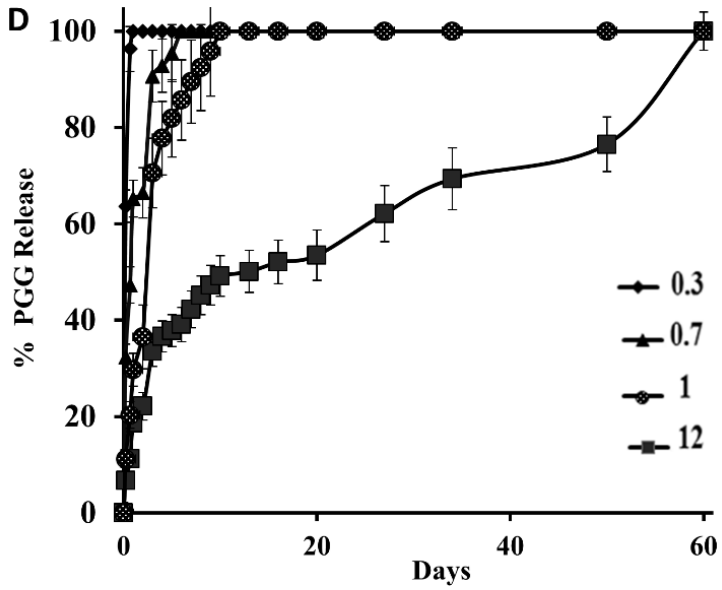

Figure 25. Release kinetics of PGG over 60 days.

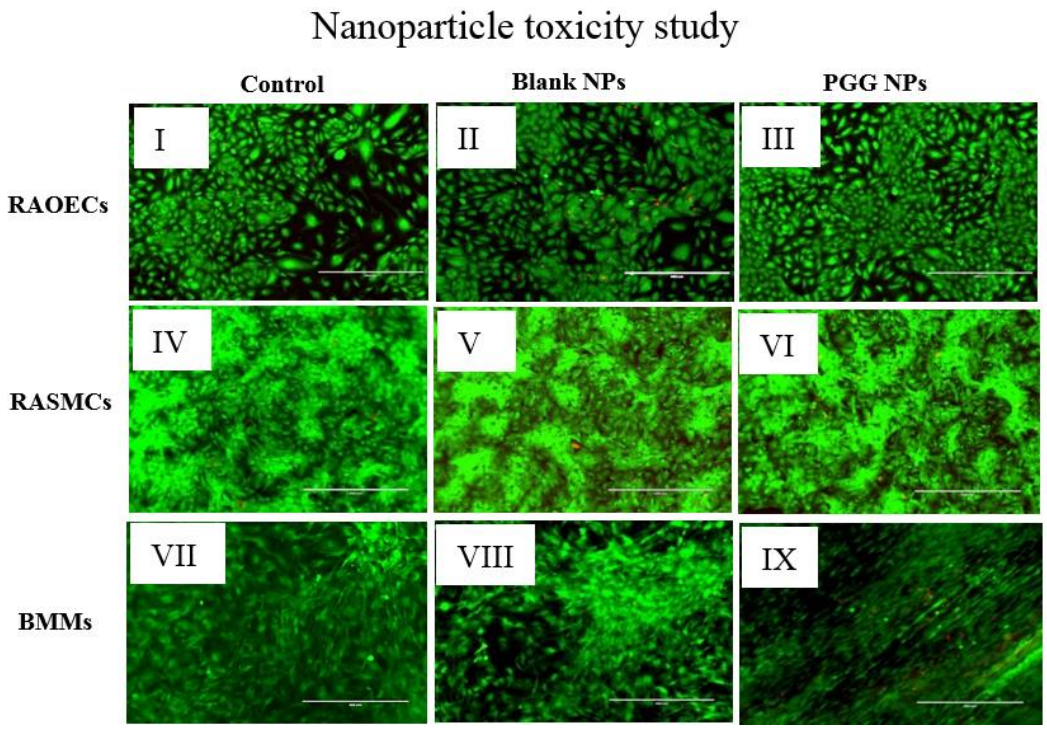

Figure 26. Cell viability.

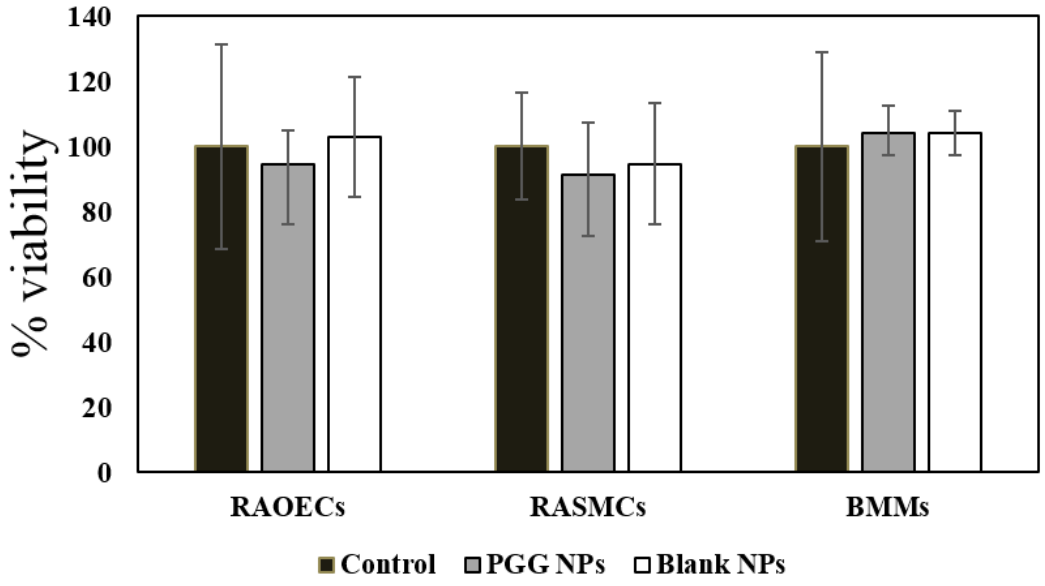

Figure 27. Cells viability quantification.

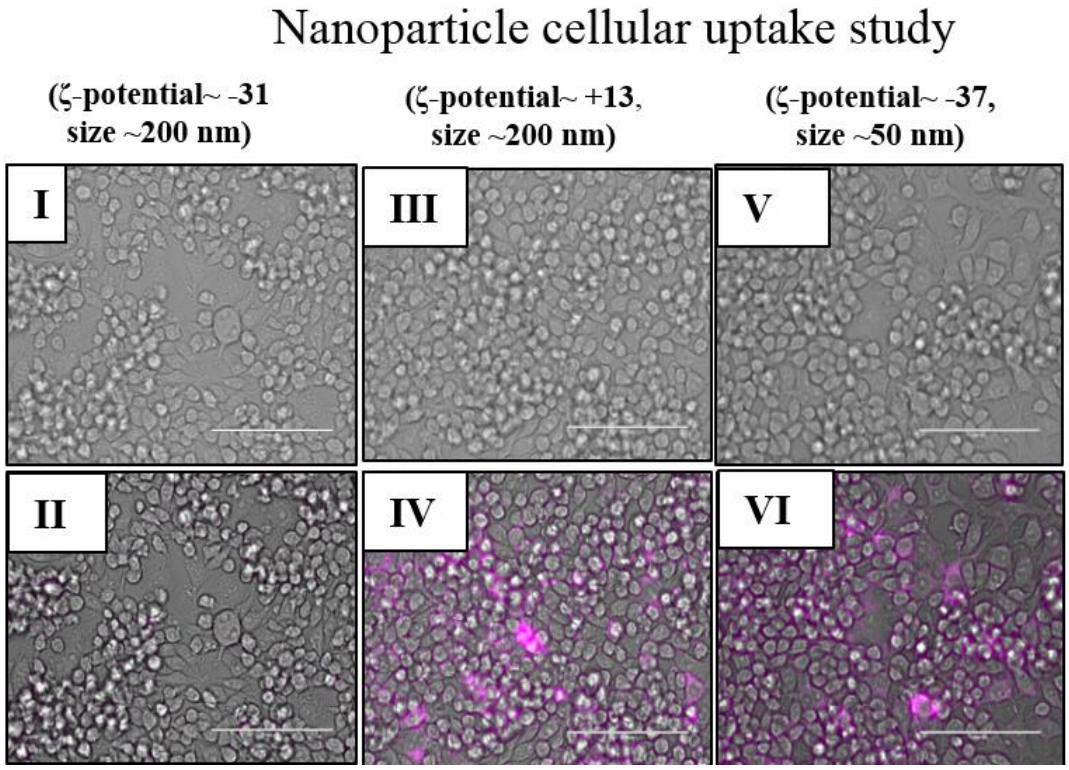

Figure 28. NPs uptake by macrophages.

used NPs with negative surface charge and ~200 nm particle size for animal studies because they were resistant to macrophage uptake.

Biodistribution of NPs

We used a calcium chloride-mediated acute perivascular injury model to cause elastin degradation and aneurysmal expansion in the infrarenal abdominal aorta of rats. Ten days after injury, DIR dye-loaded NPs were systemically administered via tail vein injection. The NPs targeted the injured aortic elastic lamina sites within the first few hours and were retained even after one week as measured by fluorescence intensity (IVIS, 59±8% targeting based on per weight basis). NPs remained at the site of elastin damage in the aorta after two weeks with no additional injections, although the amount of NPs decreased (36±5%). With the addition of another injection at two weeks, targeting to the damaged aorta was restored to 67±13% when tested at four weeks, suggesting that one injection every two weeks can successfully keep NP targeting at a high level (See Figure 29).

The fluorescence signal of DIR (% florescence/dry weight of organ) after 4 weeks decreased from 5.6% to 4.7% for the kidneys, from 2.6 to 1.6% for the liver, and from 30 to 20% for the spleen in comparison to the fluorescence observed after 1 week (See Figure 30). These results show that NPs accumulated at the injury site, while other organs were clearing non-targeted NPs.

More significantly, infiltration of the NPs was seen from the vasa vasorum on the adventitial side rather than from the luminal side (See Figure 31A) while nanoparticle did not stay in vasa vasorum (See Figure 31B).

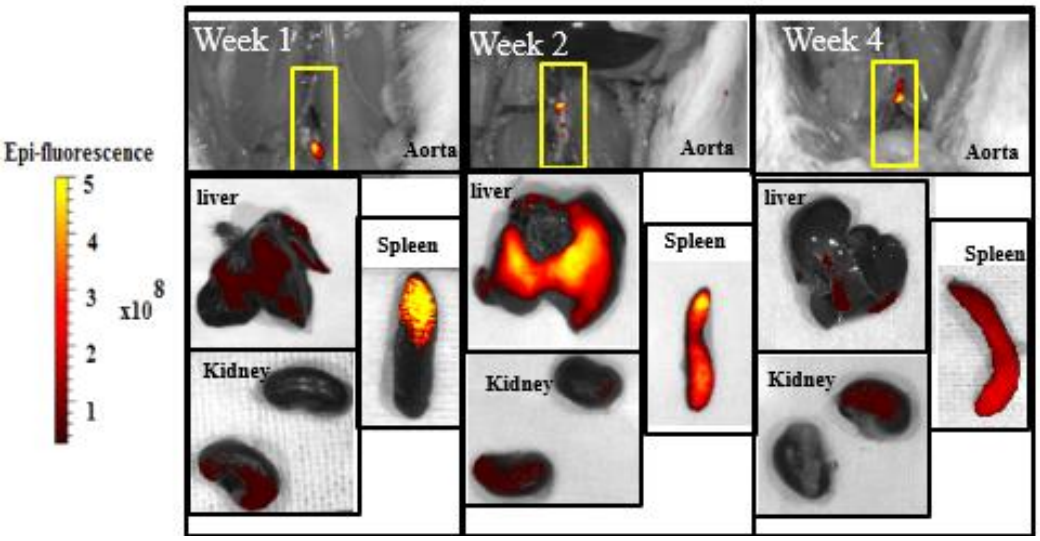

Figure 29. DIR NPs after one, two and four weeks in different organs.

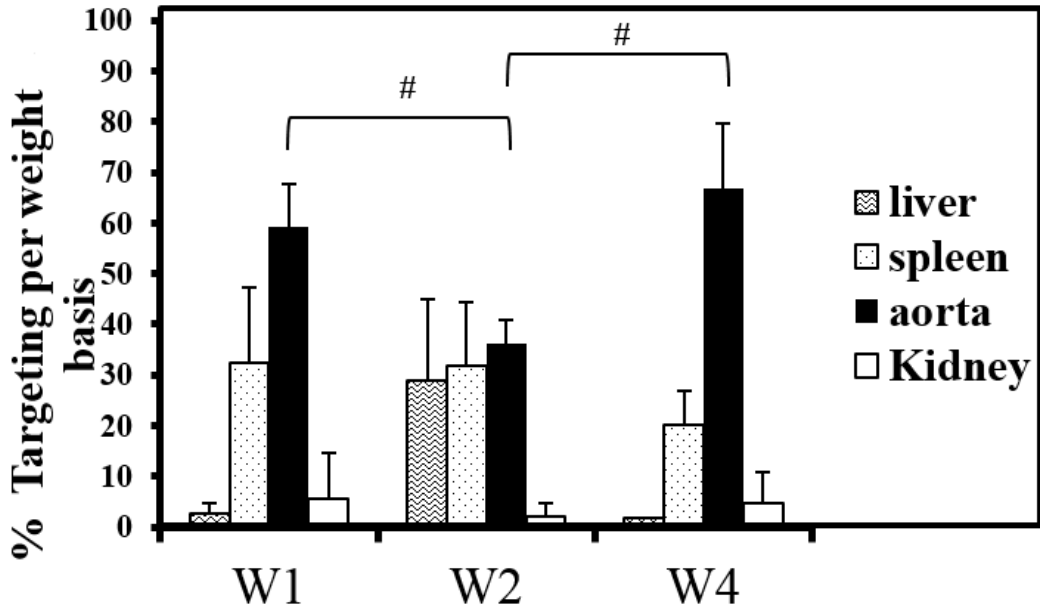

Figure 30. Organ distribution of fluorescent NPs after one, two, and four weeks. (#P < 0.05, Tukey's test, for pairwise comparison). (n=3 per time point)

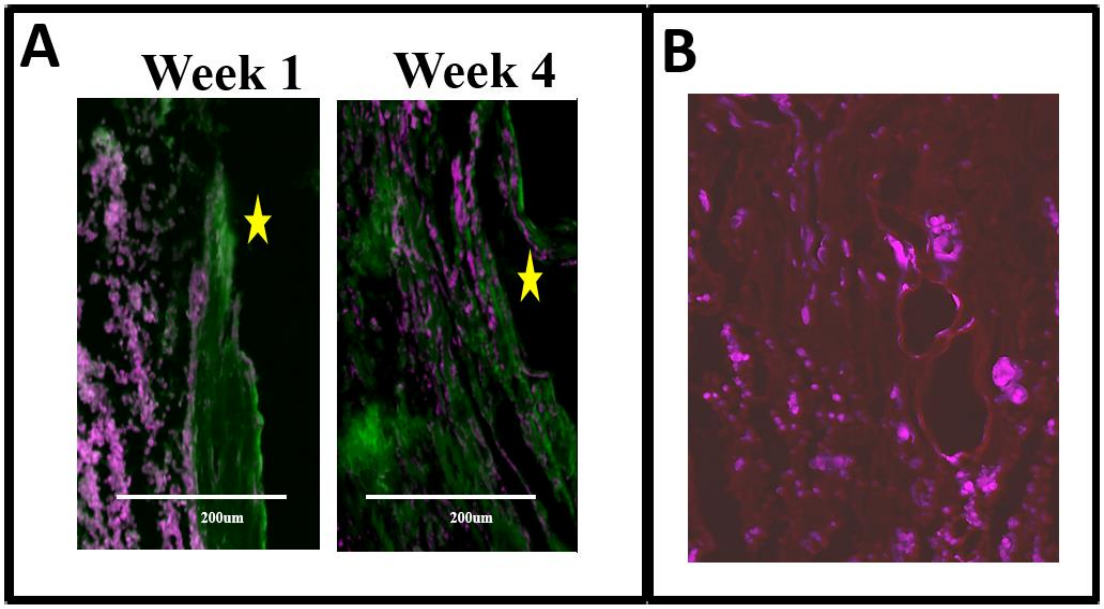

Figure 31. Cross-section of abdominal aorta showing NPs(purple) and vasa vasorum(Red).

Histological Analysis of the Abdominal Aorta

Histological sections of aortae 10 days post calcium chloride injury showed elastin damage (See Figure 32).

After confirming elastin damage 10 days post injury, in order to study the effect of targeted delivery of PGG, we systemically injected either EL-NP-PGG or EL-NP-Blank (control without PGG) NPs ten days after $CaCl_2$ injury once every two weeks. Hematoxylin and eosin staining showed significant inflammation in the adventitia in the EL-NP-Blank group with a degraded medial layer (See Figure 33A), while the EL-NP-PGG group maintained greater structural integrity and had little inflammation after 38 days (See Figure 33B). Verhoeff-van Gieson (VVG) staining revealed that the elastic lamina was broken and damaged in the EL-NP-Blank group (See See Figure 33C) while

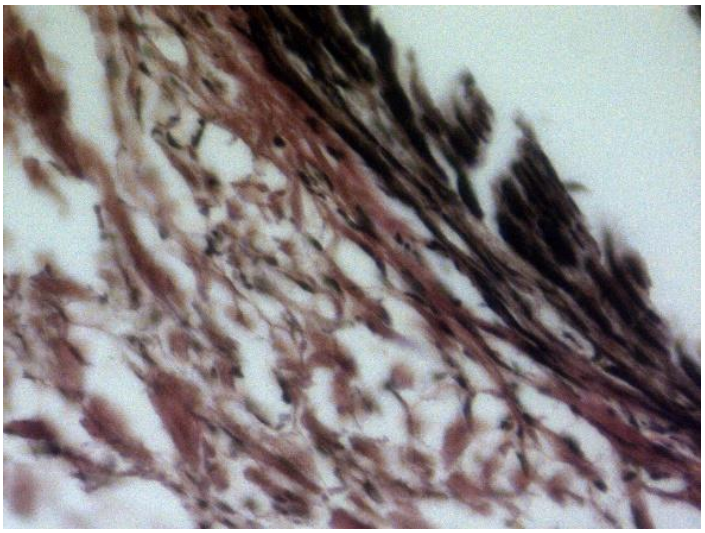

Figure 32. Histological section of abdominal aorta 10 days after calcium chloride injury.

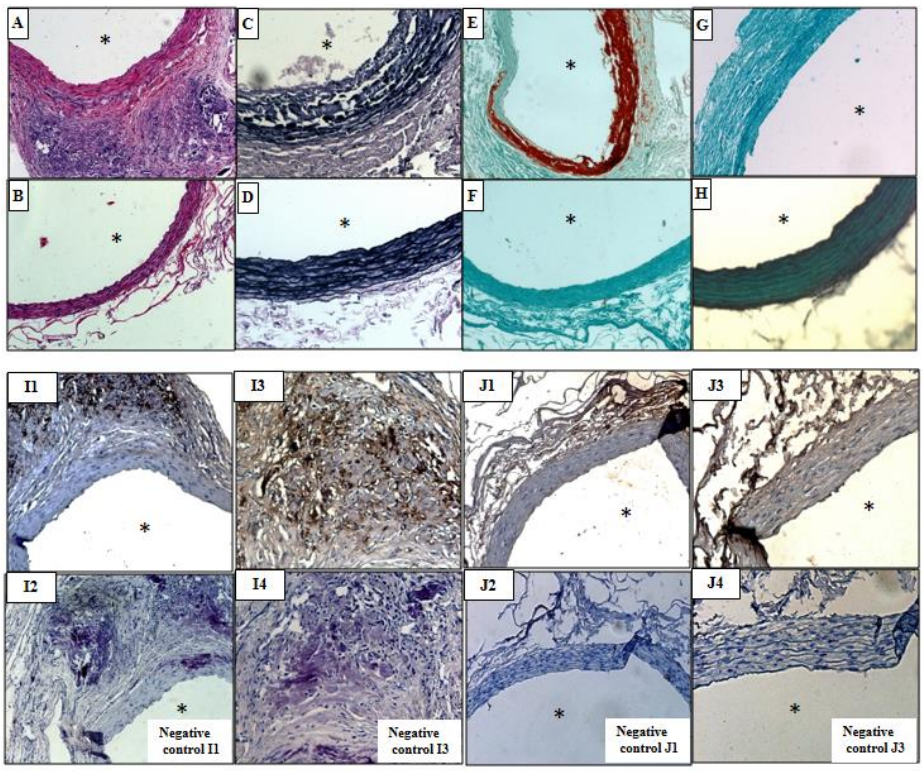

Figure 33. Histological analysis.

the elastic lamina was preserved in the EL-NP-PGG group (See Figure 33D). Alizarin Red-S staining showed heavy medial calcification in the EL-NP-Blank group (See Figure 33E), and a substantial reduction in calcification in the EL-NP-PGG group (See Figure 33F). For histological confirmation of PGG delivery by the NPs, aortic tissues were stained with a phenol-specific stain. Only the EL-NP-PGG group showed phenol specific staining surrounding the elastic lamina (See Figure 33H), while the EL-NP-Blank group showed no phenolic staining (See Figure 33G), clearly suggesting that NPs delivered PGG to the aneurysmal site. Macrophage immunohistochemistry showed pan-macrophage marker (CD68) in EL-NP-Blank group adventitia (See Figure 33I1-4) while EL-NP-PGG group doesn't show CD68 (See Figure 33J1-4).

Moreover, full aortic sections were shown in all six rats of each group (See Figure 34).

Circumferential Strain Assessment with High-Frequency Ultrasound

Circumferential strain for young healthy rats before calcium chloride injury was 12.25±1.28% (See Figure 35A). It was reduced to 3.27±2.7% for the EL-NP-Blank group at 38 days after injury suggesting stiffening of the aorta (See Figure 35B). Circumferential strain for the EL-NP-PGG group was similar to the healthy control 11.93±1.38% after 38 days, clearly suggesting that PGG maintained healthy elastic lamina and aortic elasticity (See Figure 35C).

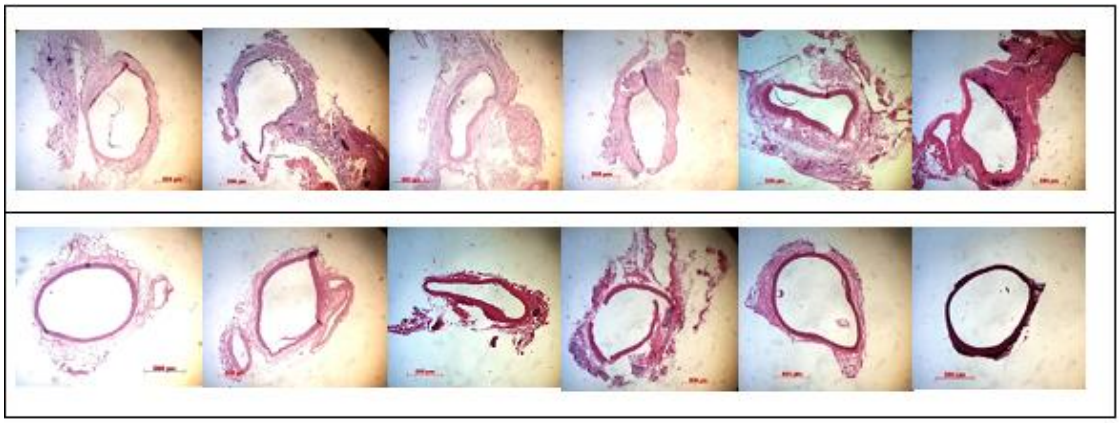

Figure 34. Hematoxylin and eosin staining of whole aortic sections.

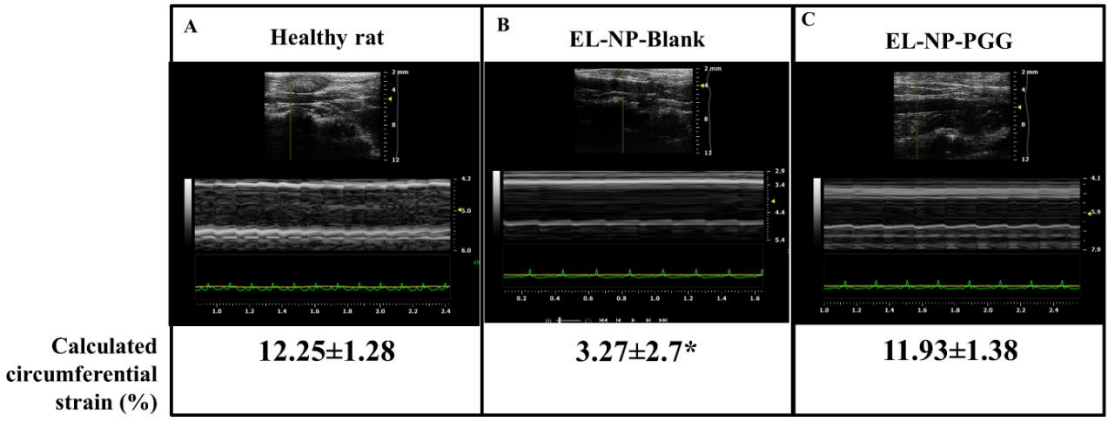

Figure 35. M-mode tracings and circumferential cyclic strain over 38 days.

MMP Activity

We next examined if NPs loaded with PGG inhibited local MMP activity at the site of AAA. Snap frozen tissues were collected, and MMP activity was measured with a MMP fluorogenic substrate assay. When normalized to total protein content and reported as abdominal/thoracic aorta, fluorescence intensity data, the EL-NP-Blank group showed

a 250% increase in MMPs as compared to the healthy thoracic aorta. In the EL-NP-PGG group, MMP activity was suppressed to healthy levels (See Figure 36A). This result was further confirmed by in situ zymography for MMPs where high activity was seen in the EL-NP-Blank group, while minimal MMP activity was seen in EL-NP-PGG group (See Figure 36A B).

Elastin Remodeling at the Aneurysm Site

Lysyl Oxidase (LOX) activity assay: When blank NPs were delivered (EL-NP-Blank), lysyl oxidase (LOX) activity in the abdominal aorta was reduced to 50% of the healthy thoracic aorta, showing suppression of elastin remodeling. When PGG loaded NPs were delivered (EL-NP-PGG), there was a 250% increase in LOX activity as compared to the healthy thoracic aorta (See Figure 37), confirming that PGG supports LOX production at the aneurysm site.

Desmosine content (characteristic of elastin crosslinking): Healthy non-injured abdominal aortas had 1606±173 pmole desmosine per mg dry tissue. Desmosine content of the aortic samples showed a significant decrease in the EL-NP-Blank group (446±110 pmole/mg dry tissue), showing degradation of elastic fibers. In contrast, the EL-NP-PGG group showed restoration of healthy desmosine levels (1405±328 pmole/per mg dry tissue) confirming elastin preservation due to PGG delivery (See Figure 38).

Aneurysmal Development

The control group (EL-NP-Blank) showed an increase in aortic diameter (158±43%) at 38 days after CaCl2-mediated injury, suggesting that targeted blank NPs

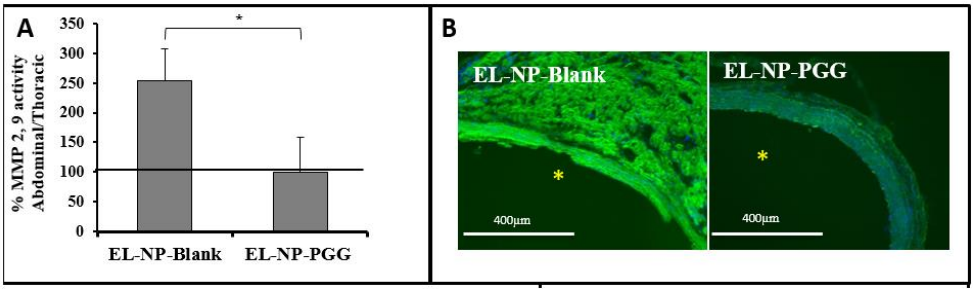

Figure 36. MMP activity (-2 and -9) by fluorogenic substrate and *in situ* zymography. * Indicates lumen. Bar = 400 µm. (*P < 0.05, Tukey's test,) (n=3).

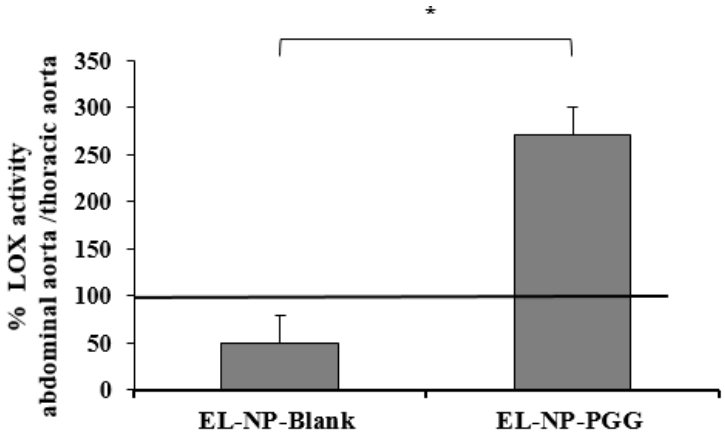

Figure 37. LOX activity. (*P < 0.05, Tukey's test,) (n=3).

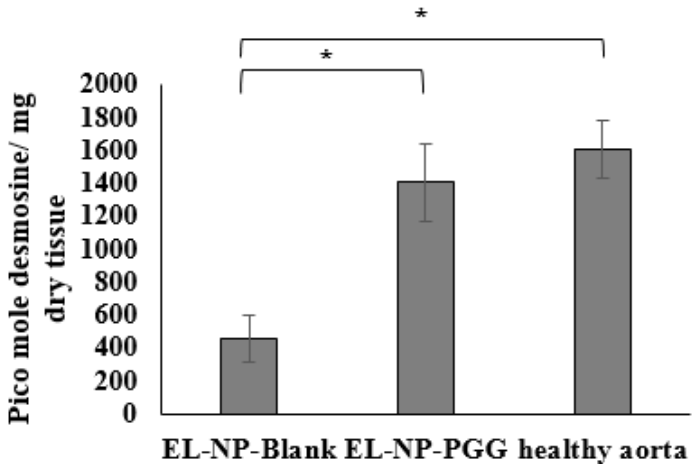

Figure 38. Desmosine content of aorta. (*P < 0.05, Tukey's test,) (n=3).

did not have any therapeutic effect on aneurysmal development. However, when PGG-loaded NPs were injected, a significant suppression of aneurysmal development was seen (3 fold) (p-value <0.05, using exact permutation test) (See Figure 39).

Hepato-Toxicity of NPs

PGG exposure had minimal cytotoxic effects in rats. Noticeable changes indicative of hepatotoxicity were not observed in hematoxylin and eosin stained sections of liver (See Figure 40). In addition, the levels of serum alanine aminotransferase (ALT), an enzyme used to assess liver function, were consistently within the acceptable range of 5 to 45 U/L (EL-NP-Blank rats, 13±0.7 U/L, and EL-NP-PGG rats, 17.8±0.9 U/L), and these results are comparable with previous studies[14].

Elastin Remodeling at the Aneurysm Site for BB-94 NPs Group

In the previous chapter, we investigated the treatment of AAA using BB-94 loaded nanoparticles. To compare PGG and Bb-94 we measure LOX and desmosine for those samples from previous study. While batimastat reduced the MMP activity, it was only slightly effective in increasing the desmosine content of the aorta, (851±192 pmole desmosine per mg dry weight of tissue) (See Figure 41).

Batimastat did not affect the LOX activity as it is shown in Figure 42.

Discussion

This study demonstrates that the use of targeted NPs carrying PGG, a potent protector of elastin, can successfully inhibit the progression of AAA, and that such delivery offers an attractive strategy for the treatment of this disease.

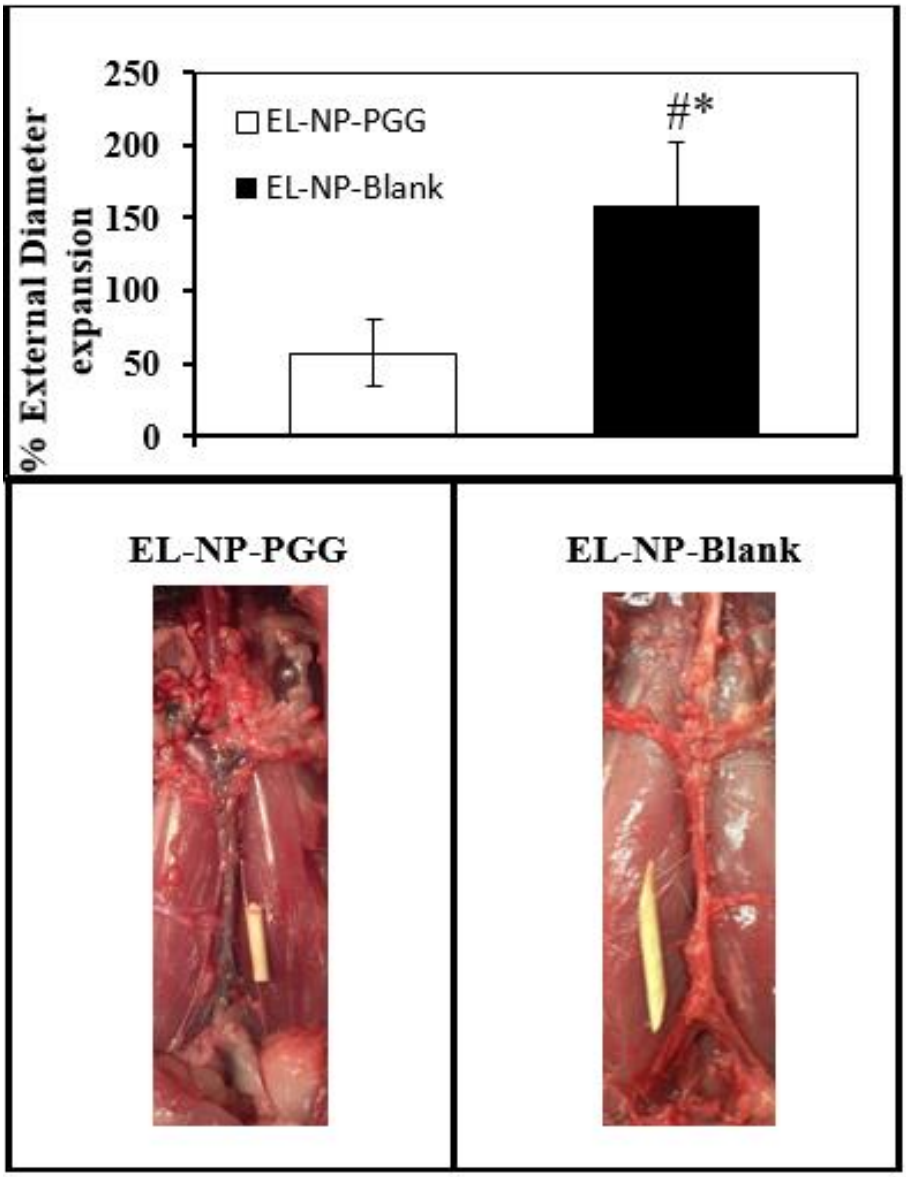

Figure 39. Expansion of external diameter in two groups after 38 days. #, $P < 0.05$, Exact permutation test compared to EL- NP-Blank group. (n=6)

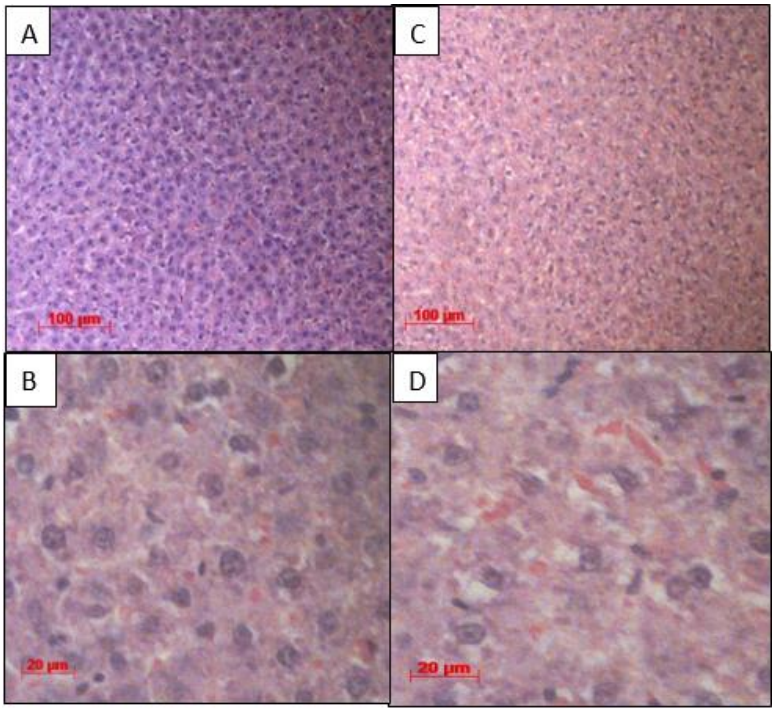

Figure 40. The liver histology data.

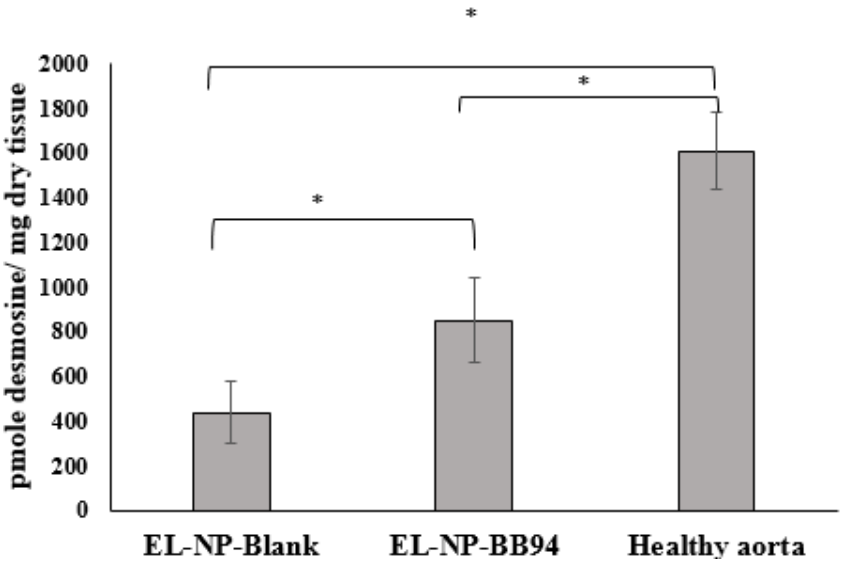

Figure 41. Desmosine content of EL-NP-Blank group vs EL-NP-BB94 group. Tukey's test, * $P < 0.05$ (n=3).

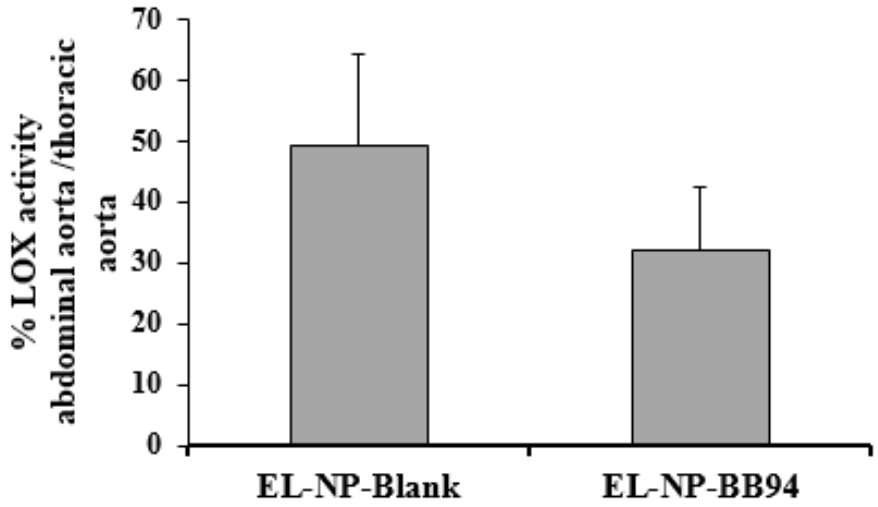

Figure 42. Analysis for LOX content of EL-NP-Blank group vs EL-NP-BB94 group.

We first optimized NP size, surface charge, and PGG loading by varying the amount of crosslinker during NP fabrication. The particle size, loading, and yield increased with increasing glutaraldehyde concentration, which is similar to what has been reported earlier_. When 12 μg glutaraldehyde/ mg BSA was used, we obtained NPs (ζ-potential~ -20mV, size ~200 nm) optimal for targeting the ECM in aortic aneurysm according to previously reported values [167]. Also, as reported previously[203], the amount of glutaraldehyde cross linking is a crucial parameter for drug release from the NPs. We found that the 12 μg glutaraldehyde/mg BSA batch had the longest release profile for PGG. Thus, these were chosen for further *in vivo* studies.

We wanted our NPs to target the degraded elastic lamina present in the ECM and not be removed by phagocytosis by resident macrophages. Macrophages are present at the aneurysmal site[204] and are responsible for phagocytosis. Our NPs showed minimal

uptake by macrophages. To confirm the mechanisms of uptake, we also made the same size NPs but with a positive surface charge or smaller NPs with negatively charged surfaces. Both were taken up by macrophages *in vitro*. This data clearly suggests that both size (~200 nm) and negative surface charge were responsible for minimizing uptake by macrophages. However, the *in vitro* results show minimal uptake but the mechanism of targeting can be a combination of both macrophages uptake and anti-elastin/elastin attachment *in vivo*.

Biodistribution data showed that NPs clearance occurs in spleen and liver as it was shown before[205]. It is possible that nanoparticles, are taken up primarily by Kupffer cells in the liver.

Phenol staining of histological sections clearly showed that PGG was indeed released at the aneurysmal site by targeted NPs, and it bound to elastin and protected it from further damage, as the aorta appeared healthy and the elastic lamina was preserved in the PGG group as compared to the blank NP group. Considering the loading, burst release of nanoparticles and targeting, 80 µg PGG will be released in first 5 hours that is enough to preserve elastin fibers.

Local inflammatory cells and vascular smooth muscle cells secrete MMPs in aneurysmal tissue[3]. MMP-9 and -2 play significant roles in AAA development as it has been shown that MMP-9 and -2 knockout mice are protected from aneurysm formation and progression[206]. The goal of targeted treatment is either to suppress MMP activity at the site of AAA or to protect elastin fibers from further degradation by blocking sites on elastin that MMPs act on during degradation. We have previously shown that PGG binds

tightly to elastic lamina and prevents its degradation by MMPs[14]. *In situ* zymography showed that the MMP activity was significantly suppressed in the EL-NP-PGG group as compared to the EL-NP-Blank group. This may be because PGG binding to elastin caused inhibition of elastin degradation and release of elastin peptides. It is known that elastin peptides are chemotactic to macrophages[207]. We also saw decreased macrophage response at the aneurysm site that may be the cause of lower MMP activity seen in the PGG group. This suggests that PGG protects elastin, and less elastin peptides are present in the EL-NP-PGG group. Therefore, elastin-derived peptide-mediated inflammatory cell recruitment is reduced[208]. However, we have looked at CD68, but more studies are needed to quantify M1 and M2 macrophages population.

Histological analysis of aortae showed inflammatory thickening of the aneurysm wall [209] that is an indicator of inflammatory AAA while EL-NP-PGG group did not show inflammation.

It has been shown in human AAA samples that desmosine content is significantly reduced in aneurysm samples in comparison to healthy aortic samples[210], which is what we have also observed in this study. Clearly, $CaCl_2$ mediated injury caused elastin degradation as seen by histology and significantly lower desmosine content (446±110 pmole/mg dry tissue), an elastin-specific cross-linking amino acid, in the blank NP group. The EL-NP-PGG group showed intact elastic lamina by histology and desmosine content similar to that of the healthy uninjured abdominal aorta (1405±328 pmole /per mg dry tissue for the EL-NP-PGG group and 1606±173 pmole desmosine per mg dry tissue for the healthy non-injured abdominal aorta). We wanted to test if these results were due to

lower inflammation and MMP activity or if there was active elastic fiber remodeling by VSMCs in the PGG group. We have previously shown that the MMP inhibitor batimastat also prevents aneurysm expansion[200]. While batimastat reduced MMP activity, it was only slightly effective in increasing the desmosine content of the aorta, (851±192 pmole desmosine per mg dry weight of tissue). PGG delivery remarkably allowed for the preservation of desmosine content similar to the healthy aorta despite aortic injury induced by calcium chloride 10 days prior to NP delivery.

To further test why PGG delivery caused restoration of healthy elastic lamina, we chose to study the activity of LOX. LOX is an extracellular copper-containing enzyme that catalyzes the formation of aldehydes from lysine residues in elastin precursors, resulting in cross-linking of elastin, which is essential for the integrity and elasticity of mature elastin[211]. In our study, tissues from the EL-NP-PGG group showed 150% increase in the production of LOX, which was significantly lower in the abdominal tissue of the EL-NP-Blank group. On the other hand, batimastat delivery did not result in a difference in LOX activity. This increased LOX production at the AAA site only in the PGG group would lead to crosslinking of tropoelastin molecules secreted by cells and may have allowed for the creation of healthier elastic lamina. This was evident in histological sections only from the PGG group. We have also shown previously that LOX production increases when aneurysmal vascular smooth muscle cells are treated with PGG in vitro and that in turn increased insoluble elastin production by cells[121]. This observation was confirmed in vivo in the present study. Although the exact mechanism by which PGG increases LOX production by cells is unknown, we hypothesize that

polyphenols like PGG lock in soluble tropoelastin molecules secreted by cells in the extracellular matrix. This then signals cells to produce more LOX to crosslink this tropoelastin and create elastic fibers. We have also shown that fibrillin levels increase *in vivo* when cells are treated with PGG. Fibrillin is an essential glycoprotein found at the periphery of mature elastic fibers[212]. Others have shown that LOX gene transfer resulted in partial prevention of the development of CaCl2-induced AAA[213]. Thus, PGG works by dual action. It binds to degraded elastic fibers and protects it from further degradation (stabilization), but at the same time it locks in tropoelastin secreted by cells to regenerate lost elastic lamina (regeneration). With targeted delivery of PGG, the protection of elastin from further damage and ongoing elastin regeneration leads to suppression of aneurysmal development in the aorta as shown by lower aneurysmal expansion in the EL-NP-PGG group (57% expansion) compared to the EL-NP-Blank group (158% expansion).

Finally, we also show that the NPs and PGG delivery were not hepato-toxic. ALT is released into the blood due to the loss of liver cells. Therefore, an increase in this enzyme is a sign of liver cell damage[214]. ALT levels were not altered by NP injection, and the livers appeared to be normal in histological stainig, suggesting that NPs are not toxic to the liver in this 38 day study.

In conclusion, we show that targeted delivery of PGG by NPs is an effective way to protect elastin fibers against further damage and restore healthy elastic lamina in an experimental rat model of AAA. Thus, such targeted PGG therapy leads to suppression of aneurysm development.

CHAPTER VI

REVERSAL OF ELASTIN CALCIFICATION AND ANEURYSM IN A RAT MODEL USING DUAL TARGETED THERAPY WITH EDTA- AND PGG-LOADED NANOPARTICLES

Rationale

Degeneration of elastin plays a crucial role in the pathology and progression of abdominal aortic aneurysms (AAA), a disease characterized by the loss of structural integrity of the arterial wall. AAA is often associated with calcification, which increases the risk of AAA rupture[4]. Current option for AAA is the replacement of weakened aorta with a vascular graft. Our group has shown earlier that treatment with pentagalloyl glucose (PGG) increased elastin matrix deposition by healthy and aneurysmal vascular smooth muscle cells in vitro[121]. Furthermore, we have shown that EDTA nanoparticles can remove calcification from calcified artery with minimal dose of EDTA using the same nanoparticles technology[172]. We would like to use EDTA and PGG and deliver it at the site of aneurysms. Such dual therapy of EDTA followed by PGG help reducing calcification and arterial elastin restoration.

Objective

Our previous study showed that EDTA loaded nanoparticles (NPs) conjugated with an anti-elastin antibody can be targeted to the site of calcification in a calcium chloride rat model. Here, we tested whether EDTA NPs can first remove calcification associated with AAA and then if PGG delivery to the site of aneurysm can regenerate damaged elastin.

Approach and Results

Albumin nanoparticles (NPs) with surface conjugated elastin-specific antibody that targets only degraded elastic lamina and loaded with either EDTA or PGG were prepared. The calcium chloride induced rat model of abdominal aortic aneurysm was used. The animals were divided into four groups. A moderate stage aneurysm and calcification was allowed to develop for four weeks and one group of animals received tail vein injection of EDTA NPs (twice a week). Two weeks after EDTA therapy (total 6 weeks), these rats received PGG loaded NPs (once every two weeks). In other three groups, aneurysm was allowed to progress for six weeks. At that point, one group received blank NPs, and one group received PGG NPs (once every two weeks). As a control, one group received an MMP inhibitor, BB-94 loaded NPs (once a week). After 12 weeks, the rats were euthanized, and disease development, calcification, and elastic lamina restoration was studied. EDTA followed by PGG NP delivery lead to reduction in macrophage recruitment, MMP activity, elastin degradation and calcification in the aorta as compared to control blank, BB-94, and PGG NPs delivery alone. It restored vascular elastic lamina and improved vascular function as observed by improvement in circumferential strain.

Conclusions

Dual targeted therapy may be an attractive option to remove mineral and restore healthy arterial structures in moderately developed aneurysmal disease.

Introduction

Clinically, abdominal aortic aneurysms (AAAs) are characterized by chronic inflammation and degradation of extracellular matrix (ECM) components by proteolytic enzymes like matrix metalloproteinases (MMPs). This can lead to inflammatory infiltration in the adventitia and calcification and degeneration of medial elastic lamina[195,215]. The infiltrating cells, including B and T cells, mast cells, macrophages, and neutrophils secrete proinflammatory mediators, leading to the acceleration of matrix degradation and causing weakening of the blood vessel wall[216]. Calcification is frequently found within the aneurysm wall, and the calcified region has a higher stiffness than the surrounding arterial wall[217]. Although abdominal aortic aneurysm is a life-threatening disease, there are no pharmacological therapies available to stop growth and reverse the disease. Several drug therapies in animal models have been shown to be successful in preventing aneurysm formation, but were started at the onset of aneurysm[218]. Such studies provide insight into the mechanisms of aneurysm formation, but do not provide therapy for already developed aneurysms. Over ninety percent of patients are diagnosed at a moderate stage of aneurysm, and therapies are critically needed to reverse these. Currently, such patients are monitored for aneurysmal expansion by ultrasound; when the diameter of the diseased aorta exceeds 5.5 cm surgical replacement, surgical replacement with a vascular graft is recommended. This threshold is arbitrary as it has been shown that at that size rupture risk exceeds interventional risk but ten percent of deaths occur below this expansion.

Perivascular application of calcium chloride to the infra-renal aorta of rats is a common model for aortic abdominal aneurysm (AAA). It shows noticeable inflammatory infiltrates including macrophages and medial elastin calcification similar to that seen clinically[67]. Our group has previously shown that systemic delivery of elastin-antibody conjugated, poly (D,L-lactide) nanoparticles loaded with hydroxamate-based MMP inhibitor batimastat (BB-94) causes suppression of AAA when delivered at the onset of disease[200]. We have also shown that EDTA-loaded bovine serum albumin (BSA) nanoparticles with a surface conjugated elastin antibody deliver EDTA to the aneurysm site and remove mineral when applied at an early stage of the disease[172]. However, both these studies were initiated at a very early stage of the disease. To mimic the clinical situation and treat moderate-size aneurysms, we designed this study to test if targeted nanoparticles can regress already developed aneurysms in rats. It has been previously shown that calcification is a sign of the inflammatory process involved with the degeneration of the arterial wall, and it is correlated with increased risk of aneurysm rupture[4]. Here, we used a dual-therapy approach: First, we employed targeted nanoparticle-based delivery of EDTA to removed mineral deposits in arteries. Then, we targeted delivery of pentagalloyl glucose (PGG), a polyphenol known to stabilize elastin and increase elastic fiber deposition[14]. We show that such dual therapy removes mineral deposits from calcified arteries and restores elastic lamina in the aneurysmal wall, leading to improvement in vascular elastance.

Materials and Methods

Study Design

The purpose of this study was to investigate the effect of calcium removal and elastin preservation on calcium chloride-induced abdominal aortic aneurysm in a rat model. We used anti-elastin conjugated nanoparticles loaded with DIR to target the injury site. Further, we loaded the nanoparticles with either EDTA, BB-94 or PGG to see their therapeutic effect, if any, on AAA. In addition to histological analysis, we measured diameter change, MMP activity, desmosine, LOX and calcium content to investigate the effect of these treatments. Sample sizes were determined by power analysis using our lab's previously published data as preliminary data. A power analysis with 90% power and $\alpha = 0.05$ indicated that a sample size of a minimum of six rats per group was required for diameter change. Data analyses were not blinded. Outliers were not excluded.

Preparation of DiR-loaded, EDTA-loaded and PGG-loaded nanoparticles

Bovine serum albumin (BSA) NPs were prepared by coacervation[201]. Briefly, DIR-loaded nanoparticles (NPs) were obtained by dissolving 250 mg of bovine serum albumin (BSA; Seracare, MA) in 4 mL of deionized water. Then, 2.5 mg of the fluorescent dye 1, 1-dioctadecyl-3, 3, 3, 3-tetramethylindotricarbocyanine iodide (DIR) was dissolved in 100 µl of acetone and added to the BSA solution. After an hour of stirring, the mixture was added dropwise to 24 mL of ethanol under continuous sonication (Omni Ruptor 400 Ultrasonic Homogenizer, Omni International Inc.,

Kennesaw, GA) for half an hour. For crosslinking, glutaraldehyde (EM grade 70%, EMS, PA) was added during stirring (42 µg per mg of BSA). Next, 10 mg of DIR-loaded NPs (DIR-NPs) were incubated with 2.5 mg heterobifunctional crosslinker α-maleimide-ω-N-hydroxysuccinimide ester poly (ethylene glycol) (Maleimide-PEG-NHS ester, MW 2000 Da, Nanocs Inc., NY) to achieve a sulfhydryl-reactive particle system. Traut's reagent (34 µg, G-Biosciences, Saint Louis, MO) was used for thiolation of 10 µg of rabbit anti-rat elastin antibody (United States Biological, Swampscott, MA), and the mixture was incubated in HEPES buffer (20 mM, pH=9.0) for an hour at room temperature. Thiolated antibodies were rinsed with HEPES buffer and were added to NPs (4 µg antibody per 1 mg NPs) and incubated overnight for conjugation.

EDTA-loaded nanoparticles were obtained by dissolving 200 mg of bovine serum albumin (BSA; Seracare, MA) and 100 mg ethylenediaminetetraacetic acid disodium salt (EDTA) (Fisher scientific, NJ) in 4 mL of deionized water and pH was adjusted to 8.5. The aqueous solution was added drop-wise to 16 mL ethanol under probe sonication for 1 hour. For crosslinking, glutaraldehyde was added during sonication (10 µg per mg of BSA). The elastin antibody conjugation procedure was similar to that of DiR-loaded NPs.

PGG-loaded nanoparticles were obtained by dissolving 250 mg of BSA (Seracare, MA) in 4 mL of deionized (DI) water. Pentagalloyl glucose (PGG, 125 mg) was dissolved in 400 µl of dimethyl sulfoxide and added slowly to the BSA solution. After an hour of stirring, the mixture was added dropwise to 24 mL of ethanol under continuous sonication for half an hour. Glutaraldehyde was added during stirring at a concentration

of 12μg/mg protein (BSA). The elastin antibody conjugation procedure was similar to that of DiR-loaded NPs.

In vivo Study

Calcium Chloride-Injury Model

Perivascular application of calcium chloride was used to create aneurysms in the abdominal aorta of the rats[69]. By 30 days, elastic lamina showed extensive calcification and degradation with a moderate increase in external diameter that mimics clinically moderate stage of the disease. We chose this time point to start the treatments to reverse AAA. The diagram in Figure 1 depicts details of the animal experimentation. Briefly, Sprague-Dawley rats (5-6-weeks-old) were placed under general anesthesia (2% to 3% isoflurane). A 0.50 mol/L CaCl2-soaked sterile cotton gauze was placed on the exposed infrarenal abdominal aorta for 15 minutes. Afterwards, the area was flushed with warm saline and sutures were used to close the abdominal incision. After surgery, the animals were given a normal diet and allowed to recover for thirty days. Either DiR dye-loaded or drug-loaded NPs were then introduced.

Targeting and Bio-distribution of NPs

Thirty days after the initial CaCl2 injury, rats were injected with elastin antibody conjugated and DIR dye-loaded NPs (EL-NP-DIR) via the tail vein. After 24 hours, the rats were euthanized. The entire body and the individual organs were imaged using a Caliper IVIS Lumina XR (Hopkinton, MA) with Ex/Em of 745/795 nm to calculate

biodistribution and targeting of NPs to the site of injury in the aorta. Biodistribution was calculated as mentioned before.

Reversal of Moderate-Size Aneurysms with Drug Therapy

Thirty days after perivascular application of calcium chloride, the rats were divided into four separate treatment groups (n=6 per group). One group of rats received tail vein injection of NPs loaded with EDTA and conjugated with elastin antibody (EL-NP-EDTA, ~10 mg/kg body wt.) suspended in 200 μL of PBS twice a week; the other three groups did not receive any treatment. After the first two weeks, the EDTA-treated group was given NPs loaded with PGG and conjugated with an elastin antibody once every two weeks for four weeks (EL-NP-EDTA+NP-PGG ~10mg/kg body wt.). The second group of six rats was given NPs loaded with PGG and conjugated elastin antibody (EL-NP-PGG, ~10mg/kg body wt.) once every two weeks over four weeks. A third group of six rats was given NPs loaded with BB-94 and conjugated elastin antibody (EL-NP-BB94, ~10mg/kg body wt.) once every week for four weeks. Finally, the last group of six rats received blank NPs conjugated with elastin antibody once every two weeks for four weeks (EL-NP-Blank~10mg/kg body wt.). Two weeks after completing treatment, the rats were then euthanized. The entire study lasted for 12 weeks total. After euthanasia, the tissues were harvested. They were either snap frozen or fixed in formalin for further examination.

MMP Activity in Rat Aorta and *In situ* Zymography

The snap frozen samples of the abdominal aorta were pulverized and homogenized in RIPA extraction buffer (50 mM Tris-HCl pH 7.4, 150 mM NaCl, 1 mM EDTA, 1% Triton X-100, 1% Sodium deoxycholate, 0.1% SDS, with protease inhibitor cocktail) (Roche Diagnostic GmbH, Germany) in accordance with the manufacturer's protocol to extract protein from the aortic tissues. A BCA protein assay (Pierce, IL) was used to quantify the total protein in the harvested aortic tissue. MMP activity was measured with an internally quenched peptide substrate (excitation 280 nm, emission 360nm, MMP Substrate III, Anaspec, CA). One mg of substrate dissolved in 50 µl of DMSO was diluted in 10 ml of development buffer (50 mM Tris Base, 5mM $CaCl_2 \cdot 2H_2O$, 200mM NaCl, 0.02% brij 35). The development buffer (96 µl) was mixed with 2 µl of extracted protein along with 2 µl of substrate stock solution and then incubated for an hour at 37°C. A fluorescence plate reader was used to read the endpoint florescence intensity.

In situ zymography was performed on frozen sections to evaluate MMP activity in the aortic tissue samples. Sections of the abdominal aorta obtained from sectioning with a cryostat (8 µm) were left to air-dry for 10 min at 4°C. One part DQ-gelatin (1mg/ml of DI water) was mixed with nine parts 1% agarose (Promega, WI) in PBS containing DAPI (1 µg/ml) (Life Technologies, IL). Each section was treated with a drop of the mixture and then incubated at 37°C for one hour in the development buffer. MMP inhibitor 1, 10-phenanthroline monohydrate (0.2 mmol/L) (Life Technologies, OR), was used to block the MMP activity of one of the samples, which was used as a positive control.

Afterwards, an EVOS® XL cell imaging system was used to capture images of the samples.

Desmosine Content of the Aorta

The snap frozen samples of the abdominal aorta were pulverized, lyophilized and hydrolyzed in 6N HCL at 95°C for 12 h[14]. Using nitrogen gas supplied in a continuous stream, the samples were dried. Afterwards, they were reconstituted in 1.0 mL of 0.01 N HCL. An ELISA kit (MyBioSource, San Diego, CA) was used to measure the desmosine content in accordance with the protocol set by the manufacturer. Another group of six healthy non-injured abdominal aortas were also studied for comparison.

Lysyl Oxidase (LOX) Activity Assay

After being snap frozen in liquid nitrogen, the aortic tissues were pulverized and then homogenized in 500 µl of 6 M urea, 10mM Tris (pH 7.4), 1mM PMSF Protease Inhibitor, 1µM pepstatin A, and 6 µM leupeptin. These homogenates were then placed on a plate shaker and shaken overnight at 4°C. The homogenized tissues were then centrifuged at 10,000 g for 30 min at 4°C. The same buffer was used again to suspend the pellets, which were subsequently homogenized and centrifuged. Using the LOX Assay Kit (AAT Bioquest, Sunnyvale, CA) to quantify the LOX concentration in the supernatant, LOX activity was measured[202].

Calcium Assay

Total calcium content was measured after lyophilizing. Lyophilized tissue was hydrolyzed in 6N HCl at 95°C and dried under a continuous stream of nitrogen gas (~45

minutes). The tissue was subsequently reconstituted in 0.01 N HCl and samples were analyzed using the Spectro Acros ICP Spectrometer (SPECTRO Analytical Instruments, Kleve, Germany) at the Clemson University Agricultural Service Laboratory.

Ultrasound Analyses of the Abdominal Aorta

A high-frequency ultrasound device (Vevo 2100, VisualSonics, Toronto, Canada) utilizing a linear array probe (MS 400D, frequency 30–55 MHz) was used to image the abdominal aorta. During imaging, the animals were kept under light anesthesia by inhalation of 2% isoflurane and fixed in the dorsal position on the imaging table.

Circumferential Strain Assessment with High-Frequency Ultrasound

Vevo 2100 analysis software was used to process M-Mode ultrasound data. Three different cardiac heart beats were recorded for each M-Mode measurement made. Systolic and diastolic diameters were measured, and this data was used to calculate the circumferential cyclic Green-Lagrange strain with the assumption that strain is uniform around the vessel according to the equation below:

$$\textit{Circumferential strain} = \frac{1}{2}((D_{sys}/D_{dia})^2-1)*100\% \qquad (10)$$

Aortic External Diameter Change

Initial external diameter was measured at the time of the $CaCl_2$ injury. Final aortic diameter was recorded before euthanasia (12 weeks after injury). Additionally, we euthanized a group of rats 30 days after injury to observe diameter change at the onset of drug therapy. Aortic external diameter change was calculated as mentioned before.

Histological Analysis

Formalin-fixed samples were embedded in paraffin, and 5 μm sections were mounted on glass slides and heated overnight to adhere the tissues to the slides and melt the paraffin. Subsequently, the slides were deparaffinized with xylenes and graded ethanol and stained with hematoxylin and eosin for tissue morphology, Verhoeff-van Gieson (VVG) for elastic fibers, phenol staining for PGG, Masson's trichrome for collagen and Alizarin Red S with a Light Green SF counterstain for calcification. Liver samples were treated the same way and stained with hematoxylin and eosin for tissue morphology.

Immunohistochemistry for Macrophages, Osteopontin (OPN) and Smooth Muscle Cells (VSMCs)

Tissues preserved with formalin were embedded in paraffin and sectioned as previously described. Subsequently, the slides were deparaffinized with xylenes and graded ethanol, and antigen retrieval was done using citrate buffer (Millipore, MA). The slides were incubated overnight at 4°C with the primary antibody, Mouse Anti Rat CD68 (Bio-Rad, Hercules, CA) or Rabbit Anti Rat Osteopontin (Rockland Immunochemical, PA). Staining was completed using a DAB kit (Enzo Life Sciences, NY). Counterstaining followed using hematoxylin or eosin. For VSMCs, the slides were incubated overnight at 4°C with the primary antibody, mouse smooth muscle actin (Santa Cruz Biotechnology, CA). Staining was completed using a mouse-HRP AEC kit (Enzo Life Sciences, NY).

IFN-γ

Blood was drawn via a heart stick with a 3 mL syringe, and after allowing 30 min for clotting, the blood was centrifuged at 3000 rpm for 3 min. Rat serum was examined for IFN-γ using a rat ELISA kit (R&D system, MN).

Alanine Aminotransferase (ALT) Analysis

The serum was examined for the activity of alanine aminotransferase (ALT) using a commercially available kit (Sigma, St. Louis, MO).

Statistical Analysis

Data were analyzed by one-way ANOVA followed by Tukey's test. Levene's test was used to verify the homogeneity of variances and normality assumption was checked using a Shapiro-Wilk test. Tukey's test was used for all pairwise comparison.

An exact permutation test was performed using the NPAR1WAY procedure in SAS. The data are expressed as the mean ± standard deviation; results were considered to be significant when P-values ≤ 0.05.

Results

Nanoparticles Delivery Design

Study designed was shown in Figure 43 for targeting or therapeutic purposes.

Aortic Disease Status at the Onset of Targeted Therapy

Aortic aneurysm and calcification were allowed to develop for 30 days after the initial $CaCl_2$ injury. Aortic external diameter increased to 127±20.6% after 30 days.

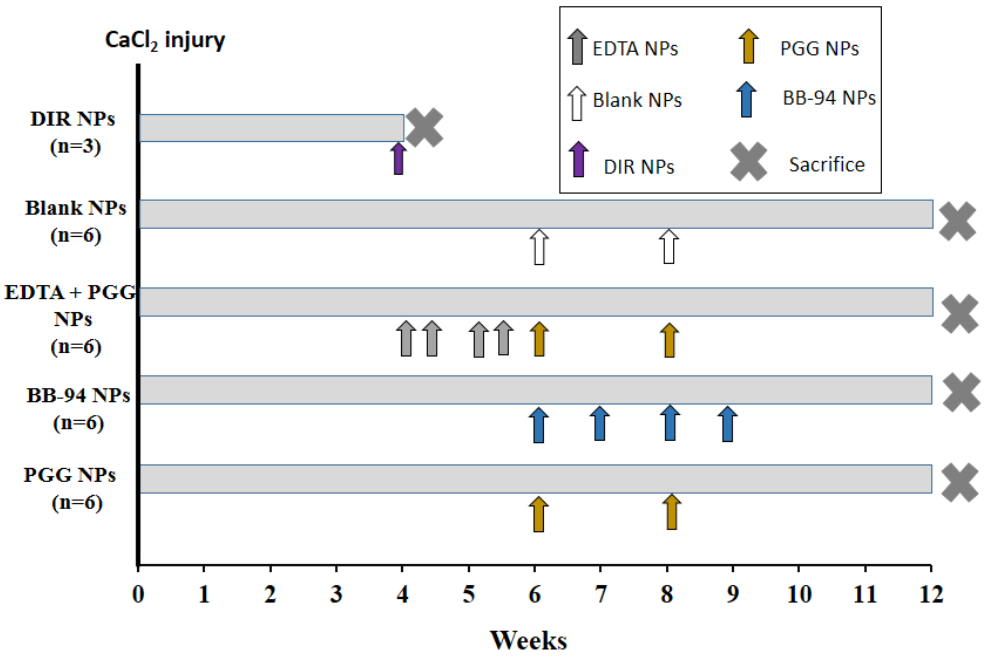

Figure 43. Schematic representation of the experiment.

Desmosine content of the aortas decreased from 1808±290.5 to 421.9±104 pmole/mg dry tissue after 30 days. Calcium content of the aortas was 43±3 µg/mg dry weight after 30 days. *In situ* zymography on frozen sections of abdominal aorta from 30 days after surgery showed high activity of MMPs (See Figure 44, A1). Histological studies further corroborated quantitative data for calcification and elastin damage 30-day post-surgery (See Figure 44, A2, A3).

NP Targeting to Diseased Aorta

Elastin antibody conjugated and DiR dye loaded NPs were injected in tail vein at 30 days' post-surgery. The NPs targeted the injured aortic elastic lamina sites within the first 24 hours as measured by fluorescence intensity (IVIS, 42±22% targeting based on

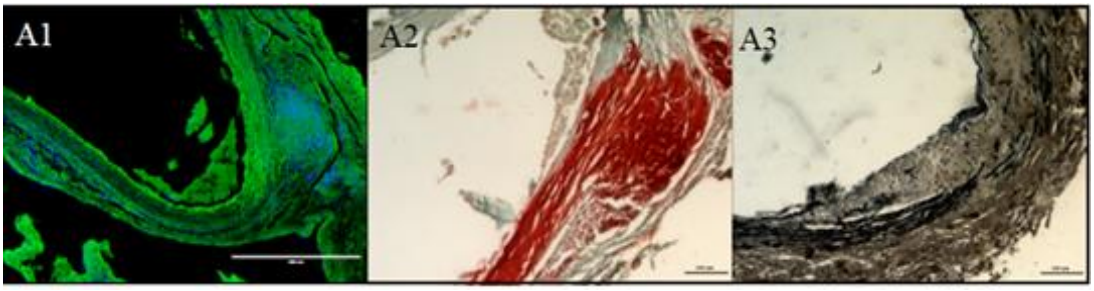

Figure 44. *In situ* zymography, alizarin red and VVG for aortic samples 30 days after injury.

per weight basis) (See Figure 45A). The fluorescence signal of DIR (% florescence/dry weight of organ) after 24 hours was 3.6±1.5% for the kidneys, 20±7% for the liver, and 20±14% for the spleen (See Figure 45B). More significantly, infiltration of the NPs was seen from adventitial section to the medial section which elastin is damaged (See Figure 45C). In a previous work we have shown, once NPs get there, they stay up to 14 days at the site of injury. Based on this information we chose to inject drug loaded NPs every two weeks for the therapeutic studies.

Dual Therapy for Calcified Aneurysms

Calcification Assessment

When blank NPs (EL-NP-Blank) or NPs loaded with an MMP inhibitor BB-94 (EL-NP-BB94) were delivered, aortic calcification increased (67.80±16 µg and 53.82±12.97 µg calcium/mg dry weight of aorta respectively). When only PGG NPs (EL-NP-PGG) were delivered, aortic calcification did not increase, but remained similar to starting levels (34.8±6 µg calcium /mg dry weight of aorta). Only when delivery of

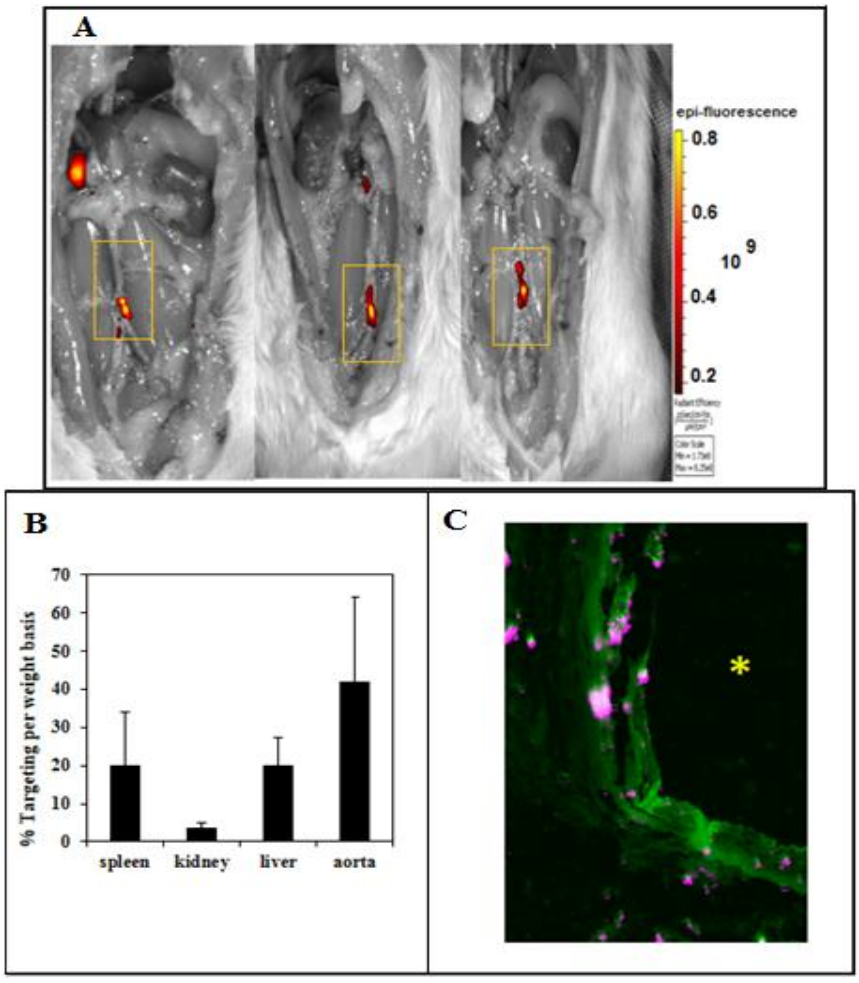

Figure 45. NP accumulation after intravenous injection of EL-NP-DIR, 30 days after injury at the site of elastin damage.

EDTA NPs was followed by PGG NPs did we see significant reduction in calcification (16.8±4.2 µg calcium /mg dry weight of aorta) (See Figure 46).

Alizarin Red S staining for calcification with a Light Green SF counterstain showed very heavy calcification in the EL-NP-Blank (See Figure 47 B1) and EL-NP-BB94 groups (See Figure 47 B2), especially in the media and adventitia. Calcification was moderate in the EL-NP-PGG group (See Figure 47 B3). Calcification was minimal

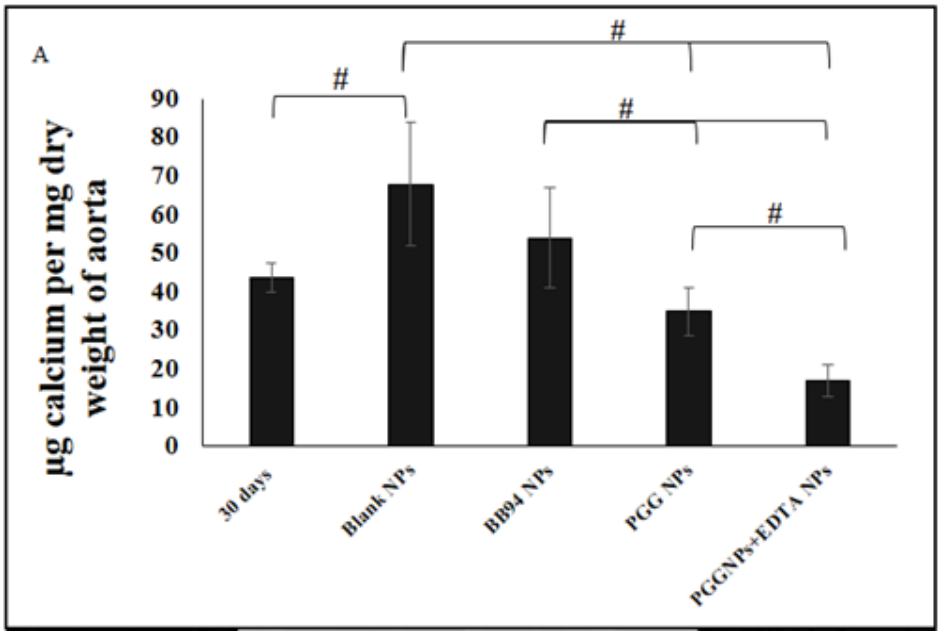

Figure 46. Calcium content of aorta in different groups. (#P < 0.05, Tukey's test,) (n=6).

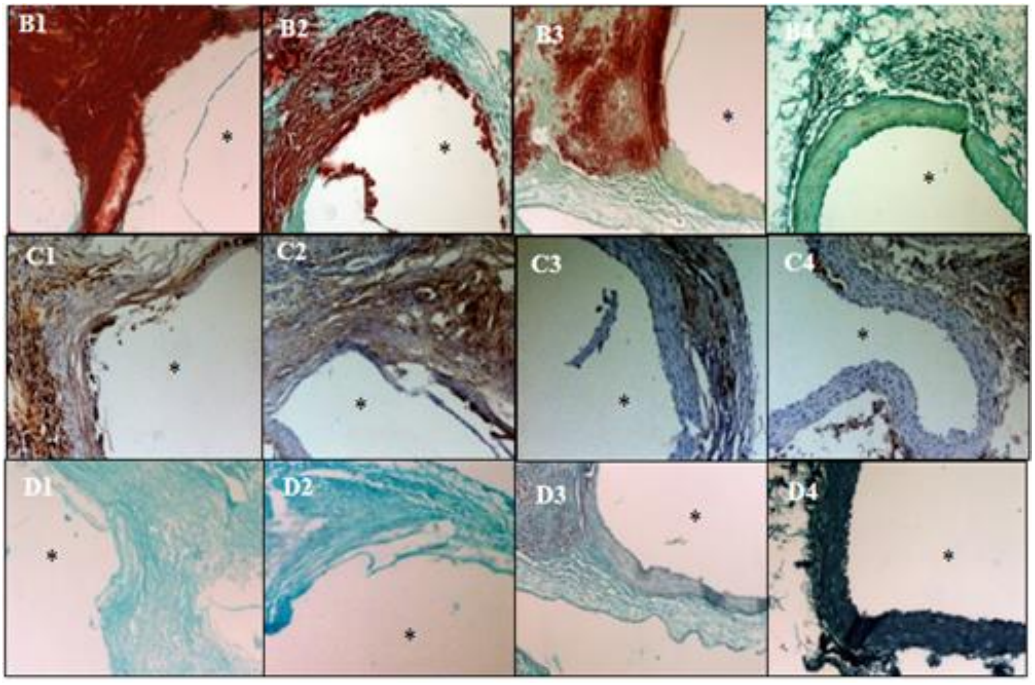

Figure 47. Histological analysis.

to nonexistent in dual therapy with EL-NP-EDTA followed by EL-NP-PGG (See Figure 47 B4). Immunohistochemical stain for osteopontin (OPN) was positive in the EL-NP-Blank (See Figure 47 C1) and EL-NP-BB94 (See Figure 47 C2) groups and correlated with high calcification. OPN was observed, but was not abundant in the other groups (See Figure 47 C3 and C4).

We used $FeCl_3$ stain to look at PGG binding to elastin. As expected, no phenol staining (black-gray for PGG) was seen in the EL-NP-Blank and EL-NP-BB94 groups (See Figure 47 D1 and D2). Staining was intense in the EL-NP-EDTA+NP-PGG group (See Figure 47 D4) as compared to the EL-NP- PGG group (See Figure 47 D3), suggesting a higher amount of PGG attached to elastin after removal of mineral by EDTA.

Aortic External Diameter Change

Aortic external diameter increased from 127±20.6% to 185±25% when control blank NPs were injected (EL-NP-Blank), suggesting that targeted blank NPs did not inhibit aneurysmal growth (See Figure 48 A, B). However, when EL-NP-PGG or EL-NP-EDTA+EL-NP-PGG NPs were injected, a significant suppression of aortic external diameter change was observed (66±21% and 25±7% respectively). Moreover, NP delivery of BB94 (EL-NP-BB94) showed no reversal of aortic external diameter (156±17%).

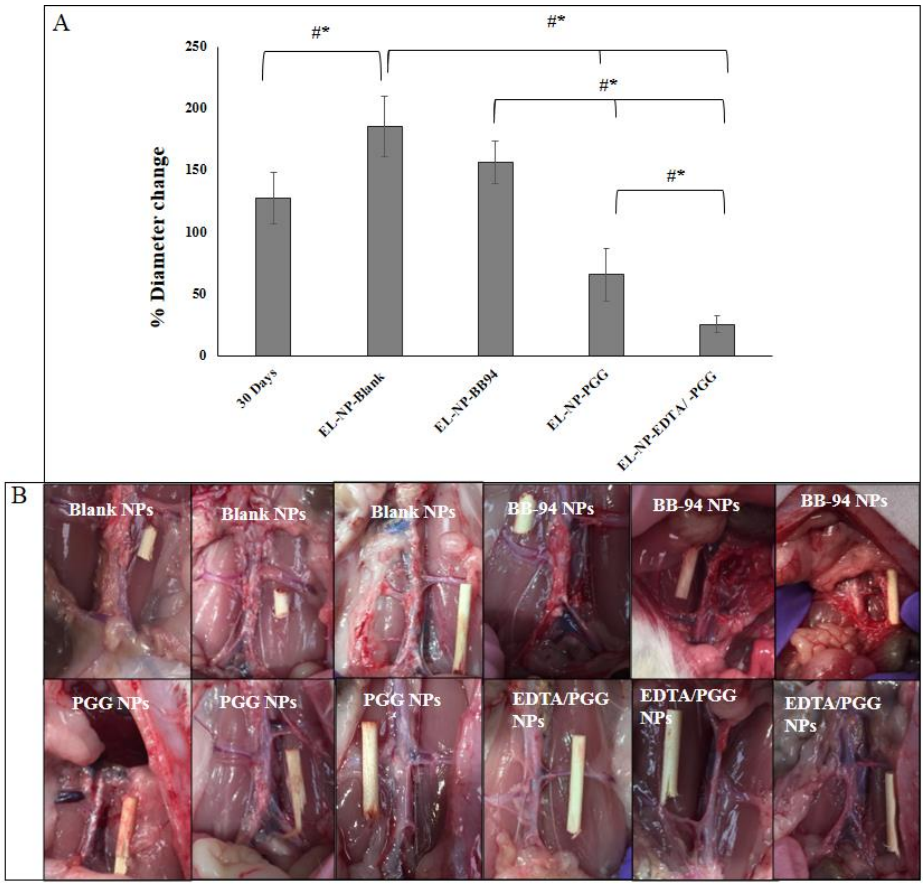

Figure 48. Diameter change. #, $P < 0.05$, exact permutation test. (n=6). Wooden sticks were kept as reference for external diameter change measurement.

MMP Activity and *In situ* Zymography

We examined if delivery of NPs loaded with PGG, BB-94 or EDTA followed by PGG would inhibit local MMP activity at the injury site. Fluorescence intensity data normalized to total protein content showed highest activity in the EL-NP-Blank group, clearly suggesting that blank NPs did not reduce MMP activity. All other groups (EL-NP-PGG, EL-NP-BB94, and EL-NP-EDTA + EL-NP-PGG) showed significant suppression of MMP activity (See Figure 49A). *In situ* zymography confirmed the quantitative results (See Figure 49B).

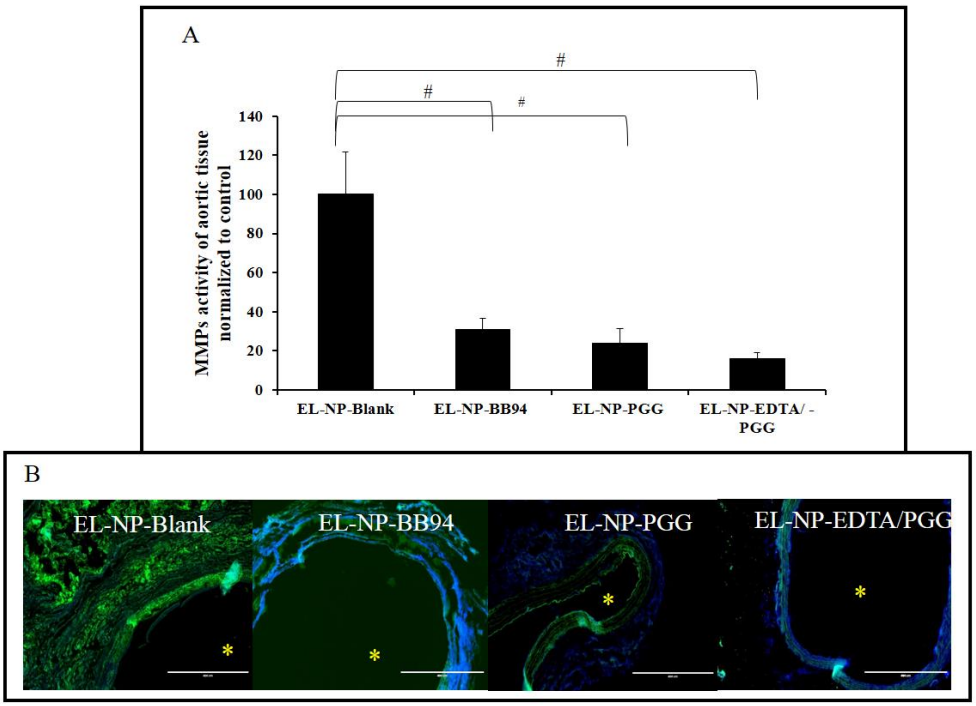

Figure 49. MMP activity (-2 and -9) by fluorogenic substrate and *in situ* zymography. . * Indicates lumen. Bar = 400 μm. (#P < 0.05, Tukey's test,) (n=6).

Histological Analysis: Aortic Inflammation

Hematoxylin and eosin staining in EL-NP-Blank and EL-NP-BB94 groups showed significant adventitial inflammation with large macrophage infiltration in the media. Minimal inflammation was seen in the EL-NP-EDTA+NP-PGG group (See Figure 50d). Masson trichrome stain revealed that collagen deposition was abundant in the EL-NP-Blank (See Figure 50e) and EL-NP-BB94 (See Figure 50f) groups while muscle fibers were minimal. Collagen deposition was lower in the EL-NP-PGG group (See Figure 50g) and minimal in EL-NP-EDTA+NP-PGG group (See Figure 50h). Smooth muscle staining was integrated where elastin fibers were regenerated in EL-NP-PGG and EL-NP-EDTA + EL-NP-PGG groups.

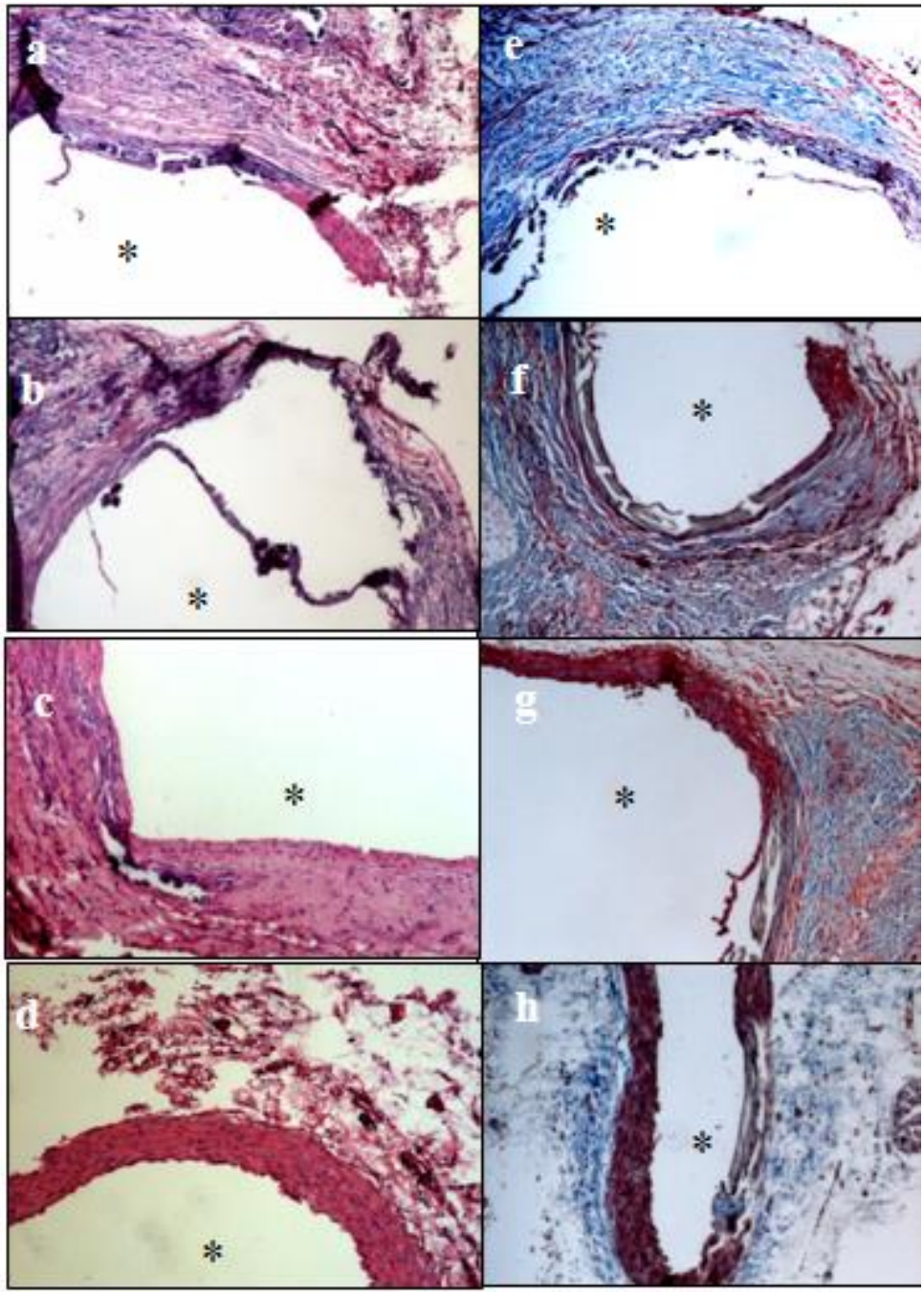

Figure 50. Hematoxylin and eosin (H&E) staining, Masson trichrome staining.

Immunostaining for Macrophages (CD68) and Smooth Muscle Cells

EL-NP-Blank group (See Figure 51i) showed adventitial granuloma and intense pan-macrophage (CD-68) stain. In EL-NP-BB94 (See Figure 51j) and EL-NP-PGG (See Figure 51k) groups adventitia was positive for pan-macrophages, but with lower staining than blank NPs. The dual therapy group EL-NP-EDTA + EL-NP-PGG group had the least amount of CD68 staining (See Figure 51l). Depletion of medial VSMCs was observed in both EL-NP-Blank (See Figure 51m) and EL-NP-BB94 (See Figure 51n) groups while more medial VSMCs were found in EL-NP-PGG (See Figure 51o) and EL-NP-EDTA + EL-NP-PGG (See Figure 51p) groups.

Systemic IFN- γ levels

EL-NP-Blank group had the highest amount of IFN- γ (23.7±7.6 pg/ml) in serum, followed by EL-NP-BB94 (11.2±4.8 pg/ml). IFN- γ levels in dual therapy group (EL-NP-EDTA + EL-NP-PGG) and EL-NP-PGG were below detectable levels.

Restoration of Elastic Lamina

We tested if drug therapy restored already degraded elastic lamina. Lysyl oxidase enzyme activity and desmosine content was measured, as was VVG histological staining for elastic lamina. We also tested circumferential strain with ultrasound at the end of the study.

LOX Activity

LOX analysis of abdominal aortic samples, as measured by ratio of thoracic aorta of the same animal showed a significant decrease in LOX in the EL-NP-Blank and EL-

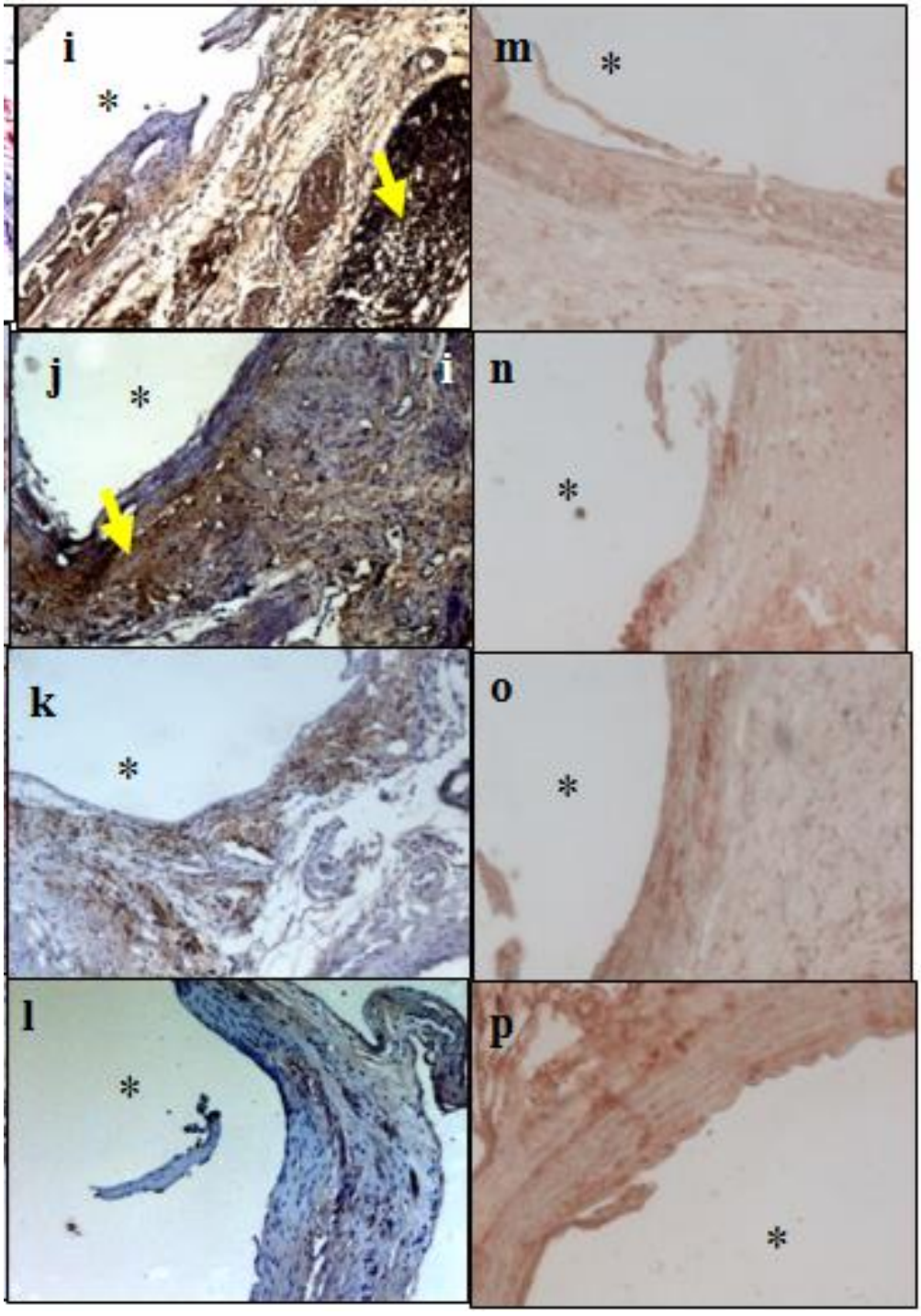

Figure 51. CD68 macrophages and VSM IHC.

NP-BB94 groups, suggesting elastin crosslinking was inhibited. However, EL-NP-PGG and EL-NP-EDTA + EL-NP-PGG groups showed a significant increase in LOX activity (See Figure 52).

Desmosine Content

Desmosine content of abdominal aortic samples in EL-NP-Blank was further reduced from 421.9±104 to 205±56 pmole desmosine/mg dry tissue, suggesting further elastin degradation. EL-NP-BB94 group had 317±177 pmole desmosine/mg dry, suggesting BB94 treatment also did not prevent elastin degradation (no significant differences between EL-NP-BB94 and EL-NP-Blank). Desmosine content in the EL-NP-PGG group was significantly higher than in the EL-NP-Blank group (571±113pmole desmosine/ mg dry tissue). The EL-NP-EDTA + EL-NP-PGG group had the highest amount of desmosine among four groups (940±261pmole desmosine/mg dry tissue), clearly showing increased elastic lamina crosslinking. A healthy non-injured aorta has 1808±290.5 pmole desmosine/ mg dry tissue (See Figure 53).

VVG Stain for Elastic Lamina

Histological evaluation of elastic lamina further confirmed quantitative results. VVG staining for elastic lamina in aortic sections showed severe damage in the EL-NP-Blank (See Figure 54C1) and EL-NP-BB94 (See Figure 54C2) groups, while the elastic lamina was partially damaged in the EL-NP-PGG (See Figure 54C3) group. However, elastic lamina had a natural wavy pattern as seen in healthy aortas in dual therapy group (EL-NP-EDTA + EL-NP-PGG) (See Figure 54C4).

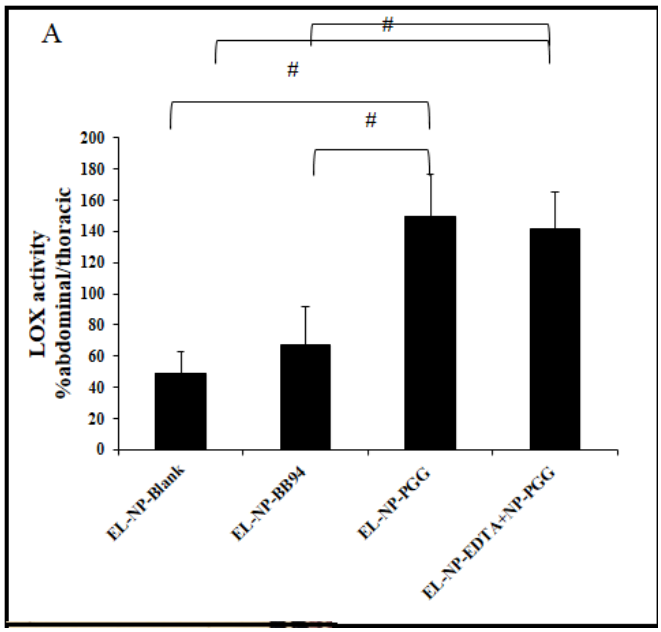

Figure 52. LOX activity in the abdominal part ($CaCl_2$ injured) over the thoracic aorta (non-injured, healthy). (#P < 0.05, Tukey's). n=6

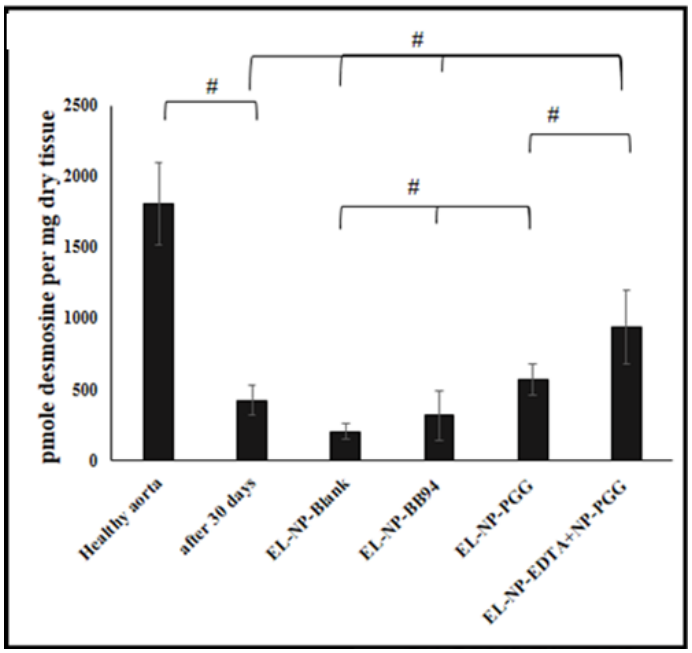

Figure 53. Desmosine content of aorta of all four-groups+healthy aorta+ 30 days post injury. (#P < 0.05, Tukey's). n=6

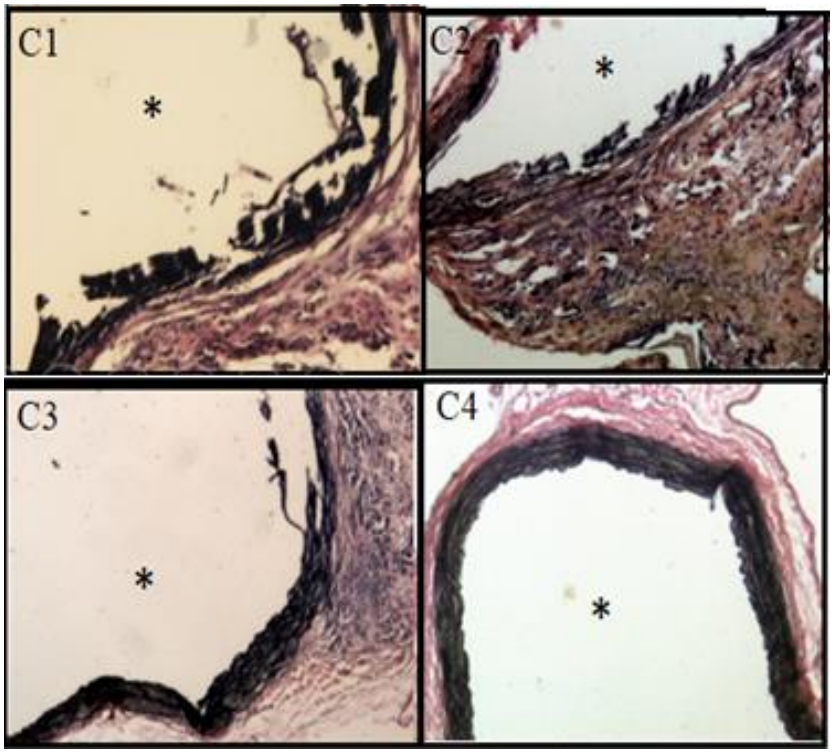

Figure 54. Verhoeff-van Gieson (VVG) staining.

Circumferential Strain

Healthy rat circumferential strain was ~13.7±1.5% (n=6). In this study, we measured circumferential strain at two time points, 30 days after injury (before any treatment began (Week 4)) and Week 12 and after the treatments finished and before euthanasia (See Figure 55). We have shown both values for each group and compared Week 4 with Week 12 in each group. At 30 days, there was significant decrease in circular strain in abdominal aortas, suggesting stiffening of the artery due to loss of elastin, deposition of collagen, and aortic mineralization. EL-NP-Blank and EL-NP-BB94 did not show any significant improvement in these values after 8 weeks, while both PGG groups (EL-NP-PGG) and (EL-NP-EDTA+EL-NP-PGG) showed significant

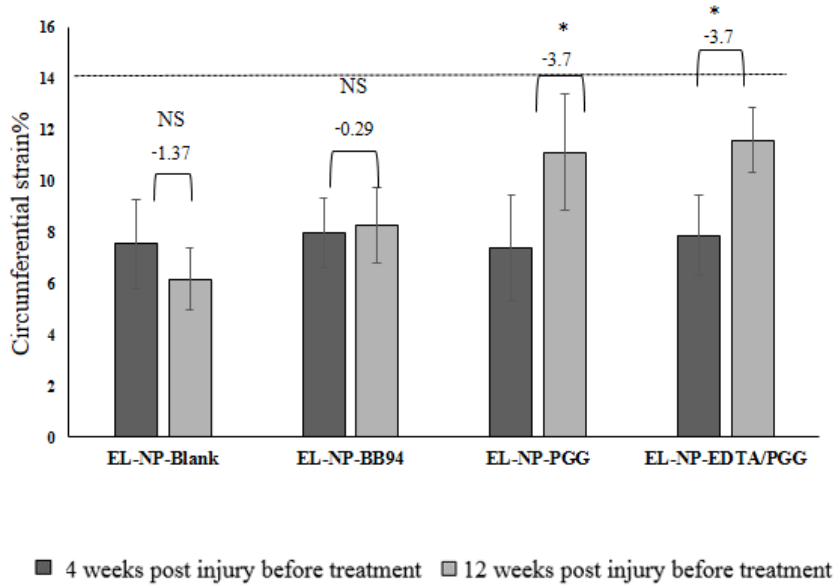

Figure 55. Circumferential strain of all four groups at week 4, after injury and before any treatment compared to Week 12 after treatment. (*P < 0.05, Tukey's test,) (n=6). Dashed line shows the circumferential strain in a healthy rat with no injury.

improvement in circumferential strain, suggesting that elastin regeneration helps restore aortic biomechanics.

Liver Function: Alanine Aminotransferase (ALT) Analysis

Serum ALT, an enzyme used to assess liver function, was consistently within the acceptable range of 5-to-45 U/L (7.8±0.5 U/L for EL-NP-Blank, 6.4±0.1 U/L for EL-NP-BB94, 5.2±0.6 U/L for EL-NP- PGG, and 6.7±0.5 U/L for EL-NP-EDTA + EL-NP-PGG rats). No differences were observed in liver histological sections stained with hematoxylin and eosin, suggesting that our treatment did not have any toxic effect on the liver.

Discussion

The ultimate goal of pharmacological therapy for AAA is to promote regression of the disease and decrease the chance of surgery and rupture. Animal studies have been performed using different medications, like statins, angiotensin-converting enzyme (ACE) inhibitors, angiotensin receptor blockers and inhibitors of MMP[218]. However, these pharmacological treatments were started at the onset of AAA induction, and these drugs reduced either inflammation or enzyme activity, but were unable to restore ECM milieu.

Contrast agent targeting to AAA for enhanced imaging has been described[219]. Our group is working on targeted therapy for AAA that can halt or regress the disease with pharmacological agents.

In our previous work, we have shown that an MMP inhibitor like BB-94, if targeted early, can halt the progression of AAA in a rat model[200]. Similarly, we have shown that EDTA targeting can remove early mineral deposits in $CaCl_2$ injury rat model[172]. Both treatments were initiated near the initiation of the diseases. However, pharmacological therapies cannot be preemptively used in patients as a precautionary measure. Once diagnosed, patients will already have developed aneurysm. Therefore, in this study, we validated the combinational use of targeted NPs carrying a chelating agent to remove calcification followed by delivery of PGG, a potent elastin protectant to reverse already developed calcified aneurysms in rats. We included delivery of BB-94, an MMP inhibitor to test if merely suppressing further degradation of ECM restores degraded elastic lamina.

Different degrees of calcification are present in most AAAs[220]. Systemic EDTA therapy has been touted and used in many countries to improve vascular function, but it is still controversial[221]. A recently concluded clinical trial (TACT) of systemic therapy for coronary disease showed slightly improved cardiovascular function that did not reach statistical significance and is therefore not FDA-approved[222]. Systemic EDTA therapy can chelate calcium in the serum and can also lead to bone loss and hypocalcemia[221]. Our approach of targeted EDTA therapy requires a 20-times-lower chelating agent that is encased in a nanoparticle and is specifically targeted to elastin calcification sites. In this study, we aimed to test if advanced calcification (30 days after injury) can be removed by targeted NP-based EDTA therapy. As expected, delivery of blank NPs did not inhibit calcification progression. Importantly, BB-94 delivery, although successful in inhibiting MMP activity at the site of AAA, was unable to prevent further calcification of the aorta. These data clearly show that suppression of a degradation pathway alone is insufficient to regress an aneurysm or existing calcification. When PGG NPs were delivered, we saw inhibition of further calcification. PGG has an affinity for proline-rich proteins like collagen and elastin, allowing for the formation of hydrogen bonds[223]. It has been shown that amino and carboxyl groups are potential nucleation site for calcification on elastin[224]. PGG has many phenolic hydroxyl groups, and they can interact with these binding sites and form hydrogen bonds. In this way, nucleation sites for calcium binding may have been blocked, and therefore, elastin was protected from further calcification. Phenolic stain confirms PGG binding to elastin. This shows that even though PGG does not have the ability to remove calcium, it can protect elastin and possibly make a hydrogen bond

and block nucleation sites on elastin. Strikingly, when we used EDTA NPs first to remove mineral deposits and then applied PGG NPs in a sequential manner, we saw not only suppression of further mineralization, but regression of deposited mineral. After EDTA treatment, we saw a higher amount of PGG bind to the elastin, which led to blocking calcification and degradation sites. Others have shown that OPN is abundant in calcified tissue and is an important regulator of arterial mineral deposition[225]. Moreover, it has been confirmed that the aortic tissues of aneurysmal patients have more OPN than non-aneurysmal patients[226]. In this study, OPN levels in the tissue correlated with the extent of calcification: The highest OPN occurred in the blank NP group, and the lowest in the dual therapy group.

Inflammation with macrophage infiltration is an important feature of AAA[227]. Pan-macrophage presence at the site of injury was abundant in the EL-NP-Blank and EL-NP-BB94 groups. MMP inhibitor BB-94 was unable to reduce inflammatory conditions. When PGG alone was delivered (EL-NP-PGG group), we saw significant reduction in macrophage presence. However, when dual EDTA therapy was followed by PGG (EL-NP-EDTA+NP-PGG group), a complete lack of macrophage presence was seen. It is known that elastin fragments (EFs) or elastin degradation products (EDPs) at the site of injury are chemotactic to macrophages, and this mechanism is mediated by elastin binding proteins[228]. Thus, suppression of elastin degradation may have further led to suppression of macrophage activity in the area and significant suppression of MMP activity in PGG groups. Another reason for suppression of macrophages in the EL-NP-EDTA+ EL-NP-PGG group may be reduction in calcification. It has been shown that

OPN is a potent chemotactic factor for macrophages[229]; we saw reversal of OPN expression after removal of mineral, and this may have also lead to suppression of macrophages. $CaCl_2$-mediated aneurysm was accompanied by depletion of the medial layer of smooth muscle cells, which others have reported[230]. In EL-NP-blank, EL-NP-BB94 and EL-NP-PGG groups, we found depletion of VSMCs where the elastin was damaged. Higher staining for viable VSMCs was observed in dual therapy (EL-NP-EDTA+EL-NP-PGG group), probably due to removal of mineral deposits and lowering of inflammatory milieu in the aorta. Systemic inflammation was tested by looking at serum IFN-γ levels in rats. IFN-γ was detected in the serum of AAA patients; additionally, AAA sections and tissue extracts from mice contained high levels of IFN-γ[231]. We observed a higher level of IFN-γ in serum of the EL-NP-Blank and EL-NP-BB94 groups compared to the EL-NP-PGG and EL-NP-EDTA+NP-PGG groups. This clearly suggests suppression of local inflammation led to suppression in systemic inflammatory markers.

Next, we looked at the elastin content of the aorta after the targeted therapy. We have shown earlier that PGG treatment of vascular smooth muscle cells from aneurysmal aortas in culture shows enhanced deposition of insoluble elastin fibers[121]. We hypothesize that due to PGG's multifunctional nature, when it binds to degraded elastin in the ECM, it has additional binding sites that can bind and anchor soluble tropoelastin precursors secreted by cells. This in turn can lead to increased lysyl oxidase (LOX) enzyme synthesis by cells to crosslink the tropoelastin. LOX is an important enzyme in elastin fiber assembly that facilitates covalent crosslinking of elastin precursors by

oxidizing peptidyl lysine to aminoadipic semialdehydes[232]. It has been shown that reduced LOX activity is involved in the pathogenesis of AAA[233,234]. As expected, aneurysmal aorta in the blank NP group showed significantly lower LOX activity as compared to healthy thoracic aorta. Delivery of BB94 did not change LOX activity, suggesting that expression of MMPs and LOX are independently controlled. When PGG was delivered either alone or after EDTA therapy, we saw significant increases in LOX activity similar to previous data from in vitro cell cultures[121].

We also looked at the desmosine content of the aorta, another marker for elastin maturation. It has been shown that levels of desmosine are significantly lower in aneurysmal specimens from human patients with AAA[210,235] than in controls, suggesting loss of mature crosslinked elastin. We have observed that desmosine content is lower in all four groups compared to healthy aortas. In our AAA model, we also observed a significant loss of desmosine as compared to healthy aorta levels, suggesting elastin degradation at the site in blank NP and BB94-NP groups. When PGG was delivered, we observed an increase in desmosine content in the aneurysmal aorta. Moreover, in the dual therapy group (EL-NP- EDTA /-PGG), desmosine content was significantly higher than in the PGG-alone group. This suggests that calcification can be a burden to elastin regeneration; when calcium was removed by EDTA delivery, elastin regeneration was facilitated. Our histological evaluation of elastin lamina with VVG stain corroborated LOX and desmosine data, showing wavy intact elastic lamina in the dual therapy group only, clearly showing regeneration of medial elastic layers after dual therapy.

We next looked at whether elastin regeneration led to improvement in tissue biomechanical parameters. It has been shown that loss of circumferential strain is the result of aneurysmal aortic degeneration[236]. Circumferential strain decreased in the EL-NP-Blank group, suggesting stiffening of the aorta. There was a very small increase in the EL-NP-BB94 group, but this increase was not statistically significant compared to the EL-NP-Blank group. Circumferential strain was increased after treatment with PGG alone and in dual therapy of EDTA and PGG (EL-NP-PGG and EL-NP-EDTA+EL-NP-PGG groups) suggesting that the functionality of the aorta in terms of elastance can be restored by elastin regeneration. Aneurysmal development as assessed by external diameter of aorta had progressed unhindered in blank NP and BB94-NP groups. Delivery of PGG led to aneurysmal regression compared to the EL-NP-Blank and EL-NP-BB94 groups. The EL-NP-EDTA+EL-NP-PGG group completely reversed aneurysmal dilation, and the aorta size was equivalent to the healthy aorta, suggesting that the combinational treatment of removing calcium by EDTA and regenerating elastin by PGG treatment may be the best strategy to reverse the disease.

A significant portion of NPs in this therapy go to kidneys, spleen, and liver although we observed a significant decrease in NP content in the liver and kidneys two weeks after injections. Thus, we hypothesize these NPs are cleared by the reticuloendothelial system (RES system)[237]. We looked at ALT levels in livers of treated rats. The ALT is the most sensitive indicator of hepatic injury[238]. The ALT level was the same among the four groups, and livers appeared normal in histological sections, suggesting that NPs were not toxic to the liver in this 12-week study.

In conclusion, we show that targeted dual NP therapy of EDTA followed by delivery of PGG is an effective way to reverse moderately developed aortic aneurysms and elastin calcification. It regenerates elastic lamina and restores healthy elastic lamina in an experimental rat model of aortic aneurysms. Thus, such therapies could be promising approach for patients with diagnosed with moderate-level AAA disease.

CHAPTER VII

CONCLUSIONS AND RECOMMENDATIONS

Conclusions

Elastin is an essential protein for maintaining elasticity of tissue. Degraded elastin can initiate inflammatory response. Also, damaged elastin can be a site of calcium nucleation. On the other hand, regeneration of elastin is impossible in adulthood. Therefore, protecting elastin from degeneration and its regeneration can be valuable in reversal of small aneurysms when it's diagnosed. We have developed nanoparticles that can be targeted to the aneurysm site by use of unique elastin antibody that recognizes only degraded elastin. First, we show that MMP inhibition with targeted nanoparticles loaded with an MMP inhibitor BB-94, we could suppress local MMP activity and inhibit initiation of elastin degradation and aneurysms in rats. Such MMP inhibitor therapy can only prevent further degradation of elastin; however, it cannot restore degraded elastin. Therefore, we chose PGG delivery as our option. We show that PGG can be loaded in polymeric nanoparticles and can be released slowly over a period of 60 days by altering nanoparticle preparation methods. When such NPs were systemically delivered, they accumulated at aneurysmal site are released active PGG that prevented aneurysmal expansion of the aorta. In advance stage of aneurysms, there is a significant calcification present in the aorta. We, therefore, tried dual therapy of EDTA (to remove mineral) followed by PGG (to stop degradation of elastin and regenerate lost elastin). Such dual therapy reversed aortic calcification and regressed aneurysmal expansion. This was the first time anyone has shown reversal of advance stage aneurysms in small animals.

Recommendation for Future Work

1. PGG is known to reduce MMPs. In our studies, we have shown that it reduces the number of macrophages *in vivo.* It would be interesting to investigate its mechanisms in macrophages suppression. Two approaches can be followed for this study: 1. Whether PGG interferes with metabolic pathways of macropahges. Macrophages can be isolated from aneurysmal tissue (human or animal) and can be characterized using flow cytometry. After culturing them *in vitro*, they can be treated by PGG or PGG NPs. To study the metabolic pathway, oxidative metabolism can be measured after incubation with PGG or PGG NPs in different time points. 2. Whether PGG alters signal transduction pathways[239]. To understand this, one of the important tests that can be done is chemotaxis assay. The chemotactic effects of the PGG conditioned media can be tested in vitro using isolated macrophages as mentioned earlier.

2. In this dissertation research, we have tried two injections of PGG nanoparticle because of lower targeting after two weeks compared to one week after injection. It's worth trying one injection of PGG nanoparticles to see if that can give the same result that two injections do as single shot treatment is preferred.

3. In this dissertation research, we used the Calcium chloride model of aneurysm. There are no animal models that faithfully recapitulate all features of human AAA. It would be useful to show that this technology is valid and useful in other animal models like the angiotensin II-induced abdominal aortic aneurysm in LDL receptor knockout mice or elastase infusion of abdominal aorta in rats. Calcium chloride model shows calcification, adventitial inflammation, and medial elastin damage but doesn't show any internal diameter change. Elastase perfusion has all the features of human AAA except calcification; however, it creates artificial faster degradation of elastin in the media causing rapid aneurysms. Ang II model is only systemic treatment model that creates AAA. It seems to show all aspects of human AAA although it is not specified to a region of interest like abdominal or thoracic aorta and AAA develop sporadically in 50% of animals. None of these three animal models led to aortic rupture as seen in humans. There is just one animal model that leads to aortic rupture. By the time they are 5 weeks old, broad-breasted white male turkeys have spontaneously developed AAA. The majority of these turkeys will die due to aneurysms that dissect the aorta when they are fed B-aminopropionitrile (BAPN). This can be a very useful model because of the size of aorta and also because it is a naturally occurring disease[240]. The only limitation is to get anti-turkey antibodies. Such antibodies can be generated in house. Another interesting model could be B-aminopropionitrile monofumarate–

induced aortic dissection in rats[241] which can be very easy if successful, because there is no surgery involved and aneurysm can be developed using diet. The only drawback is that; aneurysm won't be localized to the abdominal aorta.

4. Elastin gene in quiescent in adults, therefore finding new stimuli can be a very helpful clue to rectify the pathogenesis of diseases associated with elastin gene dysfunction. Thus, an interesting and essential experiment will be to investigate the effect of PGG on elastin gene *in vitro* and *in vivo*.

5. The contractile smooth muscle cells could switch to the synthetic phenotype in response to pathological stimuli like thoracic aortic aneurysms[242]. An in vitro experiment studying the effect of PGG on smooth muscle cells would be very interesting to see whether or not aneurysmal smooth muscle cells change phenotype from contractile to synthetic in presence of PGG. It can be done by isolating smooth muscle cells from aneurysmal tissue (human or animal). After culturing the cells, if their contractile phenotype (muscle (SM) α-actin (ACTA2), and SM22α (TAGLN)) is confirmed, PGG treatment can be started and phenotype changes can be studies using immunofluorescence at different time points.

6. It has been shown that AAAs varies from relatively non-inflammatory to inflammatory[243]. In this dissertation, we looked at CD163 and CD68 expression, but it has been shown that there are many other macrophages, T-lymphocytes and B-lymphocytes[244] present at the site of the aneurysm. It would be beneficial to look at those markers and investigate the inflammatory response more accurately when treating with PGG. Also detailed study of time course of inflammation after PGG delivery is warranted.

7. For AAAs less than 5 cm, ultrasound is the only effective way to identify size. Computed tomography (CT) or CT angiography (CTA) are recommended as the aneurysm approaches or exceeds 5 cm or rapid enlargement occurs, as these imagining techniques deliver an improved outline of the disease. Magnetic resonance imagining (MRI) and magnetic resonance angiography (MRA) are also acceptable alternatives for patients who cannot consume iodinated contrast material due to improper renal function. There is no foolproof way to predict rupture risk in human patients based merely on diameter change, although size is commonly used to predict rupture risk. Variability in aorta diameter (1.5cm-2.5cm), systolic blood pressure, growth rate, wall stress and asymmetry index between patients prevents a simple evaluation based on maximum AAA diameter from effectively evaluating all patients[245]. While our data has demonstrated that elastin-targeted NPs bind to regions of elastic lamina damage in

aneurysmal aorta, it is possible to establish a quantitative relationship between NP binding and extent of elastin degradation and the aortic rupture point. This could be a platform to predict risk of rupture by imaging a patient with aneurysm. Finding a relationship between elastic damage and nanoparticle accumulation will be a tool to predict risk of aortic rupture. Gold nanoparticles could be made with surface elastin antibody that recognizes degraded elastin only and accumulation of gold as assessed by CT can be used as a measure of rupture risk in humans.

8. In this dissertation research, we have not looked at biomechanical properties of aorta, although mechanical failure of aneurysmal aortic wall causes rupture and from a biomechanical standpoint, AAA rupture is related to mechanical wall stress. Separate groups of rats will be needed for this experiment. Biomechanical studies could be carried out on abdominal aorta close to renal and iliac bifurcations in treated rats vs control rats. Uniaxial tensile tests could be performed to measure the mechanical strength (UTS) and maximum extension at failure of aortic rings. We have shown that EDTA-PGG combination treatment removes mineral and restores elastin in the media and regresses already formed aneurysms. It will be very important to see whether this combination treatment actually improves biomechanical function of the aorta and restores it back to the healthy status.

9. Approximately 6% of the population of the United States is affected by brain aneurysms. Every year over 30,000 people in the U.S. suffer aneurysmal subarachnoid hemorrhage. Brain aneurysms also tend to occur with aging. Considering this novel nanoparticle technology targeting to elastin damage in arteries, one of the most important approach that we could follow is to test if such NPs can target brain aneurysm.

10. EL-BB-94 NPs were optimized to target degraded elastin, deliver BB-94 to the site of injury, and suppress MMPs with minimal dose. BB94 has been used already in many cancer studies[246,247] but can be a problematic drug when administered systemically because of musculoskeletal pain and inflammation[248]. So, it is entirely possible that BB-94 could be employed as a more successful therapy using the methodology of nanoparticle deployment described here. Additionally, NP surfaces could be modified to target known markers to specific cancers[249,250].

REFERENCES

1. Ascher E, Hollier LH, Strandness DE, Towne JB, Haimovici H, Calligaro K, Kent KC, Moneta GL, Pearce WH, Ricotta JJ. Haimovici's vascular surgery: John Wiley & Sons; 2008.

2. Patten DK, Layfield D, Arya S, Leff DR, Paraskeva PA. Single Best Answers in Surgery: CRC Press; 2014.

3. Longo GM, Xiong W, Greiner TC, Zhao Y, Fiotti N, Baxter BT. Matrix metalloproteinases 2 and 9 work in concert to produce aortic aneurysms. Journal of Clinical Investigation 2002;110(5):625-632.

4. Buijs R, Willems T, Tio R, Boersma H, Tielliu I, Slart R, Zeebregts C. Calcification as a risk factor for rupture of abdominal aortic aneurysm. European Journal of Vascular and Endovascular Surgery 2013;46(5):542-548.

5. Sakalihasan N, Limet R, Defawe O. Abdominal aortic aneurysm. The Lancet 2005;365(9470):1577-1589.

6. Grundmann RT. The Abdominal Aortic Aneurysm-Prognosis, Treatment, Screening and Cost-Effectiveness: INTECH Open Access Publisher; 2011.

7. Lu H, Rateri DL, Bruemmer D, Cassis LA, Daugherty A. Novel mechanisms of abdominal aortic aneurysms. Current atherosclerosis reports 2012;14(5):402-412.

8. Gadowski GR, Pilcher DB, Ricci MA. Abdominal aortic aneurysm expansion rate: effect of size and beta-adrenergic blockade. Journal of vascular surgery 1994;19(4):727-731.

9. Karlsson L, Gnarpe J, Bergqvist D, Lindbäck J, Pärsson H. The effect of azithromycin and Chlamydophilia pneumonia infection on expansion of small abdominal aortic aneurysms-A prospective randomized double-blind trial. Journal of vascular surgery 2009;50(1):23-29.

10. Dalman RL, Mell M, Mills Sr JL, Eidt JF, Mohler III ER, Clement DL, Collins KA. Management of asymptomatic abdominal aortic aneurysm.

11. Mosorin M, Juvonen J, Biancari F, Satta J, Surcel H-M, Leinonen M, Saikku P, Juvonen T. Use of doxycycline to decrease the growth rate of abdominal aortic aneurysms: a randomized, double-blind, placebo-controlled pilot study. Journal of vascular surgery 2001;34(4):606-610.

12. Shifren A, Mecham RP. The stumbling block in lung repair of emphysema: elastic fiber assembly. Proceedings of the American Thoracic Society 2006;3(5):428-433.

13. Hoffman GS, Weyand CM, Langford CA, Goronzy JJ. Inflammatory diseases of blood vessels: Wiley Online Library; 2012.

14. Isenburg JC, Simionescu DT, Starcher BC, Vyavahare NR. Elastin stabilization for treatment of abdominal aortic aneurysms. Circulation 2007;115(13):1729-1737.

15. Saphirstein RJ, Morgan KG. The contribution of vascular smooth muscle to aortic stiffness across length scales. Microcirculation 2014;21(3):201-207.

16. Kilarski W. Mechanisms of Tissue Vascularization. 2005.

17. Holman ME, Kasby C, Suthers M, Wilson JA. Some properties of the smooth muscle of rabbit portal vein. The Journal of physiology 1968;196(1):111.

18. Junqueira L, Carneiro J, Kelley R. Basic histology. 9th. Stamford, Conn.: Appleton & Lange. x; 1998.

19. Rhodin JA. Architecture of the vessel wall. Comprehensive Physiology 2011.

20. Fortier A, Gullapalli V, Mirshams RA. Review of biomechanical studies of arteries and their effect on stent performance. IJC Heart & Vessels 2014;4:12-18.

21. Vorp DA. Biomechanics of abdominal aortic aneurysm. Journal of biomechanics 2007;40(9):1887-1902.

22. Xiong J, Wang SM, Zhou W, Wu JG. Measurement and analysis of ultimate mechanical properties, stress-strain curve fit, and elastic modulus formula of human abdominal aortic aneurysm and nonaneurysmal abdominal aorta. Journal of vascular surgery 2008;48(1):189-195.

23. Roach MR, Burton AC. The effect of age on the elasticity of human iliac arteries. Canadian journal of biochemistry and physiology 1959;37(4):557-570.

24. Kassab GS. Biomechanics of the cardiovascular system: the aorta as an illustratory example. Journal of the Royal Society Interface 2006;3(11):719-740.

25. Lanzer P, Topol EJ. Pan vascular medicine: integrated clinical management: Springer; 2013.

26. Carew TE, VAISHNAV RN, PATEL DJ. Compressibility of the arterial wall. Circulation Research 1968;23(1):61-68.

27. Bäck M, Gasser TC, Michel J-B, Caligiuri G. Biomechanical factors in the biology of aortic wall and aortic valve diseases. Cardiovascular research 2013;99(2):232-241.

28. Shu C, Assar A, Xu C, Zarins C. Sustained Increase in Aortic Wall Tension Induces Aneurysmal Enlargement in the Abdominal Aorta of the Rat. 2012. WILEY-BLACKWELL 111 RIVER ST, HOBOKEN 07030-5774, NJ USA. p 84-84.

29. Biewener A. Overview of structural mechanics. Biomechanics—Structures and Systems 1992:1-20.

30. Lindeman JH, Ashcroft BA, Beenakker J-WM, van Es M, Koekkoek NB, Prins FA, Tielemans JF, Abdul-Hussien H, Bank RA, Oosterkamp TH. Distinct defects in collagen microarchitecture underlie vessel-wall failure in advanced abdominal aneurysms and aneurysms in Marfan syndrome. Proceedings of the National Academy of Sciences 2010;107(2):862-865.

31. Li RX, Luo J, Balaram SK, Chaudhry FA, Lantis JC, Shahmirzadi D, Konofagou EE. In-vivo pulse wave imaging for arterial stiffness measurement under normal and pathological conditions. 2011. IEEE. p 567-570.

32. Tomlinson LA. Methods for assessing arterial stiffness: technical considerations. Current opinion in nephrology and hypertension 2012;21(6):655-660.

33. Trachet B, Fraga-Silva RA, Londono FJ, Swillens A, Stergiopulos N, Segers P. Performance comparison of ultrasound-based methods to assess aortic diameter and stiffness in normal and aneurysmal mice. PloS one 2015;10(5):e0129007.

34. Rosenbloom J, Abrams W, Mecham R. Extracellular matrix 4: the elastic fiber. The FASEB Journal 1993;7(13):1208-1218.

35. Vrhovski B, Weiss AS. Biochemistry of tropoelastin. European Journal of Biochemistry 1998;258(1):1-18.

36. Vasconcelos A. Protein matrices for wound dressings. 2011.

37. Fritze O, Romero B, Schleicher M, Jacob MP, Oh D-Y, Starcher B, Schenke-Layland K, Bujan J, Stock UA. Age-related changes in the elastic tissue of the human aorta. Journal of vascular research 2011;49(1):77-86.

38. Dietz HC, Pyeritz R. Mutations in the human gene for fibrillin-1 (FBN1) in the Marfan syndrome and related disorders. Human Molecular Genetics 1995;4(suppl 1):1799-1809.

39. Thomassin L, Werneck CC, Broekelmann TJ, Gleyzal C, Hornstra IK, Mecham RP, Sommer P. The Pro-regions of lysyl oxidase and lysyl oxidase-like 1 are required for deposition onto elastic fibers. Journal of Biological Chemistry 2005;280(52):42848-42855.

40. Nivison-Smith L, Weiss A. Elastin based constructs: INTECH Open Access Publisher; 2011.

41. Akhtar K, Broekelmann TJ, Song H, Turk J, Brett TJ, Mecham RP, Adair-Kirk TL. Oxidative modifications of the C-terminal domain of tropoelastin prevent cell binding. Journal of Biological Chemistry 2011;286(15):13574-13582.

42. Zaret BL, Cohen LS, Moser M. Yale university school of medicine heart book: William Morrow and Co.; 1992.

43. Control CfD, Prevention. Million hearts: strategies to reduce the prevalence of leading cardiovascular disease risk factors--United States, 2011. MMWR. Morbidity and mortality weekly report 2011;60(36):1248.

44. Ardies CM. Diet, Exercise, and Chronic Disease: The Biological Basis of Prevention: Crc Press; 2014.

45. Association AH. Heart and stroke facts: The Association; 1993.

46. Powell J. Non-operative or medical management of abdominal aortic aneurysm. Scandinavian Journal of Surgery 2008;97(2):121-124.

47. Maiora J, Graña M. Abdominal cta image analisys through active learning and decision random forests: Aplication to aaa segmentation. 2012. IEEE. p 1-7.

48. Mozaffarian D, Benjamin EJ, Go AS, Arnett DK, Blaha MJ, Cushman M, de Ferranti S, Despres J-P, Fullerton HJ, Howard VJ. Heart disease and stroke statistics-2015 update: a report from the american heart association. Circulation 2015;131(4):e29.

49. Gasser TC, Gallinetti S, Xing X, Forsell C, Swedenborg J, Roy J. Spatial orientation of collagen fibers in the abdominal aortic aneurysm's wall and its relation to wall mechanics. Acta biomaterialia 2012;8(8):3091-3103.

50. García-Herrera CM, Atienza J, Rojo F, Claes E, Guinea G, Celentano DJ, García-Montero C, Burgos R. Mechanical behaviour and rupture of normal and pathological human ascending aortic wall. Medical & biological engineering & computing 2012;50(6):559-566.

51. Finlayson SR, Birkmeyer JD, Fillinger MF, Cronenwett JL. Should endovascular surgery lower the threshold for repair of abdominal aortic aneurysms? Journal of vascular surgery 1999;29(6):973-985.

52. Haug ES, Romundstad P, Aadahl P, Myhre H. Emergency non-ruptured abdominal aortic aneurysm. European journal of vascular and endovascular surgery 2004;28(6):612-618.

53. Brown PM, Pattenden R, Vernooy C, Zelt DT, Gutelius JR. Selective management of abdominal aortic aneurysms in a prospective measurement program. Journal of vascular surgery 1996;23(2):213-222.

54. Sun Z-H. Abdominal aortic aneurysm: Treatment options, image visualizations and follow-up procedures. Journal of geriatric cardiology: JGC 2012;9(1):49.

55. Jones G. Diagnosis, Screening and Treatment of Abdominal, Thoracoabdominal and Thoracic Aortic Aneurysms. 2011.

56. Wilt TJ, Lederle FA, MacDonald R, Jonk YC, Rector TS, Kane RL. Comparison of endovascular and open surgical repairs for abdominal aortic aneurysm. Evidence report/technology assessment 2006(144):1-113.

57. Schermerhorn ML, O'Malley AJ, Jhaveri A, Cotterill P, Pomposelli F, Landon BE. Endovascular vs. open repair of abdominal aortic aneurysms in the Medicare population. New England Journal of Medicine 2008;358(5):464-474.

58. Heikkinen M, Salenius J-P, Auvinen O. Ruptured abdominal aortic aneurysm in a well-defined geographic area. Journal of vascular surgery 2002;36(2):291-296.

59. Trollope A, Moxon JV, Moran CS, Golledge J. Animal models of abdominal aortic aneurysm and their role in furthering management of human disease. Cardiovascular Pathology 2011;20(2):114-123.

60. Czerski A, Bujok J, Gnus J, Hauzer W, Ratajczak K, Nowak M, Janeczek M, Zawadzki W, Witkiewicz W, Rusiecka A. Experimental methods of abdominal aortic aneurysm creation in swine as a large animal model. J Physiol Pharmacol 2013;64(2):185-192.

61. Allaire E, Guettier C, Bruneval P, Plissonnier D, Michel J-B. Cell-free arterial grafts: morphologic characteristics of aortic isografts, allografts, and xenografts in rats. Journal of vascular surgery 1994;19(3):446-456.

62. Powell J, Greenhalgh RM. Cellular, enzymatic, and genetic factors in the pathogenesis of abdominal aortic aneurysms. Journal of vascular surgery 1989;9(2):297-304.

63. Blumenthal HT, Lansing A, Wheeler PA. Calcification of the media of the human aorta and its relation to intimal arteriosclerosis, ageing and disease. The American journal of pathology 1944;20(4):665.

64. Economou SG, Taylor CB, Beattie Jr E, Davis Jr C. Persistent experimental aortic aneurysms in dogs. Surgery 1960;47:21-28.

65. Maier A, Gee M, Reeps C, Eckstein H-H, Wall W. Impact of calcifications on patient-specific wall stress analysis of abdominal aortic aneurysms. Biomechanics and modeling in mechanobiology 2010;9(5):511-521.

66. Gertz SD, Kurgan A, Eisenberg D. Aneurysm of the rabbit common carotid artery induced by periarterial application of calcium chloride in vivo. Journal of Clinical Investigation 1988;81(3):649.

67. Wang Y, Krishna S, Golledge J. The calcium chloride-induced rodent model of abdominal aortic aneurysm. Atherosclerosis 2013;226(1):29-39.

68. Freestone T, Turner R, Higman D, Lever M, Powell J. Influence of hypercholesterolemia and adventitial inflammation on the development of aortic aneurysm in rabbits. Arteriosclerosis, thrombosis, and vascular biology 1997;17(1):10-17.

69. Chiou AC, Chiu B, Pearce WH. Murine aortic aneurysm produced by periarterial application of calcium chloride. Journal of Surgical Research 2001;99(2):371-376.

70. Basalyga DM, Simionescu DT, Xiong W, Baxter BT, Starcher BC, Vyavahare NR. Elastin degradation and calcification in an abdominal aorta injury model role of matrix metalloproteinases. Circulation 2004;110(22):3480-3487.

71. Tsuruda T, Kato J, Hatakeyama K, Kojima K, Yano M, Yano Y, Nakamura K, Nakamura-Uchiyama F, Matsushima Y, Imamura T. Adventitial mast cells contribute to pathogenesis in the progression of abdominal aortic aneurysm. Circulation research 2008;102(11):1368-1377.

72. Carrell T, Smith A, Burnand K. Experimental techniques and models in the study of the development and treatment of abdominal aortic aneurysm. British journal of surgery 1999;86(3):305-312.

73. King VL, Trivedi DB, Gitlin JM, Loftin CD. Selective cyclooxygenase-2 inhibition with celecoxib decreases angiotensin II-induced abdominal aortic aneurysm formation in mice. Arteriosclerosis, thrombosis, and vascular biology 2006;26(5):1137-1143.

74. Wang Y-X, Martin-McNulty B, da Cunha V, Vincelette J, Lu X, Feng Q, Halks-Miller M, Mahmoudi M, Schroeder M, Subramanyam B. Fasudil, a Rho-kinase inhibitor, attenuates angiotensin II–induced abdominal aortic aneurysm in apolipoprotein E–deficient mice by inhibiting apoptosis and proteolysis. Circulation 2005;111(17):2219-2226.

75. Fleming C, Whitlock EP, Beil TL, Lederle FA. Screening for abdominal aortic aneurysm: a best-evidence systematic review for the US Preventive Services Task Force. Annals of Internal Medicine 2005;142(3):203-211.

76. Ducajú GM, Farré AL, Modrego J, Serrano J. Actual Pharmacological Treatment to Reduce Growth of Small Abdominal Aneurysm: INTECH Open Access Publisher; 2011.

77. Valentine RJ, DeCaprio JD, Castillo JM, Modrall JG, Jackson MR, Clagett GP. Watchful waiting in cases of small abdominal aortic aneurysms—appropriate for all patients? Journal of vascular surgery 2000;32(3):441-450.

78. Thompson RW, Timothy, B. MMP Inhibition in Abdominal Aortic Aneurysms: Rationale for a Prospective Randomized Clinical Trial. Annals of the New York Academy of Sciences 1999;878 (1):159-178.

79. Brophy CM, Reilly JM, Smith GW, Tilson MD. The role of inflammation in nonspecific abdominal aortic aneurysm disease. Annals of vascular surgery 1991;5(3):229-233.

80. Tsamis A, Krawiec JT, Vorp DA. Elastin and collagen fibre microstructure of the human aorta in ageing and disease: a review. Journal of the Royal Society Interface 2013;10(83):20121004.

81. Freestone T, Turner RJ, Coady A, Higman DJ, Greenhalgh RM, Powell JT. Inflammation and matrix metalloproteinases in the enlarging abdominal aortic aneurysm. Arteriosclerosis, thrombosis, and vascular biology 1995;15(8):1145-1151.

82. Sami N. Autoimmune Bullous Diseases: Approach and Management: Springer; 2016.

83. Devulapalli Narasimha Swamy SS, Moogla S, Kapalavai V. Chemically modified tetracyclines: The novel host modulating agents. Journal of Indian Society of Periodontology 2015;19(4):370.

84. Smith MB, Lee NJ, Haney E, Carson S, Helfand M. Drug Class Review HMG-CoA Reductase Inhibitors (Statins) and Fixed-dose Combination Products Containing a Statin. Update 2009.

85. Van Kuijk JP, Flu W, Witteveen O, Voute M, Bax J, Poldermans D. The influence of statins on the expansion rate and rupture risk of abdominal aortic aneurysms. Journal of Cardiovascular Surgery 2009;50(5):599.

86. Takagi H, Matsui M, Umemoto T. A meta-analysis of clinical studies of statins for prevention of abdominal aortic aneurysm expansion. Journal of vascular surgery 2010;52(6):1675-1681.

87. Steinmetz EF, Buckley C, Shames ML, Ennis TL, Vanvickle-Chavez SJ, Mao D, Goeddel LA, Hawkins CJ, Thompson RW. Treatment with simvastatin suppresses the development of experimental abdominal aortic aneurysms in normal and hypercholesterolemic mice. Annals of surgery 2005;241(1):92-101.

88. Shiraya S, Miyake T, Aoki M, Yoshikazu F, Ohgi S, Nishimura M, Ogihara T, Morishita R. Inhibition of development of experimental aortic abdominal aneurysm in rat model by atorvastatin through inhibition of macrophage migration. Atherosclerosis 2009;202(1):34-40.

89. Feeney JM, Burns K, Staff I, Bai J, Rodrigues N, Fortier J, Jacobs LM. Prehospital HMG Co-A reductase inhibitor use and reduced mortality in ruptured abdominal aortic aneurysm. Journal of the American College of Surgeons 2009;209(1):41-46.

90. Sukhija R, Aronow WS, Sandhu R, Kakar P, Babu S. Mortality and size of abdominal aortic aneurysm at long-term follow-up of patients not treated surgically and treated with and without statins. The American journal of cardiology 2006;97(2):279-280.

91. Schouten O, van Laanen JH, Boersma E, Vidakovic R, Feringa HH, Dunkelgrün M, Bax JJ, Koning J, van Urk H, Poldermans D. Statins are associated with a reduced infrarenal abdominal aortic aneurysm growth. European journal of vascular and endovascular surgery 2006;32(1):21-26.

92. Hadi H, Mahmeed W, Suwaidi J, Ellahham S. Pleiotropic effects of statins in atrial fibrillation patients: the evidence. Vasc Health Risk Manag 2009;5(3):533-551.

93. Mateos-Caceres PJ, Lopez-Farre AJ, Morata PC, Ramos-Mozo P, Macaya C, Serrano FJ, Moñux G. Pravastatin increases the expression of the tissue inhibitor of matrix metalloproteinase-1 and the oncogene Bax in human aortic abdominal aneurysms. Canadian journal of physiology and pharmacology 2008;86(7):431-437.

94. Verma RP, Hansch C. Matrix metalloproteinases (MMPs): chemical–biological functions and (Q) SARs. Bioorganic & medicinal chemistry 2007;15(6):2223-2268.

95. Karsdal MA, Nielsen MJ, Sand JM, Henriksen K, Genovese F, Bay-Jensen A-C, Smith V, Adamkewicz JI, Christiansen C, Leeming DJ. Extracellular matrix remodeling: the common denominator in connective tissue diseases possibilities for evaluation and current understanding of the matrix as more than a passive architecture, but a key player in tissue failure. Assay and drug development technologies 2013;11(2):70-92.

96. Reitz AB. Frontiers in Medicinal Chemistry: Bentham Science Publishers; 2005.

97. Benjamin MM, Khalil RA. Matrix metalloproteinase inhibitors as investigative tools in the pathogenesis and management of vascular disease. Matrix Metalloproteinase Inhibitors: Springer; 2012. p 209-279.

98. Gupta SP. Matrix metalloproteinase inhibitors: specificity of binding and structure-activity relationships: Springer Science & Business Media; 2012.

99. Woessner JF. Matrix metalloproteinase inhibition: from the Jurassic to the third millennium. Annals of the New York Academy of Sciences 1999;878(1):388-403.

100. Ali HA, Dembitsky VM, Srebnik M. Contemporary Aspects of Boron: Chemistry and Biological Applications: Chemistry and Biological Applications: Elsevier; 2005.

101. Vandenbroucke RE, Libert C. Is there new hope for therapeutic matrix metalloproteinase inhibition? Nature reviews Drug discovery 2014;13(12):904-927.

102. Botos I, Scapozza L, Zhang D, Liotta LA, Meyer EF. Batimastat, a potent matrix mealloproteinase inhibitor, exhibits an unexpected mode of binding. Proceedings of the National Academy of Sciences 1996;93(7):2749-2754.

103. Bigatel DA, Elmore JR, Carey DJ, Cizmeci-Smith G, Franklin DP, Youkey JR. The matrix metalloproteinase inhibitor BB-94 limits expansion of experimental abdominal aortic aneurysms. Journal of vascular surgery 1999;29(1):130-139.

104. Peterson M, Porter K, Loftus I, Thompson M, London N. Marimastat Inhibits Neointimal Thickening in aModel of Human Arterial Intimal Hyperplasia. European Journal of Vascular and Endovascular Surgery 2000;19(5):461-467.

105. Durrant JD, de Oliveira CA, McCammon JA. Pyrone-Based Inhibitors of Metalloproteinase Types 2 and 3 May Work as Conformation-Selective Inhibitors. Chemical biology & drug design 2011;78(2):191-198.

106. Hua H, Li M, Luo T, Yin Y, Jiang Y. Matrix metalloproteinases in tumorigenesis: an evolving paradigm. Cellular and Molecular Life Sciences 2011;68(23):3853-3868.

107. Fisher JF, Mobashery S. Recent advances in MMP inhibitor design. Cancer and Metastasis Reviews 2006;25(1):115-136.

108. Kasaoka T, Nishiyama H, Okada M, Nakajima M. Matrix metalloproteinase inhibitor, MMI270 (CGS27023A) inhibited hematogenic metastasis of B16 melanoma cells in both experimental and spontaneous metastasis models. Clinical & experimental metastasis 2008;25(7):827-834.

109. Daugherty A, Cassis LA, Lu H. Complex pathologies of angiotensin II-induced abdominal aortic aneurysms. Journal of Zhejiang University Science B 2011;12(8):624-628.

110. Claridge M, Hobbs S, Quick C, Day N, Bradbury A, Wilmink A. ACE inhibitors increase type III collagen synthesis: a potential explanation for reduction in acute vascular events by ACE inhibitors. European journal of vascular and endovascular surgery 2004;28(1):67-70.

111. Liao S, Miralles M, Kelley BJ, Curci JA, Borhani M, Thompson RW. Suppression of experimental abdominal aortic aneurysms in the rat by treatment with angiotensin-converting enzyme inhibitors. Journal of vascular surgery 2001;33(5):1057-1064.

112. Alsac J-M, Journe C, Louedec L, Dai J, Julia P, Fabiani J-N, Michel J-B. Downregulation of remodelling enzymatic activity induced by an angiotensin-converting enzyme inhibitor (perindopril) reduces the degeneration of experimental abdominal aortic aneurysms in a rat model. European Journal of Vascular and Endovascular Surgery 2011;41(4):474-480.

113. Hackam DG, Thiruchelvam D, Redelmeier DA. Angiotensin-converting enzyme inhibitors and aortic rupture: a population-based case-control study. The Lancet 2006;368(9536):659-665.

114. Sweeting MJ, Thompson SG, Brown LC, Greenhalgh RM, Powell JT. Use of angiotensin converting enzyme inhibitors is associated with increased growth rate of abdominal aortic aneurysms. Journal of vascular surgery 2010;52(1):1-4.

115. Fujiwara Y, Shiraya S, Miyake T, Yamakawa S, Aoki M, Makino H, Nishimura M, Morishita R. Inhibition of experimental abdominal aortic aneurysm in a rat model by the angiotensin receptor blocker valsartan. International journal of molecular medicine 2008;22(6):703-708.

116. Habashi JP, Judge DP, Holm TM, Cohn RD, Loeys BL, Cooper TK, Myers L, Klein EC, Liu G, Calvi C. Losartan, an AT1 antagonist, prevents aortic aneurysm in a mouse model of Marfan syndrome. Science 2006;312(5770):117-121.

117. Gavrila D, Li WG, McCormick ML, Thomas M, Daugherty A, Cassis LA, Miller FJ, Oberley LW, Dellsperger KC, Weintraub NL. Vitamin E inhibits abdominal aortic aneurysm formation in angiotensin II–infused apolipoprotein E–deficient mice. Arteriosclerosis, thrombosis, and vascular biology 2005;25(8):1671-1677.

118. Munin A, Edwards-Lévy F. Encapsulation of natural polyphenolic compounds; a review. Pharmaceutics 2011;3(4):793-829.

119. Manach C, Scalbert A, Morand C, Rémésy C, Jiménez L. Polyphenols: food sources and bioavailability. The American Journal of Clinical Nutrition 2004;79(5):727-747.

120. Pei Y, Xiang Y-F, Chen J-N, Lu C-H, Hao J, Du Q, Qu C, Li S, Ju H-Q, Ren Z. Pentagalloylglucose downregulates cofilin1 and inhibits HSV-1 infection. Antiviral research 2011;89(1):98-108.

121. Sinha A, Nosoudi N, Vyavahare N. Elasto-regenerative properties of polyphenols. Biochemical and biophysical research communications 2014;444(2):205-211.

122. Isenburg JC, Karamchandani NV, Simionescu DT, Vyavahare NR. Structural requirements for stabilization of vascular elastin by polyphenolic tannins. Biomaterials 2006;27(19):3645-51.

123. Hagerman A. Tannin Handbook. Miami University. Oxford OH; 2002.

124. Bae YH, Park K. Targeted drug delivery to tumors: myths, reality and possibility. Journal of Controlled Release 2011;153(3):198.

125. Kumar A, Patel A, Duvalsaint L, Desai M, Marks ED. Thymosin β4 coated nanofiber scaffolds for the repair of damaged cardiac tissue. J Nanobiotechnol 2014;12(10).

126. Hasan A, Memic A, Annabi N, Hossain M, Paul A, Dokmeci MR, Dehghani F, Khademhosseini A. Electrospun scaffolds for tissue engineering of vascular grafts. Acta biomaterialia 2014;10(1):11-25.

127. Cho YW, Kim K, Park K, Kwon IC. Molecular imaging in the aid of drug delivery technology. Macromolecular Research 2014;22(9):926-931.

128. Arayne MS, Sultana N, Qureshi F. Review: nanoparticles in delivery of cardiovascular drugs. Pakistan journal of pharmaceutical sciences 2007;20(4):340-348.

129. de La Zerda A, Gambhir SS. Drug delivery: keeping tabs on nanocarriers. Nature nanotechnology 2007;2(12):745-746.

130. Tiwari G, Tiwari R, Sriwastawa B, Bhati L, Pandey S, Pandey P, Bannerjee SK. Drug delivery systems: An updated review. International journal of pharmaceutical investigation 2012;2(1):2.

131. Yildirimer L, Thanh NT, Loizidou M, Seifalian AM. Toxicology and clinical potential of nanoparticles. Nano today 2011;6(6):585-607.

132. Yu B, Tai HC, Xue W, Lee LJ, Lee RJ. Receptor-targeted nanocarriers for therapeutic delivery to cancer. Molecular membrane biology 2010;27(7):286-298.

133. Mitra A, Lee CH, Cheng K. Advanced drug delivery: John Wiley & Sons; 2013.

134. Teicher BA, Chari RV. Antibody conjugate therapeutics: challenges and potential. Clinical Cancer Research 2011;17(20):6389-6397.

135. Rapaka R. Membranes and Barriers: Targeted Drug Delivery. National Institute on Drug Abuse, Research Monograph 154. US DEPARTMENT OF HEALTH AND HUMAN SERVICES. Public Health Service, National Institutes of Health, National Institute on Drug Abuse, Division of Preclinical Research 1995;5600.

136. Meyers JD, Doane T, Burda C, Basilion JP. Nanoparticles for imaging and treating brain cancer. Nanomedicine 2013;8(1):123-143.

137. Katz J. Developments in medical polymers for biomaterials applications. Medical Device and Diagnostic Industry 2001;23(1):122-133.

138. Makadia HK, Siegel SJ. Poly lactic-co-glycolic acid (PLGA) as biodegradable controlled drug delivery carrier. Polymers 2011;3(3):1377-1397.

139. Marin E, Briceño MI, Caballero-George C. Critical evaluation of biodegradable polymers used in nanodrugs. International journal of nanomedicine 2013;8:3071.

140. Bao G, Mitragotri S, Tong S. Multifunctional nanoparticles for drug delivery and molecular imaging. Annual review of biomedical engineering 2013;15:253-282.

141. Coelho JF, Ferreira PC, Alves P, Cordeiro R, Fonseca AC, Góis JR, Gil MH. Drug delivery systems: Advanced technologies potentially applicable in personalized treatments. The EPMA journal 2010;1(1):164-209.

142. Fonte P, Araújo F, Silva C, Pereira C, Reis S, Santos HA, Sarmento B. Polymer-based nanoparticles for oral insulin delivery: Revisited approaches. Biotechnology advances 2015;33(6):1342-1354.

143. Li J, Fan C, Pei H, Shi J, Huang Q. Smart Drug Delivery Nanocarriers with Self-Assembled DNA Nanostructures. Advanced materials 2013;25(32):4386-4396.

144. van Hell AJ, Fretz MM, Crommelin DJ, Hennink WE, Mastrobattista E. Peptide nanocarriers for intracellular delivery of photosensitizers. Journal of Controlled Release 2010;141(3):347-353.

145. Babu A, Templeton AK, Munshi A, Ramesh R. Nanodrug delivery systems: a promising technology for detection, diagnosis, and treatment of cancer. AAPS PharmSciTech 2014;15(3):709-721.

146. Kobayashi H, Watanabe R, Choyke PL. Improving conventional enhanced permeability and retention (EPR) effects; what is the appropriate target. Theranostics 2014;4(1):81-89.

147. Friedman AD, Claypool SE, Liu R. The smart targeting of nanoparticles. Current pharmaceutical design 2013;19(35):6315.

148. Georgieva JV, Hoekstra D, Zuhorn IS. Smuggling drugs into the brain: an overview of ligands targeting transcytosis for drug delivery across the blood–brain barrier. Pharmaceutics 2014;6(4):557-583.

149. Mansour HM, Sohn M, Al-Ghananeem A, DeLuca PP. Materials for pharmaceutical dosage forms: molecular pharmaceutics and controlled release drug delivery aspects. International journal of molecular sciences 2010;11(9):3298-3322.

150. Valo H. Biopolymer-Based Nanoparticles for Drug Delivery. 2012.

151. Mukherjee B, Santra K, Pattnaik G, Ghosh S. Preparation, characterization and in-vitro evaluation of sustained release protein-loaded nanoparticles based on biodegradable polymers. International journal of nanomedicine 2008;3(4):487.

152. Ma P, Mumper RJ. Paclitaxel nano-delivery systems: a comprehensive review. Journal of nanomedicine & nanotechnology 2013;4(2):1000164.

153. Jain I. Crosslinking Albumin for Drug Release from Spray Dried Particles: University of Louisville; 2014.

154. Niknejad H, Mahmoudzadeh R. Comparison of Different Crosslinking Methods for Preparation of Docetaxel-loaded Albumin Nanoparticles. Iranian journal of pharmaceutical research: IJPR 2015;14(2):385.

155. Singh R, Lillard JW. Nanoparticle-based targeted drug delivery. Experimental and molecular pathology 2009;86(3):215-223.

156. Bamrungsap S, Zhao Z, Chen T, Wang L, Li C, Fu T, Tan W. Nanotechnology in therapeutics: a focus on nanoparticles as a drug delivery system. Nanomedicine 2012;7(8):1253-1271.

157. Champion JA, Katare YK, Mitragotri S. Particle shape: a new design parameter for micro-and nanoscale drug delivery carriers. Journal of Controlled Release 2007;121(1):3-9.

158. Yoo J-W, Chambers E, Mitragotri S. Factors that control the circulation time of nanoparticles in blood: challenges, solutions and future prospects. Current pharmaceutical design 2010;16(21):2298-2307.

159. Owens DE, Peppas NA. Opsonization, biodistribution, and pharmacokinetics of polymeric nanoparticles. International journal of pharmaceutics 2006;307(1):93-102.

160. Perrie Y, Rades T. FASTtrack Pharmaceutics: Drug Delivery and Targeting: Pharmaceutical press; 2012.

161. Peracchia M, Harnisch S, Pinto-Alphandary H, Gulik A, Dedieu J, Desmaele D, d'Angelo J, Müller R, Couvreur P. Visualization of in vitro protein-rejecting properties of PEGylated stealth® polycyanoacrylate nanoparticles. Biomaterials 1999;20(14):1269-1275.

162. Fröhlich E. The role of surface charge in cellular uptake and cytotoxicity of medical nanoparticles. Int J Nanomedicine 2012;7:5577-5591.

163. Fleischer CC, Payne CK. Nanoparticle–cell interactions: molecular structure of the protein corona and cellular outcomes. Accounts of chemical research 2014;47(8):2651-2659.

164. Panyam J, ZHOU W-Z, PRABHA S, SAHOO SK, LABHASETWAR V. Rapid endo-lysosomal escape of poly (DL-lactide-co-glycolide) nanoparticles: implications for drug and gene delivery. The FASEB Journal 2002;16(10):1217-1226.

165. Bonnard T, Yang G, Petiet A, Ollivier V, Haddad O, Arnaud D, Louedec L, Bachelet-Violette L, Derkaoui SM, Letourneur D. Abdominal aortic aneurysms targeted by functionalized polysaccharide microparticles: a new tool for SPECT imaging. Theranostics 2014;4(6):592.

166. Sivaraman B, Ramamurthi A. Multifunctional nanoparticles for doxycycline delivery towards localized elastic matrix stabilization and regenerative repair. Acta biomaterialia 2013;9(5):6511-6525.

167. Sinha A, Shaporev A, Nosoudi N, Lei Y, Vertegel A, Lessner S, Vyavahare N. Nanoparticle targeting to diseased vasculature for imaging and therapy. Nanomedicine-Nanotechnology Biology and Medicine 2014;10(5):1003-1012.

168. Vandenbroucke RE, Libert C. Is there new hope for therapeutic matrix metalloproteinase inhibition? Nature Reviews Drug Discovery 2014.

169. Investigators PAT. Propranolol for small abdominal aortic aneurysms: results of a randomized trial. Journal of Vascular Surgery 2002;35(1):72-79.

170. Fingleton B. MMPs as therapeutic targets—still a viable option? ; 2008. Elsevier. p 61-68.

171. Wiernicki I, Cnotliwy M, Baranowska-Bosiacka I, Urasinska E, Kwas A, Bober J, Gutowski P. Elastin degradation within the abdominal aortic aneurysm wall–relationship between intramural pH and adjacent thrombus formation. European journal of clinical investigation 2008;38(12):883-887.

172. Lei Y, Nosoudi N, Vyavahare N. Targeted chelation therapy with EDTA-loaded albumin nanoparticles regresses arterial calcification without causing systemic side effects. Journal of Controlled Release 2014;196:79-86.

173. Kuivaniemi H, Platsoucas, C., and Tilson, III M.D. Aortic Aneurysms: An Immune Disease With a Strong Genetic Component. Circulation. 2008;117(2):242.

174. Woessner JF, & Nagase, H. . Matrix metalloproteinases and TIMPs. Oxford; New York: Oxford University Press; , 2000.

175. Morris DR, Biros, E., Cronin, O., Kuivaniemi, H., & Golledge, J. . The association of genetic variants of matrix metalloproteinases with abdominal aortic aneurysm: a systematic review and meta-analysis. Heart Heart 2014;100(4):295-302.

176. Sun J. Matrix Metalloproteinases and Tissue Inhibitor of Metalloproteinases Are Essential for the Inflammatory Response in Cancer Cells. Journal of Signal Transduction Journal of Signal Transduction 2010(2):1-7.

177. Raffetto JD, Khalil, R.A,. Matrix metalloproteinases and their inhibitors in vascular remodeling and vascular disease. Biochemical pharmacology 2008;75(2):346-59.

178. Kadoglou NP, Liapis CD. Matrix metalloproteinases: contribution to pathogenesis, diagnosis, surveillance and treatment of abdominal aortic aneurysms. Current Medical Research and Opinion® 2004;20(4):419-432.

179. Prescott MS, W. K, Von Linden-Reed, J., Jeune, M., Chou, M., Caplan, S. L., Jeng, A. Y. Effect of matrix metalloproteinase inhibition on progression of atherosclerosis and aneurysm in LDL receptor-deficient mice overexpressing MMP-3, MMP-12, and MMP-13 and on restenosis in rats after balloon injury. Annals of the New York Academy of Sciences 1999;878:179-90.

180. Brown PD. Matrix metalloproteinase inhibitors in the treatment of cancer. Medical Oncology 1997;14(1):1-10.

181. Mannello F, Tonti, G., Papa, S. . Matrix Metalloproteinase Inhibitors as Anticancer Therapeutics. Current Cancer Drug Targets 2005;5(4):285-98.

182. Abbruzzese TA, Guzman, R. J., Martin, R. L., Yee, C., Zarins, C. K., & Dalman, R. L. Matrix metalloproteinase inhibition limits arterial enlargements in a rodent arteriovenous fistula model. Surgery 1998;124(2):328-34.

183. Erba E, Ronzoni, S., Bassano, L., Giavazzi, R., D'Incalci M. The metalloproteinase inhibitor batimastat (BB-94) causes cell cycle phase perturbations in ovarian cancer cells. Annals of oncology : official journal of the European Society for Medical Oncology / ESMO 1999;10(5):589-91.

184. Moore G, Liao, S., Curci, J. A., Starcher, B. C., Martin, R. L., Hendricks, R. T., Chen, J. J. Suppression of experimental abdominal aortic aneurysms by systemic treatment with a hydroxamate-based matrix metalloproteinase inhibitor (RS 132908). Journal of vascular surgery 1999;29(3):522-32.

185. Epstein CJ, Erickson RP, Wynshaw-Boris AJ. Inborn errors of development: the molecular basis of clinical disorders of morphogenesis: Oxford University Press; 2004.

186. Liu J, Xiong W, Baca-Regen L, Nagase H, Baxter BT. Mechanism of inhibition of matrix metalloproteinase-2 expression by doxycycline in human aortic smooth muscle cells. J Vasc Surg 2003;38(6):1376-83.

187. Chronopoulou L, Massimi, M., Giardi, M. F., Cametti, C., Devirgiliis, L. C., Dentini, M., & Palocci, C. (Chitosan-coated PLGA nanoparticles: A sustained drug release strategy for cell cultures. COLSUB Colloids and Surfaces B: Biointerfaces 2013;103:310-317.

188. Kilicarslan M, & Baykara, T. . The effect of the drug/polymer ratio on the properties of the verapamil HCl loaded microspheres. International journal of pharmaceutics 2003;252(1-2):1-2.

189. Botelho MA, Queiroz DB, Barros G, Guerreiro S, Fechine P, Umbelino S, Lyra A, Borges B, Freitas A, Queiroz DC and others. Nanostructured transdermal hormone replacement therapy for relieving menopausal symptoms: a confocal Raman spectroscopy study. Clinics (Sao Paulo) 2014;69(2):75-82.

190. Patel PJ, Gohel, M. C., & Acharya, S. R. Exploration of statistical experimental design to improve entrapment efficiency of acyclovir in poly (d, l) lactide nanoparticles. PHARMACEUTICAL DEVELOPMENT AND TECHNOLOGY 2014;19(2):200-212.

191. Sledge GWJ, Qulali, M., Goulet, R., Bone, E. A., & Fife, R. . Effect of matrix metalloproteinase inhibitor batimastat on breast cancer regrowth and metastasis in athymic mice. Journal of the National Cancer Institute 1995;87(20):1546-50.

192. Houard X, Leclercq A, Fontaine V, Coutard M, Martin-Ventura J-L, Ho-Tin-Noé B, Touat Z, Meilhac O, Michel J-B. Retention and Activation of Blood-Borne Proteases in the Arterial WallImplications for Atherothrombosis. Journal of the American College of Cardiology 2006;48(9s1):A3-A9.

193. Della PP, Soeltl, R., Krell, H. W., Collins, K., O'Donoghue, M., Schmitt, M., & Kruger, A. . Combined treatment with serine protease inhibitor aprotinin and matrix metalloproteinase inhibitor Batimastat (BB-94) does not prevent invasion of human esophageal and ovarian carcinoma cells in vivo. Anticancer research 1999;19(5B).

194. Boucek RJ, Gunja-Smith Z, Noble NL, Simpson CF. Modulation by propranolol of the lysyl cross-links in aortic elastin and collagen of the aneurysm-prone turkey. Biochemical Pharmacology 1983;32(2):275-280.

195. Assar AN, Zarins C. Ruptured abdominal aortic aneurysm: a surgical emergency with many clinical presentations. Postgraduate medical journal 2009;85(1003):268-273.

196. Golledge J, Muller J, Daugherty A, Norman P. Abdominal aortic aneurysm pathogenesis and implications for management. Arteriosclerosis, thrombosis, and vascular biology 2006;26(12):2605-2613.

197. Abdul-Hussien H, Soekhoe RG, Weber E, von der Thusen JH, Kleemann R, Mulder A, van Bockel JH, Hanemaaijer R, Lindeman JH. Collagen degradation in the abdominal aneurysm: a conspiracy of matrix metalloproteinase and cysteine collagenases. Am J Pathol 2007;170(3):809-17.

198. Huang J. Role of matrix metalloproteinase-2 in therosclerosis and abdominal aortic aneurysms in apolipoprotein e deficient mice. 2005.

199. Sierevogel MJ, Pasterkamp G, Velema E, de Jaegere PP, de Smet BJ, Verheijen JH, de Kleijn DP, Borst C. Oral Matrix Metalloproteinase Inhibition and Arterial Remodeling After Balloon Dilation An Intravascular Ultrasound Study in the Pig. Circulation 2001;103(2):302-307.

200. Nosoudi N, Nahar-Gohad P, Sinha A, Chowdhury A, Gerard P, Carsten CG, Gray BH, Vyavahare NR. Prevention of Abdominal Aortic Aneurysm Progression by Targeted Inhibition of Matrix Metalloproteinase Activity With Batimastat-Loaded Nanoparticles. Circulation research 2015;117(11):e80-e89.

201. Merodio M, Arnedo A, Renedo MJ, Irache JM. Ganciclovir-loaded albumin nanoparticles: characterization and in vitro release properties. European Journal of Pharmaceutical Sciences 2001;12(3):251-259.

202. Choudhary B, Zhou J, Li P, Thomas S, Kaartinen V, Sucov HM. Absence of TGFβ signaling in embryonic vascular smooth muscle leads to reduced lysyl oxidase expression, impaired elastogenesis, and aneurysm. Genesis 2009;47(2):115-121.

203. Rajith B, Ravindran A. BSA nanoparticle loaded atorvastatin calcium—a new facet for an old drug. PloS one 2014;9:e86317.

204. Xiong W, Knispel RA, Dietz HC, Ramirez F, Baxter BT. Doxycycline delays aneurysm rupture in a mouse model of Marfan syndrome. Journal of vascular surgery 2008;47(1):166-172.

205. Weissleder R, Nahrendorf M, Pittet MJ. Imaging macrophages with nanoparticles. Nature materials 2014;13(2):125-138.

206. Cronenwett JL, Johnston KW. Rutherford's vascular surgery: Elsevier Health Sciences; 2014.

207. Senior RM, Griffin GL, Mecham RP. Chemotactic activity of elastin-derived peptides. Journal of Clinical Investigation 1980;66(4):859.

208. Dale MA, Xiong W, Carson JS, Ruhlman MK, Baxter B. Elastin-derived Peptides Induce M1 Macrophage Polarization Promoting Abdominal Aortic Aneurysm Formation. Arteriosclerosis, Thrombosis, and Vascular Biology 2015;35(Suppl 1):A252-A252.

209. Hellmann DB, Grand DJ, Freischlag JA. Inflammatory abdominal aortic aneurysm. Jama 2007;297(4):395-400.

210. Carmo M, Colombo L, Bruno A, Corsi F, Roncoroni L, Cuttin M, Radice F, Mussini E, Settembrini P. Alteration of elastin, collagen and their cross-links in abdominal aortic aneurysms. European journal of vascular and endovascular surgery 2002;23(6):543-549.

211. Mäki JM, Sormunen R, Lippo S, Kaarteenaho-Wiik R, Soininen R, Myllyharju J. Lysyl oxidase is essential for normal development and function of the respiratory system and for the integrity of elastic and collagen fibers in various tissues. The American journal of pathology 2005;167(4):927-936.

212. Ross MH, Kaye GI, Pawlina W. Histology: a text and atlas: with cell and molecular biology: Lippincott Williams & Wilkins; 2003.

213. Yoshimura K, Aoki H, Ikeda Y, Fujii K, Akiyama N, Furutani A, Hoshii Y, Tanaka N, Ricci R, Ishihara T. Regression of abdominal aortic aneurysm by inhibition of c-Jun N-terminal kinase. Nature medicine 2005;11(12):1330-1338.

214. Adeyemi O, Akanji M. Biochemical changes in the kidney and liver of rats following administration of ethanolic extract of Psidium guajava leaves. Human & experimental toxicology 2011;30(9):1266-74.

215. Ishizaka N, Sohmiya K, Miyamura M, Umeda T, Tsuji M, Katsumata T, Miyata T. Infected aortic aneurysm and inflammatory aortic aneurysm—in search of an optimal differential diagnosis. Journal of cardiology 2012;59(2):123-131.

216. Mäyränpää MI, Trosien JA, Fontaine V, Folkesson M, Kazi M, Eriksson P, Swedenborg J, Hedin U. Mast cells associate with neovessels in the media and adventitia of abdominal aortic aneurysms. Journal of vascular surgery 2009;50(2):388-395.

217. Li Z-Y, Jean U, Tang TY, Soh E, See TC, Gillard JH. Impact of calcification and intraluminal thrombus on the computed wall stresses of abdominal aortic aneurysm. Journal of vascular surgery 2008;47(5):928-935.

218. Miyake T, Morishita R. Pharmacological treatment of abdominal aortic aneurysm. Cardiovascular research 2009:cvp155.

219. Botnar RM, Wiethoff AJ, Ebersberger U, Lacerda S, Blume U, Warley A, Jansen CH, Onthank DC, Cesati RR, Razavi R. In vivo assessment of aortic aneurysm wall integrity using elastin-specific molecular magnetic resonance imaging. Circulation: Cardiovascular Imaging 2014;7(4):679-689.

220. O'Leary SA, Mulvihill JJ, Barrett HE, Kavanagh EG, Walsh MT, McGloughlin TM, Doyle BJ. Determining the influence of calcification on the failure properties of abdominal aortic aneurysm (AAA) tissue. Journal of the mechanical behavior of biomedical materials 2015;42:154-167.

221. Seely DM, Wu P, Mills EJ. EDTA chelation therapy for cardiovascular disease: a systematic review. BMC Cardiovascular Disorders 2005;5(1):32.

222. Lamas GA, Goertz C, Boineau R, Mark DB, Rozema T, Nahin RL, Drisko JA, Lee KL. Design of the trial to assess chelation therapy (TACT). American heart journal 2012;163(1):7-12.

223. Luck G, Liao H, Murray NJ, Grimmer HR, Warminski EE, Williamson MP, Lilley TH, Haslam E. Polyphenols, astringency and proline-rich proteins. Phytochemistry 1994;37(2):357-371.

224. Scrutton MC. Proteinmetal interactions. FEBS Letters 1976;70(1-2):291-292.

225. Giachelli CM, Speer MY, Li X, Rajachar RM, Yang H. Regulation of vascular calcification roles of phosphate and osteopontin. Circulation Research 2005;96(7):717-722.

226. Pei H, Tian C, Sun X, Qian X, Liu P, Liu W, Chang Q. Overexpression of MicroRNA-145 Promotes Ascending Aortic Aneurysm Media Remodeling through TGF-β1. European Journal of Vascular and Endovascular Surgery 2015;49(1):52-59.

227. Gabriel EA, Gabriel SA. Inflammatory Response in Cardiovascular Surgery: Springer; 2013.

228. Guo G, Gehle P, Doelken S, Martin-Ventura JL, Von Kodolitsch Y, Hetzer R, Robinson PN. Induction of macrophage chemotaxis by aortic extracts from patients with Marfan syndrome is related to elastin binding protein. PLoS One 2011;6(5):e20138.

229. Nakazato Y, Yamaji Y, Oshima N, Hayashi M, Saruta T. Calcification and osteopontin localization in the peritoneum of patients on long-term continuous ambulatory peritoneal dialysis therapy. Nephrology Dialysis Transplantation 2002;17(7):1293-1303.

230. Yamanouchi D, Morgan S, Stair C, Seedial S, Lengfeld J, Kent KC, Liu B. Accelerated aneurysmal dilation associated with apoptosis and inflammation in a newly developed calcium phosphate rodent abdominal aortic aneurysm model. Journal of vascular surgery 2012;56(2):455-461.

231. Sun J, Sukhova GK, Yang M, Wolters PJ, MacFarlane LA, Libby P, Sun C, Zhang Y, Liu J, Ennis TL. Mast cells modulate the pathogenesis of elastase-induced abdominal aortic aneurysms in mice. The Journal of clinical investigation 2007;117(117 (11)):3359-3368.

232. Kothapalli CR, Ramamurthi A. Lysyl oxidase enhances elastin synthesis and matrix formation by vascular smooth muscle cells. Journal of tissue engineering and regenerative medicine 2009;3(8):655-661.

233. Rowe DW, McGoodwin EB, Martin GR, Grahn D. Decreased lysyl oxidase activity in the aneurysm-prone, mottled mouse. Journal of Biological Chemistry 1977;252(3):939-942.

234. Mäki JM, Räsänen J, Tikkanen H, Sormunen R, Mäkikallio K, Kivirikko KI, Soininen R. Inactivation of the lysyl oxidase gene Lox leads to aortic aneurysms, cardiovascular dysfunction, and perinatal death in mice. Circulation 2002;106(19):2503-2509.

235. Krettek A, Sukhova GK, Libby P. Elastogenesis in Human Arterial Disease A Role for Macrophages in Disordered Elastin Synthesis. Arteriosclerosis, thrombosis, and vascular biology 2003;23(4):582-587.

236. Favreau JT, Nguyen BT, Gao I, Yu P, Tao M, Schneiderman J, Gaudette GR, Ozaki CK. Murine ultrasound imaging for circumferential strain analyses in the angiotensin II abdominal aortic aneurysm model. Journal of vascular surgery 2012;56(2):462-469.

237. Liu L, Hitchens TK, Ye Q, Wu Y, Barbe B, Prior DE, Li WF, Yeh F-C, Foley LM, Bain DJ. Decreased reticuloendothelial system clearance and increased blood half-life and immune cell labeling for nano-and micron-sized superparamagnetic iron-oxide particles upon pre-treatment with Intralipid. Biochimica et Biophysica Acta (BBA)-General Subjects 2013;1830(6):3447-3453.

238. Venkatasubbu GD, Ramasamy S, Gaddam PR, Kumar J. Acute and subchronic toxicity analysis of surface modified paclitaxel attached hydroxyapatite and titanium dioxide nanoparticles. International journal of nanomedicine 2015;10(Suppl 1):137.

239. van Rooijen N, van Kesteren-Hendrikx E. In vivo" depletion of macrophages by liposome-mediated "suicide. Methods in enzymology 2003;373:3-16.

240. Simpson CF. Sotalol for the protection of turkeys from the development of β-aminopropionitrile-induced aortic ruptures. British journal of pharmacology 1972;45(3):385-390.

241. Nagashima H, Uto K, Sakomura Y, Aoka Y, Sakuta A, Aomi S, Hagiwara N, Kawana M, Kasanuki H. An angiotensin-converting enzyme inhibitor, not an angiotensin II type-1 receptor blocker, prevents β-aminopropionitrile monofumarate-induced aortic dissection in rats. Journal of vascular surgery 2002;36(4):818-823.

242. Mao N, Gu T, Shi E, Zhang G, Yu L, Wang C. Phenotypic switching of vascular smooth muscle cells in animal model of rat thoracic aortic aneurysm. Interactive cardiovascular and thoracic surgery 2015;21(1):62-70.

243. Koch A, Haines G, Rizzo R, Radosevich J, Pope R, Robinson P, Pearce W. Human abdominal aortic aneurysms. Immunophenotypic analysis suggesting an immune-mediated response. The American journal of pathology 1990;137(5):1199.

244. Tang T, Boyle J, Dixon A, Varty K. Inflammatory abdominal aortic aneurysms. European journal of vascular and endovascular surgery 2005;29(4):353-362.

245. Kleinstreuer C, Li Z. Analysis and computer program for rupture-risk prediction of abdominal aortic aneurysms. Biomed Eng Online 2006;5(19).

246. Low JA, Johnson MD, Bone EA, Dickson RB. The matrix metalloproteinase inhibitor batimastat (BB-94) retards human breast cancer solid tumor growth but not ascites formation in nude mice. Clinical cancer research 1996;2(7):1207-1214.

247. O'Byrne K, Macaulay V, Saunders M, Long L, Gleeson F, Ganesan T, Harris A, Talbot D. 951 Phase I study of batimastat (BB94) in the treatment of malignant pleural effusions. European Journal of Cancer 1995;31:S198.

248. Pavlaki M, Zucker S. Matrix metalloproteinase inhibitors (MMPIs): the beginning of phase I or the termination of phase III clinical trials. Cancer and metastasis reviews 2003;22(2-3):177-203.

249. Chen L-S, Wang A-X, Dong B, Pu K-F, Yuan L-H, Zhu Y-M. A new prospect in cancer therapy: targeting cancer stem cells to eradicate cancer. Chinese journal of cancer 2012;31(12):564.

250. Sarkar FH. MicroRNA Targeted Cancer Therapy: Springer; 2014.